Core (COR) Package
Reference Manual

The MELCOR Core (COR) package calculates the thermal response of the core and lower plenum internal structures, including the portion of the lower head directly below the core. The package also models the relocation of core and lower plenum structural materials during melting, slumping, and debris formation, including failure of the reactor vessel and ejection of debris into the reactor cavity. Energy transfer to and from the Control Volume Hydrodynamics package and the Heat Structure package is calculated. This Reference Manual gives a description of the physical models in the COR package, including the nodalization scheme and calculational framework of the package, the heat transfer and oxidation models, the mass relocation models, and the default lower head model. An alternate (and more detailed) model for debris behavior in the lower plenum of a reactor (BWR or PWR) is available by invoking the Bottom Head package, described in the BH Package Reference Manual.

User input for running MELGEN and MELCOR with the COR package activated is described in the COR Package Users' Guide.

Contents

1 Introduction 6
1.1 Nodalization Scheme 7
1.1.1 Core/Lower Plenum 7
1.1.2 Lower Head 13
1.2 Calculation Framework 15

2 Heat Transfer and Oxidation Models 16
2.1 Radiation 17
2.1.1 Emissivities 18
2.1.2 View Factors 20
2.1.3 Implementation Logic 23
2.2 Conduction 26
2.2.1 Axial Conduction 27
2.2.2 Radial Conduction 30
2.2.3 Intra-Cell Conduction 30
2.2.4 Fuel-Cladding Gap Heat Transfer 31
2.2.5 Consideration of Heat Capacity of Components 33
2.2.6 Effective Heat Capacity of Cladding 33
2.2.7 Conduction to Boundary Heat Structures 34
2.3 Convection 35
2.3.1 Laminar Forced Convection 36
2.3.2 Turbulent Forced Convection 37
2.3.3 Laminar and Turbulent Free Convection 37
2.3.4 Convection from Particulate Debris 38
2.3.5 Boiling 38
2.3.6 Heat Transfer from Horizontal Surfaces of Plates 39
2.3.7 Debris Quenching and Dryout 40
2.4 Oxidation 42
2.4.1 Zircaloy and Steel 44
2.4.2 Simple Boron Carbide Reaction Model 47
2.4.3 Advanced Boron Carbide Reaction Model 49
2.4.4 Steam/Oxygen Allocation 50
2.5 Control Volume Temperature Distribution (dT/dz) Model 52
2.6 Power Generation 55
2.6.1 Fission Power Generation 55
2.6.2 Decay Power Distribution 58
2.7 Material Interactions (Eutectics) 60
2.7.1 Mixture Formation 60
2.7.2 Mixture Properties 61
2.7.3 Chemical Dissolution of Solids 63

3 Core/In-Vessel Mass Relocation Models 65

3.1 Candling 65
3.1.1 Steady Flow 65
3.1.2 Flow Blockages 69
3.1.3 Holdup by Oxide Shells 71
3.1.4 Solid Material Transport 72
3.1.5 Radial Relocation of Molten Materials 73
3.1.6 Surface Area Effects of Conglomerate Debris 74
3.2 Particulate Debris 77
3.2.1 Formation of Particulate Debris 78
3.2.2 Debris Addition from Heat Structure Melting 80
3.2.3 Exclusion of Particulate Debris 80
3.2.4 Radial Relocation of Particulate Debris 84
3.2.5 Gravitational Settling 84
3.3 Displacement of Fluids in CVH 86

4 Structure Support Model 88
4.1 Model for OS 88
4.2 Models for SS 88
4.2.1 The PLATEG Model 89
4.2.2 The PLATE Model 90
4.2.3 The PLATEB Model 92
4.2.4 The COLUMN Model 92
4.2.5 User Flexibility in Modeling 93
4.3 SS Failure Models 94
4.3.1 Failure by Yielding 94
4.3.2 Failure by Buckling 94
4.3.3 Failure by Creep 95

5 Lower Head Model 96
5.1 Heat Transfer 97
5.2 Failure 103
5.3 Debris Ejection 106

6 Discussion and Development Plans 109
6.1 Radiation 109
6.2 Reflood Behavior 109
6.3 Lower Plenum Debris Behavior and Vessel Failure 109
6.4 Updating of Core Degradation Models 110

References 117

List of Figures

Figure 1.1 Core/lower plenum nodalization. 8
Figure 1.2 Core cell components. 9
Figure 1.3 Typical COR-CVH nodalization interface (2D). 12
Figure 1.4 Typical COR-CVH nodalization interface (3D). 13
Figure 1.5 Lower head nodalization (one ring). 14
Figure 2.1 Radiative heat transfer framework -- BWR cell cross-section. 21
Figure 2.2 Component axial temperature gradient across liquid level. 28
Figure 2.3 Two-phase construction for material mixture [22]. 62
Figure 3.1 Candling process steps. 69
Figure 3.2 Flow blockage formation during candling. 71
Figure 3.3 Conglomerate debris geometry in fuel rod bundles. 75
Figure 5.1 Lower head nodalization. 96

List of Tables

Table 1.1 Components modeled in COR package 9
Table 2.1 Steam emissivity vs. temperature and optical depth [6]. 20
Table 2.2 Core eutectic reactions [20, 21]. 61
Table 2.3 Solid dissolution hierarchy. 63
Table 3.1 Alternate refreezing components. 68
Table 3.2 Exclusion of particulate debris by core components 83

1 Introduction

The MELCOR COR package calculates the thermal response of the core and lower plenum structures, including the portion of the lower head directly beneath the core, and models the relocation of core materials during melting, slumping, and debris formation. Fuel pellets, cladding, grid spacers, canister walls (for BWRs), other structures (e.g., control rods or guide tubes), and particulate debris are modeled separately within individual cells, the basic nodalization unit in the COR package. Either BWR or PWR systems may be modeled, as specified on record COR00002. (For the convenience of the user and the sake of clarity, numerous cross-references are made in this document to specific input records and quantities in the COR Package Users' Guide. Both documents should be consulted by the user for a more complete understanding of the models and their implementation.)

All important heat transfer processes are modeled in each COR cell. Thermal radiation within a cell and between cells in both the axial and radial directions is calculated, as well as radiation to boundary structures (e.g., the core shroud or upper plenum, which are modeled by the Heat Structure package) from the outer and upper COR cells. Radiation to a liquid pool (or the lower head if a pool is absent) and to steam is also included. Heat transfer within fuel pellets and across the fuel-cladding gap is evaluated. Axial conduction between segments of components in adjacent cells is modeled, as is radial conduction within core plates and within debris beds that are not interrupted by BWR canister walls. Intracell conduction is calculated between particulate debris and other components with which it is in intimate contact. An option is available to include radial conduction between the core and radial boundary heat structures. An analytical model for axial conduction is applied within structures that are partially covered with liquid pool. Convection to the control volume fluids is modeled for a wide range of fluid conditions and structure surface temperatures, including nucleate and film boiling.

Oxidation of Zircaloy and steel is modeled as limited by both solid-state diffusion of oxygen through the oxide layer and gaseous diffusion of steam or oxygen through the mixture. The reaction of B_4C with steam is also modeled.

The core degradation model treats eutectic liquefaction and dissolution reactions, *candling* of molten core materials (i.e., downward flow and refreezing), and the formation and relocation of particulate debris. Geometric variables (e.g., cell surface areas and volumes) are updated for changing core geometry.

Many of the various physics models can be selectively disabled by setting the flags on MELCOR input record CORTST01. This action might be appropriate for testing purposes or to bypass phenomena that are not expected to arise during a particular calculation.

1.1 Nodalization Scheme

1.1.1 Core/Lower Plenum

The core and lower plenum regions of the reactor vessel are divided into concentric radial rings and axial levels, as shown in Figure 1.1; the numbers of rings and levels are input by the user on record COR00000. The number of levels defining the lower plenum alone (which should include the core plate) is defined by the user on this record also. A particular radial ring and a particular axial level designate a COR cell, whose cell number is defined as a three-digit number; the first digit represents the radial ring number and the last two digits represent the axial level number. For example, cell 307 denotes the third radial ring and the seventh axial level. Radial rings are numbered from the center out and axial levels are numbered from the bottom head up. *This nodalization scheme applies only to structures treated by the COR package, and is independent of the control volume nodalization specified for the Control Volume Hydrodynamics (CVH) package.* The interface between the COR and CVH packages is discussed later in this section.

Each cell may contain one or more components, as shown in Figure 1.2. Seven possible intact components are modeled: (1) fuel, (2) cladding, (3) and (4) BWR canister walls, split into two parts: one part not adjacent to the control blade and another part that is, (5) supporting structure, (6) nonsupporting structure, and (7) "other structure". The primary difference between the "supporting" and "nonsupporting" structure components is the ability to support other core components (core support structures) or not (control rods or blades). The "other structure" component has a limited ability to represent either. It has been retained from older versions of MELCOR, and may not be used in combination with either of the "supporting" or "nonsupporting structure" components. The structure shown in Figure 1.2 may represent supporting and/or nonsupporting structures in the new representation *or* "other structure" in the old representation.

A core cell may also contain particulate debris ("rubble") resulting from the collapse of fuel rods and other core components. In a BWR, such debris may reside either inside or outside the channel box, in the channel or bypass region, respectively. Unlike previous versions, MELCOR 1.8.5 distinguishes particulate debris in the channel from that in the bypass, using separate components for each. The distinction exists only for a BWR, and only for core cells that have distinct channel and bypass regions. Even then, most of the distinction is lost when the channel box fails, and the two debris fields are assumed to be mixed and equilibrated. However, both types of particulate debris must continue to be tracked after canister failure because they typically occupy space in different CVH control volumes. When the canister fails, the transfer of debris between the channel and the bypass is not instantaneous. It is controlled by a time constant with a default value of 1 s, adjustable through sensitivity coefficient array C1021.

Conglomerate debris, i.e., core material that has melted and resolidified, is modeled as an integral part of the component onto which it has frozen, which may be any one of the seven listed above except for intact fuel.

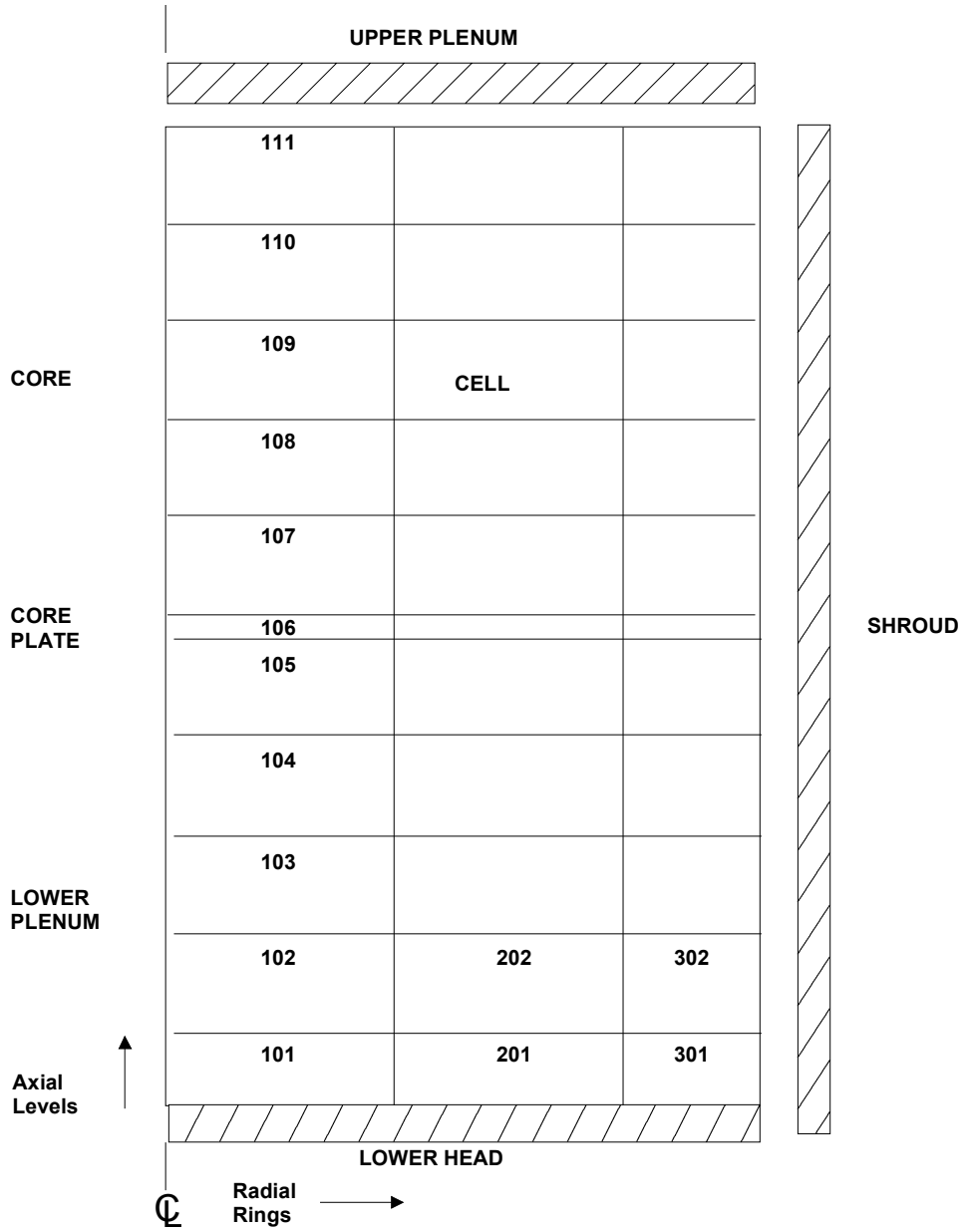

Figure 1.1 Core/lower plenum nodalization.

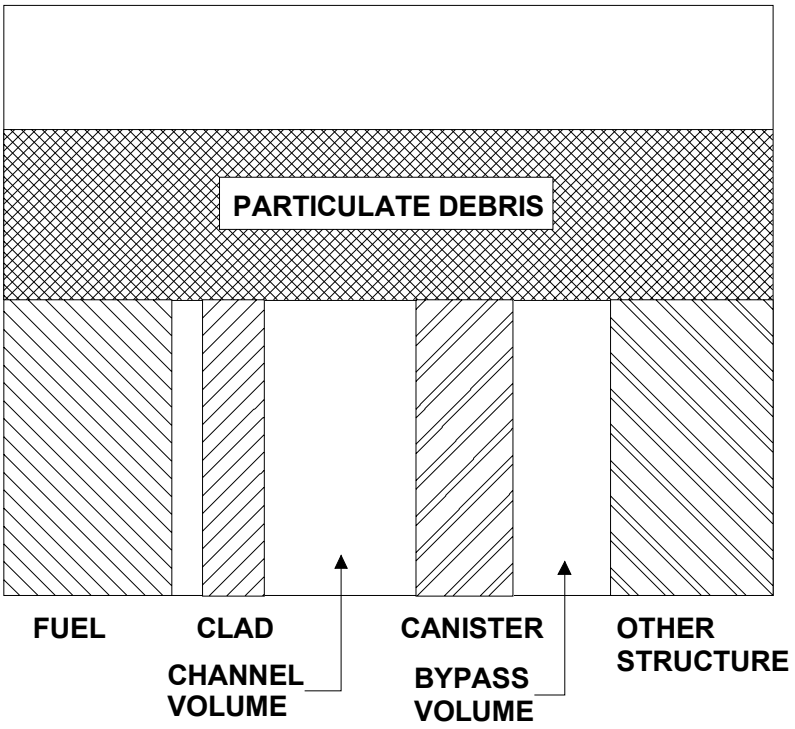

Figure 1.2 Core cell components.

The following table identifies each component by its component number and component identifier, which are often used in the COR package documentation.

Table 1.1 Components modeled in COR package

1	FU	intact fuel component
2	CL	intact cladding component
3	CN	intact canister component (portion not adjacent to control blade
4	CB	intact canister component (portion adjacent to control blade)
5	OS	“other structure" component
6	PD	particulate debris component (portion in the channel for a BWR)
7	SS	supporting structure component
8	NS	nonsupporting structure component
9	PB	particulate debris component in the bypass (for a BWR)

Eight materials are currently modeled in the COR package: (1) UO_2, (2) Zircaloy, (3) steel, (4) ZrO_2, (5) steel oxide, (6) control rod poison, which may be either boron carbide (B_4C)

or silver-indium-cadmium alloy (Ag-In-Cd) as specified on record COR00002, (7) Inconel, and (8) an electric heating element material, specified on record COR00002. Each component may be composed of one or more of these materials. For example, the cladding component may be composed of Zircaloy, Inconel (to simulate grid spacers), and ZrO_2 (either initially present or calculated by the COR package oxidation models). The melting and candling of materials results in the possibility of any or all materials being found in a given component. The “heating element material” is intended for use in analysis of electrically heated experiments. Its use requires that the user modify subroutine ELHEAT to provide a calculation of the associated heating power in all cells containing the material.

Zircaloy is considered as single material in the COR package, with no distinction made between zirconium and the zircaloy alloying elements. Steel and steel oxide are also each modeled as single materials within the COR package, but the user must specify the fractions of iron, nickel, and chromium in the steel so that oxidation can be properly treated and the right amounts of each species can be transmitted to the Cavity (CAV) package during debris ejection. Inconel is treated as a single material, and currently it has the same properties as steel (and is ejected as steel), but it is not permitted to oxidize. Properties of the materials are obtained from MELCOR’s Material Properties (MP) package. In MELCOR versions after 1.8.4, the user was given increased flexibility to use properties other than those of the default materials.

Several geometric variables are defined by the user to further describe the cells and components. Representative dimensions for the intact components are specified on record COR00001, and elevations and lengths (heights) for each cell are input on record CORZjj01. Equivalent diameters for each component in each cell for use in various heat transfer correlations also must be specified on record CORijj04. Cell boundary areas for inter-cell radiation (both axially and radially) are defined by the user on records CORijj05 and CORRii01. Initial volumes of components and the "empty" CVH fluid volume are calculated based on user input for component masses and cell flow areas (records CORijj02 and CORijj05), and are then tracked during core slumping and flow blockage calculations.

For each intact component in each cell, a surface area is input by the user on record CORijj06 for convection and oxidation calculations. (The single surface area value input for a canister is multiplied by elements in sensitivity coefficient array C1501 to obtain values for each side of each canister component to communicate separately with the channel and bypass control volumes.) For particulate debris, a surface area is calculated from the total mass and a user-defined particle size input on record CORijj04. (For oxidation of particulate debris, separate Zircaloy and steel surface areas are calculated.) The effects of conglomerate debris on component surface areas are factored into the heat transfer, oxidation, and candling calculations; this model is described in Section 3.1.5.

As discussed later in Sections 2.3 and 2.5, the Control Volume Hydrodynamics (CVH) package supplies fluid conditions for use by the COR package in calculating heat transfer

and oxidation rates, which are then multiplied by the time step and passed back to the CVH package as energy and mass sources or sinks. The nodalization for the reactor vessel used in the CVH package is typically much coarser than that used in the COR package, but finer CVH nodalizations can be used to simulate in-vessel natural circulation. The COR nodalization applies only to those components in the core and lower plenum treated by the COR package, and is independent of the CVH nodalization, with some restrictions imposed.

Figure 1.3 gives a 2-D representation of the interface between the COR and CVH packages, but to more accurately depict the relationship between the two nodalizations requires a 3-D illustration, shown in Figure 1.4. Each COR cell interfaces with a CVH control volume (input on record CORijj01) representing the primary flow (channel volume), which provides boundary conditions for most core surfaces. Typically many core or lower plenum cells will interface with the same control volume. For BWRs, a separate CVH control volume (shown behind the channel volume in Figure 1.4) may also be specified for COR cells on record CORijj01 to represent the interstitial space between fuel assemblies (bypass volume). The outer canister surfaces and the supporting and nonsupporting structure (or "other structure") surfaces, as well as the surface of any particulate debris in the bypass of a BWR, all communicate with this bypass control volume if it is distinguished from the channel control volume. The total number of control volumes interfaced to the COR package is a required input quantity on record COR00000. The only restrictions between CVH and COR nodalizations are that control volumes occupy a rectangular grid of core cells and have boundaries lying either on cell boundaries or entirely outside the core nodalization.

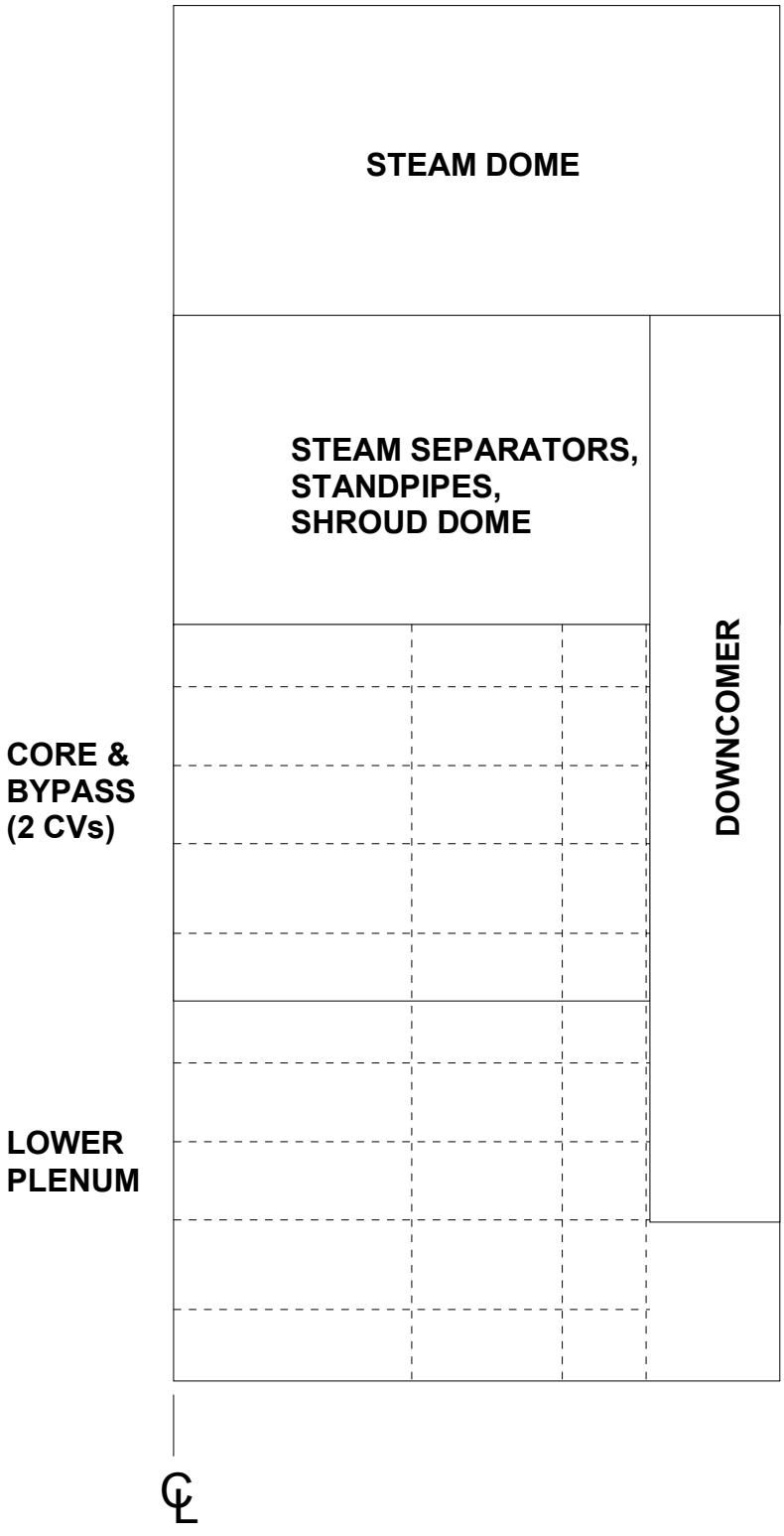

Figure 1.3 Typical COR-CVH nodalization interface (2D).

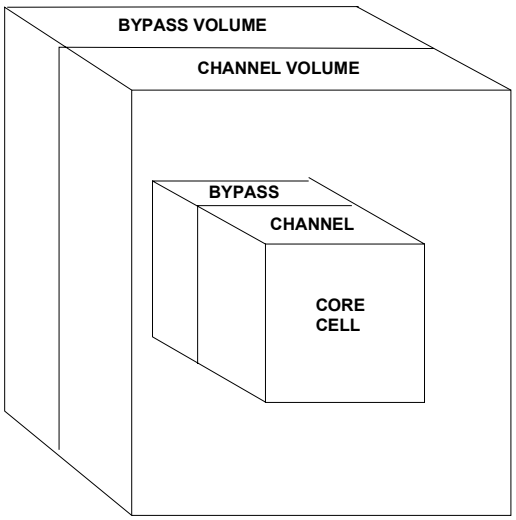

Figure 1.4 Typical COR-CVH nodalization interface (3D).

1.1.2 Lower Head

The basic elements of the COR package lower head heat transfer model are the portion of the lower head hemisphere directly beneath the core, head penetrations such as instrumentation tubes or guide tubes, the layer of debris on top of the lower head and the CVH heat sink available in the reactor cavity. Note that all core cells in an axial level have the same height. This forces the bottom head to be flat out to the outer boundary of the outer COR cell ring. The lower head is divided into radial rings corresponding to the core/lower plenum nodalization, and its thickness (defined by entry DZLH on record COR00001) is divided axially into a number (defined by entry NLH on record COR00000) of finite-difference temperature nodes for treating conduction. Both the composition and mesh spacing in the lower head may be defined by the user (by default the lower head is divided into NLH-1 equal mesh layers of stainless steel, each of thickness DZLH/(NLH-1)). The NLH temperature nodes are located at the mesh layer boundaries. Heat transfer from hot debris to the inner surface of the lower head is modeled parametrically, with a user-specified constant heat transfer coefficient. Heat transfer from the outer surface of the lower head to the reactor cavity is treated parametrically if the cavity is dry, using a constant, user-adjustable heat transfer coefficient with a default value of 10 W/m^2-K, or with a simple downward-facing boiling model if the cavity is flooded. The calculated temperature profile through the lower head is used in a mechanical response model that determines stress and strain in the lower head to predict creep-rupture failure. Creep (plastic strain) is calculated from the Larson-Miller parameter and a life-fraction rule.

Figure 1.5 illustrates the lower head nodalization for a single radial ring. For each lower head ring, the user can define up to three representative types of penetrations (only one is shown in the figure), specifying the total mass and heat transfer areas associated with

each penetration type and the initial effective diameter of the opening created when a penetration fails. Each penetration communicates thermally with the top lower head node and with the debris. The Heat Structure (HS) package should not be used to model the center portion of the lower head treated by the COR package, but should only be used to model the upper portion of the head hemisphere that does not directly contact the debris. There should be no duplication of head mass or surface area between HS and COR packages. Neither should there be any duplication of mass or surface area between penetrations and structures modeled as ordinary core components in the first axial level of core cells; the user may divide such structures between penetrations and supporting or nonsupporting structure (or “other structure”) arbitrarily, but the thermal modeling interface is somewhat indirect. The user should also realize that penetration masses are not currently added to core/lower plenum debris masses and cannot be ejected from the reactor vessel. The total number of penetrations in all rings is a required input quantity on record COR00000.

The Bottom Head (BH) package has been developed by Oak Ridge National Laboratories for more detailed treatment of lower plenum debris behavior and bottom head heatup and failure following debris bed dryout. That package may be activated by optional user input and is documented in the BH Package Users' Guide and Reference Manual.

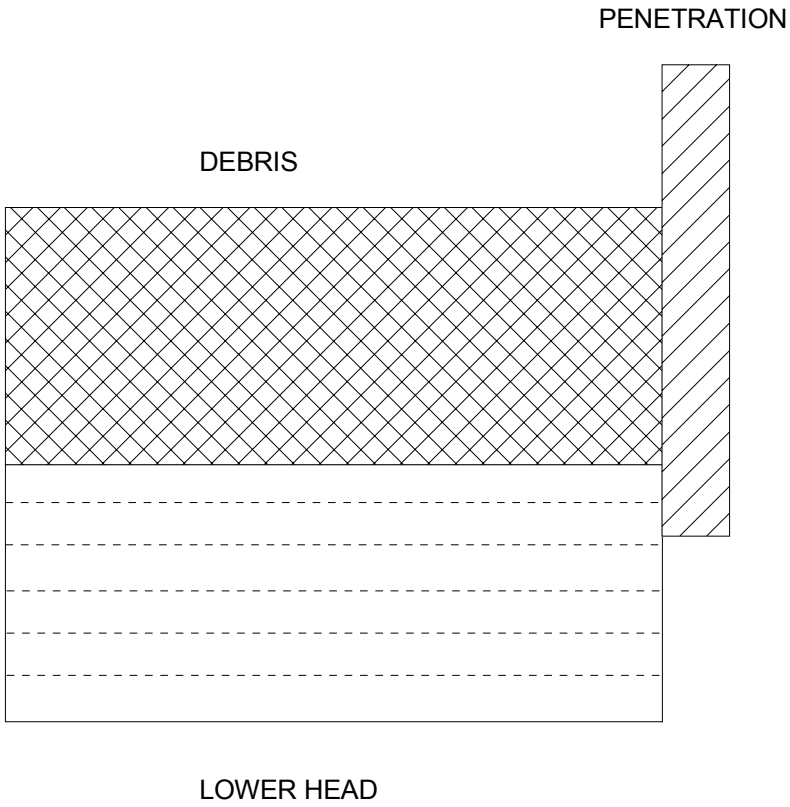

Figure 1.5 Lower head nodalization (one ring).

1.2 Calculation Framework

All thermal calculations in the COR package (both in the core/lower plenum components and in the lower head) are done using internal energies of the materials (i.e., temperature is a derived variable calculated from the material internal energies; initial temperatures are defined on record CORijj03). The mass and internal energy of each material in each component are tracked separately to conserve total mass and energy to within machine roundoff accuracy.

The COR package uses an explicit numerical scheme for advancing the thermal state of the core, lower plenum, and lower head through time. To mitigate numerical instabilities, a subcycling capability has been developed to allow the COR package to take multiple time steps across a single Executive package time step. All energy generation, heat transfer, and oxidation rates are evaluated at the beginning of a COR package subcycle based on current temperatures, geometric conditions, and an estimate of the local fluid conditions (calculated by the COR package dT/dz model to reflect the temperature variation within a control volume containing many individual COR cells). The net energy gain (or loss) across the subcycle is determined for each component by multiplying these rates by the COR package time step.

The temperature change of most components is limited to a user-input maximum; if the calculated temperature change for a component is greater than this limit, the COR package subcycle time step is reduced accordingly, but not lower than the minimum time step input by the user for the COR package. Components with a total mass below a critical minimum are not subjected to this limit. If the energy input to any fluid volume changes from previous values in such a way as to possibly result in numeric instability between the COR and control volume packages, the system time step may be cut immediately, or a reduction may be requested for the next Executive time step. The various time step control parameters may be specified by the user on record CORDTC01 and using sensitivity coefficient arrays C1401 and C1502 (see COR Package Users' Guide).

At the end of a COR package time step, after the thermal state of the core has been updated by the heat transfer and oxidation models described in Section 2, relocation of core materials and debris formation are calculated by the core degradation models described in Section 3. Molten portions of intact structures are transferred to the conglomerate debris associated with the structure. Liquefaction of intact structures caused by eutectic reactions between materials within the structure and dissolution of intact structures by existing molten material within the core cell are calculated, if the materials interactions model has been activated. Molten materials are relocated downward by the candling model (provided there is no flow blockage) and intact components are converted to debris if various debris formation criteria are met.

Downward relocation of particulate debris from one cell to a lower one by gravitational settling is generally modeled as a logical process and relocation is completed over a single time step, with consideration given only to constraints imposed by the porosity of the

debris, the availability of free (open) volume to hold it, and support by structures such as the core plate. (These constraints are not imposed on molten debris, which will always relocate to lower regions unless the path is totally blocked.) However, numerical limits are imposed to ensure that the mass relocated goes to zero in the limit of small timesteps, and a rate limitation is imposed for the falling debris quench heat transfer model. In MELCOR 1.8.5, debris in the bypass of a BWR is distinguished from that in the channel. In core cells containing a canister, the downward relocation of particulate or molten debris can be blocked separately in the channel and in the bypass. After the canister has failed, debris in the channel and that in the bypass are mixed and equilibrated. As long as the canister is intact, the majority of the particulate debris in the bypass of a BWR will be the remnants of control blades. Most of the space available to it will be in the bladed bypass region, adjacent to canister component CB. Therefore, the existence of CB is taken as the criterion for separation of particulate debris in the bypass from that in the channel.

Reactor components such as control rods and blades may be supported from above or below, with parametric models for failure based on the temperature and the remaining thickness of the structural metal. Either load-based structural models or simpler parametric models may be used for the failure of components such as the core plate and the Control Rod Guide Tubes (CRGTs) in a BWR.

Gravitational leveling of molten pools and debris beds across the core rings is calculated with a user-adjustable time constant. In a BWR, this leveling is blocked by the presence of intact canisters, so that no leveling is possible until any distinction between the debris in the channel and that in the bypass has disappeared. Debris beds are completely leveled; the angle of repose is not considered. Whenever mass is relocated or debris formed, material energies in the new or changed components are re-evaluated and the temperature updated to maintain thermal equilibrium, and any relevant geometric variables are recalculated to reflect the change in geometry.

2 Heat Transfer and Oxidation Models

This section describes the models implemented in the COR package to treat various modes of heat transfer and oxidation within the core and lower plenum; lower head heat transfer models are discussed separately in Section 5. Radiation, conduction, and convection are covered in Sections 2.1, 2.2 and 2.3, respectively, and oxidation is covered in Section 2.4. Section 2.5 describes the "dT/dz" model used by the COR package to provide approximate local (core cell) fluid temperatures and gas compositions within the possibly larger CVH control volume. Fission power generation in ATWS accident sequences (and in some experiments) is covered in Section 2.6.

Most of the constants (including exponents) used in the correlations described in this section have been implemented as sensitivity coefficients, thus allowing the user to change them from the default values described in this document if desired. Sensitivity coefficients are grouped into numbered arrays, Cnnnn(k), where 'nnnn' is an identifying number that

refers to a set of related coefficients, such as the several constants appearing in a single correlation (see the MELGEN/MELCOR Users' Guide). Appendix A gives a table of sensitivity coefficients used in the COR package and their default values. Unless otherwise noted, all variables and dimensional constants are in SI units, in conformance to MELCOR coding conventions.

2.1 Radiation

Thermal radiation among components within COR cells, across cell boundaries, and from components to steam is modeled as exchange of radiation between pairs of gray surfaces with an intervening gray medium; the model is constructed following the description provided in Kreith [1]. The radiosity, J_I, is defined as the total energy flux leaving the i-th surface (i=1 or 2 in this model), both reflected and emitted:

$$J_i = (1 - \varepsilon_i) G_i + \varepsilon_i E_{bi} \tag{2.1}$$

where

ε_i = emissivity of surface i

G_i= radiation flux incident on surface i

E_{bi}= blackbody emissive power of surface i, σT_i^4

The net heat transfer rate from the i-th surface is the difference between the radiosity and the incident radiation, multiplied by the area of surface i, A_i:

$$q_i = A_i (J_i - G_i) \tag{2.2}$$

Combining Equations (2.1) and (2.2) gives q_i in terms of the radiosity and blackbody emissive power:

$$q_i = A_i \frac{\varepsilon_i}{1 - \varepsilon_i} (E_{bi} - J_i) \tag{2.3}$$

The net heat transfer rate from surface i to surface j is given in terms of the surface radiosities by the expression:

$$q_{ij} = A_i F_{ij} \tau_{ij} \left(J_i - J_j\right) \tag{2.4}$$

where

F_{ij}= geometric view factor from surface i to surface j

τ_{ij} = geometric mean transmittance between surfaces i and j

Radiation heat transfer also occurs between each of the surfaces and the steam medium, according to the expression:

$$q_{i,m} = A_i \, \varepsilon_m \, (J_i - E_{b,m}) \tag{2.5}$$

where

ε_m = steam emissivity/absorptivity = $(1 - \tau_{ij})$

$E_{b,m}$= blackbody emissive power of medium, $\sigma \, T_m^4$

With the additional requirement:

$$q_i = q_{im} + q_{ij} \tag{2.6}$$

Equations (2.3), (2.4), (2.5), and (2.6) are solved in the COR package to obtain q_i and q_{im} (i = 1, 2) for various pairs of surfaces. The subsections below discuss the calculation of surface and steam emissivities ε_i and ε_m, the geometric view factors F_{ij}, and the implementation logic (i.e., how pairs of surfaces are chosen for multiple cell components that may relocate during the course of a calculation).

2.1.1 Emissivities

The surface and steam emissivities are evaluated by models adapted from MARCON 2.1B [2], an extended version of MARCH 2 [3]. For cladding and canister components, the surface emissivity of Zircaloy is used, which is calculated in these models as a function of temperature and oxide thickness from the equations used in MATPRO [4]. For Zircaloy surfaces whose maximum temperature has never reached 1500 K, the surface emissivity is given by:

$$\varepsilon_i = 0.325 + 0.1246 \, x \, 10^6 \, \Delta r_{ox} \quad \left[\Delta r_{ox} < 3.88 \, x \, 10^{-6}\right] \tag{2.7}$$

$$\varepsilon_i = 0.808642 - 50.0 \, \Delta r_{ox} \quad \left[\Delta r_{ox} \geq 3.88 \, x \, 10^{-6}\right] \tag{2.8}$$

where Δr_{ox} is the oxide thickness. For surfaces that have reached temperatures greater than 1500 K at some time, the emissivity is calculated by Equation (2.7) or (2.8) and then multiplied by the factor:

$$f = \exp\left[\frac{1500.0 - T_{i,max}}{300.0}\right] \tag{2.9}$$

where $T_{i,max}$ is the maximum temperature the surface has reached. This factor is limited to a lower bound of 0.325.

The surface emissivity of SS and NS (or OS) components in these models is calculated from the relation used in MARCON 2.1B for stainless steel, taken from Reference [5]:

$$\varepsilon_i = 0.042 + 0.000347 \cdot T_i \tag{2.10}$$

The steam emissivities, ε_m, are evaluated in these models from a table taken from Reference [6] (see Table 2.1), which specifies the steam emissivity versus steam temperature and optical depth (steam partial pressure times mean beam length L_e) at the high-pressure limit. Mean beam lengths are supplied for each component type based only on representative distances for an intact core geometric configuration using these equations [7]:

$$L_{e,cl} = 3.5\left(P - 2r_{cl}\right) \tag{2.11}$$

$$L_{e,cn} = L_{e,cb} = 1.8\ r_{cl,cn} \tag{2.12}$$

$$L_{e,cbb} = L_{e,os} = 1.8\ r_{cn,cb} \tag{2.13}$$

$$L_{e,cnb} = 1.8\ r_{cn,cn} \tag{2.14}$$

$$L_{e,pd} = L_{e,pb} = 0 \tag{2.15}$$

where the second subscripts on the mean beam length represent cladding (cl); canister (not by blade) inner surface (cn); canister (by blade) inner surface (cb); canister (by blade) outer surface (cbb); other structure (xs, representing ss, ns, or os); canister (not by blade) outer surface (cnb); and particulate debris (pd and pb); and where P is the fuel rod pitch, r_{cl} is the cladding radius, $r_{cl,cn}$ is the distance between the outer fuel rods and the canister wall, $r_{cn,cb}$ is the distance between the canister and control blade, and $r_{cn,cn}$ is the distance between adjacent canister walls. For the particulate debris component, a surface emissivity of unity is assumed.

Table 2.1 Steam emissivity vs. temperature and optical depth [6].

Optical Depth (cm-atm)	Temperature (K)						
	370	600	1000	1500	2000	2500	3000
1.0	0.12	0.09	0.041	0.02	0.01	0.0063	0.004
3.2	0.25	0.195	0.11	0.06	0.03	0.019	0.011
10.0	0.37	0.315	0.23	0.145	0.085	0.053	0.033
32.0	0.47	0.425	0.37	0.29	0.20	0.135	0.086
100.0	0.56	0.533	0.55	0.47	0.365	0.277	0.193
320.0	0.65	0.625	0.70	0.66	0.555	0.47	0.35
1000.0	0.73	0.71	0.82	0.80	0.74	0.65	0.52
3200.0	0.79	0.78	0.92	0.90	0.88	0.78	0.65
10000.0	0.85	0.85	1.00	0.92	0.92	0.85	0.73

2.1.2 View Factors

The view factors F_{ij} used in Equation (2.4) model the effects of surface orientation and are implemented as user-specified parameters. The surface areas A_i used with F_{ij} are the actual component areas for radiation between components within a cell and are cell boundary areas for inter-cell radiation. Values for the view factors are input by the user as “exchange factors” on record COR00003. These values should be based on standard expressions for simple geometries, where possible, or on experimental data or detailed radiation calculations for complicated geometries involving intervening surfaces, such as for radiation between "representative" structures in cells containing a number of similar structures (e.g., fuel rod bundles). In the absence of any information to aid in selection of view factors, they should be used as arbitrarily varied parameters to examine the effects of radiation on the course of a calculation. View factors are not dynamic, that is they do not change as the core degrades; however, they may be changed across a MELCOR restart. Because of reciprocity (i.e., $F_{12}A_1 = F_{21}A_2$), the user-input component surface areas, unmodified by the effects of conglomerate debris, of intact components are always used with these constant view factors. Only the areas of particulate debris are treated as time dependent.

Figure 2.1 depicts the conceptual framework for radiative heat transfer in MELCOR. The framework is geared toward intact BWR cores but is general enough to treat PWR cores, as well as degraded cores and lower plenum radiation. (The precise situation represented, with *part* of the control blade and *part* of the fuel rods failed, cannot exist within a single core cell in MELCOR. The Figure is for illustration only, as an aid to visualizing which surfaces can radiate to other surfaces under various conditions.)

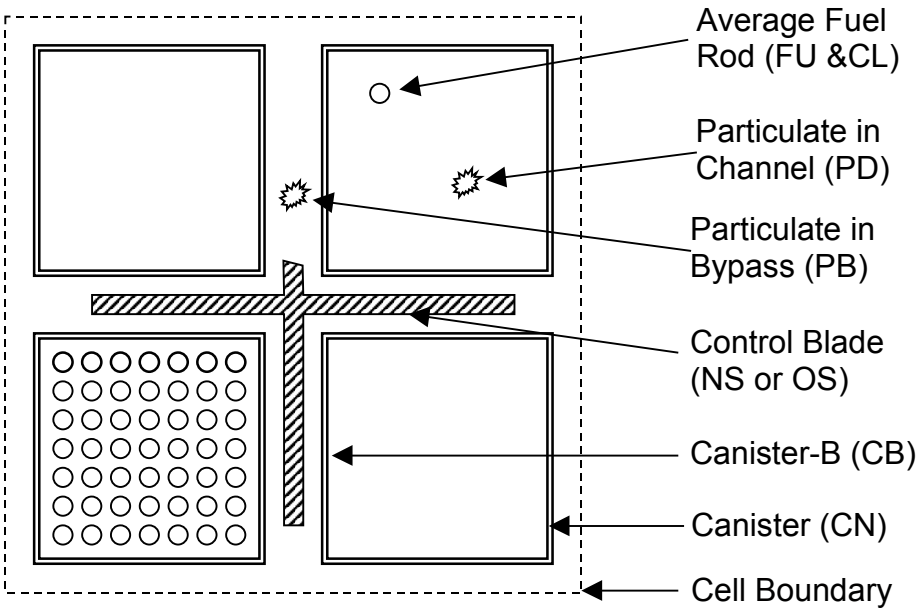

Figure 2.1 Radiative heat transfer framework -- BWR cell cross-section.

Other structures (SS and NS, *or* OS) representing core support structures and control elements are always treated as the innermost component in a cell; these components can radiate to adjacent cells only if no other component exists in the cell. The canister component not adjacent to the control blade (CN) is always treated as the outermost component in a cell; no other cell components can radiate to adjacent radial cells if the canister component CN is present. Particulate debris can exist in the channel (PD) and/or in the bypass region outside the canisters (PB).

For intra-cell radiation, the user must input two view factors that control radiation between the "average" fuel rod (cladding component, or perhaps "bare" fuel) and canister walls (used for both canister components), and between the canister wall (component CB only) and other structures (SS, and/or NS, *or* OS):

$F_{cn,cl}$ - view factor for radiation between canister (both components CN and CB) and fuel rods or particulate debris, used with the canister component inside surface areas

$F_{os,cn}$ - view factor for radiation between any other structure (SS, NS, *or* OS) and canister (component CB only), used with the structure surface area

In radiation to or from a fuel bundle or a debris bed, the view of interior surfaces will be partially obstructed by outer rods or particles. Whenever radiation is an important

mechanism for heat transfer, a temperature gradient will be established within the fuel bundle or debris bed. Therefore, the effective temperature difference for radiative exchange with another surface will be less than would be predicted from the average temperature of the bundle or bed. This effect can be important in reducing the radiation to a surrounding canister, and may be captured by assigning the view factor $F_{cn,cl}$ a value significantly less than unity. The value input for $F_{os,cn}$, on the other hand, should ordinarily be some value close to unity since the entire control blade surface is directly adjacent to the surface to which it radiates.

For radiation between any other structure (SS, NS, *or* OS) and another component within the same cell, the "other structure" surface area and the view factor $F_{os,cn}$ are used in Equation (2.4). For radiation between either of the two canister components and the cladding, the canister surface areas and the view factor $F_{cn,cl}$ are used.

As discussed in Section 1.2, particulate debris in the bypass of a BWR (PB) can exist separated from that in the channel (PD) only in the presence of intact canister component CB. Otherwise, the two are assumed to be mixed and equilibrated. In the following discussion, “PD” will therefore be used to mean all particulate debris (including any in the bypass region of a BWR) in a cell unless there is intact canister component CB in that cell.

If particulate debris is present in a cell containing fuel rods, an implicit view factor $F_{cl,pd}$ of 1.0 is used with the cladding (or bare fuel) surface area to model radiation from the rods to the debris. Otherwise, if debris is present in a cell with either canister or “other structure” (SS, NS, *or* OS) components, implicit view factors $F_{cn,pd}$ and $F_{os,pd}$ of 1.0 are used with the canister or "other structure" surface areas to model radiation between these components and the debris.

If a cell contains both components of a BWR canister (CN and CB) but no fuel rods, the view factor from the inner surface of CN to the inner surface of CB, $F_{cn,cb}$, is taken as $2^{-1/2}$ (from standard tables, assuming a square canister), used with the area of the inner surface of CN.

For inter-cell radiation the user must input two view factors that control radiation in the radial and axial directions:

- $F_{cell,r}$ - view factor for radiation radially from one cell to the next outer one, used with cell outer radial boundary area
- $F_{cell,a}$ - view factor for radiation axially from one cell to the next higher one, used with cell axial boundary area

Intra-cell radiation is calculated for the outermost (“most visible”) components. Again, because of temperature gradients, the effective temperature difference for radiative exchange will be less than would be predicted from cell-average temperatures. This effect, which is dependent on the coarseness of the nodalization, should be considered in

choosing the values input for these view factors. For radiation from any component to another cell, the appropriate cell boundary area and $F_{cell,r}$ or $F_{cell,a}$ are used in Equation (2.4), although the actual component temperatures are used. For radiation between the liquid pool or lower head and the first cell containing a component, the lower head surface area and $F_{lp,up}$ (defined below) are used in Equation (2.4).

If no components exist in the next outer or higher cell, the radial ring or axial level beyond that is used, until a boundary heat structure is reached. Thus, components in one cell can communicate to nonadjacent cells all the way across the core if there are no components in intervening cells. The boundary heat structures, both radially and axially, specified on records CORZjj02 and CORRii02, respectively, receive energy from the outermost cells that contain a component. An additional view factor controls radiation to the liquid pool, if one exists, or to the lower head:

$F_{lp,up}$ - view factor for radiation axially from lowermost uncovered COR cell to lower head or liquid pool, used with lower head surface area

2.1.3 Implementation Logic

As already noted, the radiation model employs a superposition of pairwise surface-to-surface radiation calculations. The determination of which surfaces "see" which other surfaces is not exhaustive, but is intended to assure that (1) the most important radiation exchange paths are included and (2) no surface is isolated, with each being allowed to radiate to at least one other surface. Assumptions about which terms dominate in a BWR are based largely on Figure 2.1, as qualitatively described above.

When a dominant radiation path for some surface involves an adjacent radial or axial cell, only a single "selected" surface in that cell is considered. In considering other structures, NS takes precedence over SS; OS can occur only in a calculation that does not employ SS or NS. In the radial case, surfaces in the next cell are considered in the following order: outside of CN, CL, FU, inside of CB, NS, SS, OS, and PD. If none of these exist, the next radial cell is considered. In the axial case, the order is: CL, FU, inside of CN, inside of CB, NS, SS, OS, and PD. If none of these exist, the next axial cell is considered. Note that particulate debris in the bypass (PB) does not appear in either of these lists. This is because if it exists independent of particulate in the channel (PD), CB must also be present which will define a more important radiation path (in the axial direction), or shield it from external view (in the radial direction).

View factors are used only in combination with areas, as the product $A_1F_{12} = A_2F_{21} = AF$, where the equality is required by reciprocity. In some cases, limits are imposed because direct use of the view factors and areas cited Section 2.1.2 would result in an implied reciprocal view factor greater than unity.

1. For radiation exchange between surfaces 1 and 2 that crosses a cell boundary, the product actually used is $F_{\text{cell,x}}$ MIN($A_{cell,x}$, A_1, A_2), where x may be r or a.

2. For radiation exchange involving particulate debris PD, the product actually used is F MIN(A_1, A_{PD}), where F is the view factor cited in Section 2.1.2.

The following describes the model implementation in MELCOR 1.8.5. It is based on the logic used in MELCOR 1.8.4, with the treatment of OS generalized to apply to SS and NS and the addition of PB and a more careful distinction of channel and bypass. It is clear that improvements are possible.

The logic begins by considering the outer surfaces of an intact canister in a BWR.

1a. That portion of the outer surface of intact canister CB in a core cell that does not see other outer CB surface in the same cell must radiate to "other structure" xS representing the control blade and/or to PB in the same core cell. Here x is N or O; NS and OS cannot be used in the came calculation. Similarly, some portion of the xS surface may radiate to PB. The fraction of the surface of xS and of the outer surface of CB, that sees PB is proportional to the fraction f of the available space in the bypass that is occupied by PB. AF = MIN ($f\,A_{surf}$, $A_{pb}/2$) where surf is xs or cbb.

1b. The remaining portions of these surfaces, A'_{surf} = MAX(A_{surf} - $AF_{surf,pb}$, 0) see each other with AF = MAX($A'_{xs}\,F_{os,cn}$, A'_{cbb}). This formulation, rather than simple use of a factor (1-f), accounts for that fact that porosity may result in large "holes" through the debris bed.

2. That portion of the outer surface of intact canister CN in a core cell that does not see other outer CN surface in the same cell radiates to a component in the next radial cell. AF = MIN($A_{cell,r}$, A_{cnb}, $A_{s,out}$) $F_{cell,r}$.

If fuel rods are present in a core cell in a BWR or PWR, their view factors are considered next. If intact CL is present, only its outer surface is included, with FU-to-CL radiation treated as part of the gap model. The surface of bare FU, however, can radiate to other components.

3a. Fuel rods radiate to the inner surface of canister CB in the same cell, if present ($AF = A_{cb}\,F_{cn,cl}$); otherwise they radiate to other structure (SS, NS, or OS) present in the same core cell, ($AF = A_{xs}\,F_{os,cn}$) with the same precedence as in item 1.

3b. Fuel rods radiate to PD in the same core cell (AF = MIN(A_{rod}, A_{pd}) 1), if any is present.

3c. If intact canister CN is present in the same core cell, fuel rods radiate to its inner surface ($AF = A_{cn}\ F_{cn,cl}$); otherwise they radiate to a selected component in the next radial cell (AF = MIN($A_{cell,r}$, A_{rod}, $A_{s,out}$) $F_{cell,r}$).

3d. Fuel rods also radiate to a selected component in the next axial cell, with AF = MIN($A_{cell,a}$, A_{rod}, $A_{s,up}$) $F_{cell,a}$.

If there is canister but no fuel rods in a core cell, the view factors for the inner canister surfaces are considered next.

4. If there are no fuel rods in a cell, the inner surface of canister CN radiates to the next axial level (AF = MIN($A_{cell,a}$, A_{cn}, $A_{s,up}$) $F_{cell,a}$) *unless* there is PD in the same cell. This case is covered later.

5. If there are no fuel rods in a cell, the inner surface of canister CB radiates to the inner surface of CN in the same cell, if present ($AF = A_{cb}\ \ 2^{-1/2}$); or to a selected component in the next radial cell (AF = MIN($A_{cell,r}$, A_{cb}, $A_{s,out}$) $F_{cell,r}$).

The major view factors for "other structures" in a cell are the outer surface of canister CB, or fuel rods, if either or both exist. Canister CB will block the view of fuel rods. These are covered by items 1 and 3a above. Otherwise, the dominant radiative heat transfer for "other structures" will involve some other surface.

6a. In the absence of fuel rods *and* canister CB in a cell, "other structures" radiate to the inner surface of canister CN ($AF = A_{xs}\ F_{os,cn}$) *unless* there is PD in the same cell. This case is covered later.

6b. In the absence of fuel rods *and* both canister components (CN and CB) in a cell, "other structures" partition radiation between any PD in the same cell and selected surfaces in the next axial and radial cells. The fraction going to other cells is taken to be MAX(0, 1-A_{pd}/A_{xS}), where xS represents NS, SS, or OS, with NS taking precedence over SS, as previously discussed. AF = MIN($A_{cell,y}$, A_{xs}, $A_{s,out}$) $F_{cell,y}$, where y is a or r. Radiation to PD is covered later.

Radiative heat transfer for PD is assumed to be dominated by any fuel rods in the same cell. This is covered by item 3b above. If there is no PD in the core cell, other surfaces must be considered.

7a. In the absence of fuel rods PD radiates to the inner surface of canister CB with AF = MIN(A_{cb}, A_{pd}) $F_{cn,cl}$ or, if there is no CB, to some "other structure" in the same cell with AF = MIN(A_{xs}, A_{pd}) $F_{os,cn}$. (As with intercell radiation, NS takes precedence over SS). The latter case completes items 6a and 6b.

7b. In the absence of fuel rods PD also radiates to the inner surface of canister CN (AF = MIN(A_{cn}, A_{pd}) $F_{cn,cl}$) or, if there is no CN, to a selected component in the next radial cell (AF = MIN($A_{cell,r}$, A_{pd}, $A_{s,out}$) $F_{cell,r}$). The former case completes item 4.

7c. In the absence of fuel rods PD also radiates to a selected component in the next axial cell (AF = MIN($A_{cell,a}$, A_{pd}, $A_{s,up}$) $F_{cell,a}$).

If a water pool is present, radiation is considered between its surface in each radial ring and a selected component in the first non-empty core cell in the same ring above the pool. If there is no water pool, radiation is considered between the lower head and a selected component in the first axial level in each ring. MELCOR 1.8.5 allows additional control of the emissivity and view factor to be used when this component is a supporting structure, through input on COR000PR, CORZjjPR, CORRiiPR, and/or CORijjPR records. This can aid in modeling radiation to the core support plate.

2.2 Conduction

Conduction heat transfer between components in axially adjacent cells is described in Section 2.2.1. Cell-to-cell radial conduction is treated for supporting structure (SS) representing a continuous plate, and for particulate debris (PD and/or PB) following failure of any intact canister component in the two cells. In addition, a component in the outermost ring may optionally be designated to conduct heat directly to the boundary heat structures. (This is useful in simulating some experiment geometries.) Conduction between particulate debris (PD and/or PB) and other components within the same cell is also treated, as described in Section 2.2.3. Radial conduction through the fuel pellets and across the gap to the cladding is calculated by an analytic expression, as described in Section 2.2.4. Conduction within the lower head is discussed in Section 5.

The core package does not treat convection in molten debris pools. Hence, whenever the larger of the two component temperatures used to calculate inter-component conduction exceeds an assumed "melt" temperature, TKMIN, the rate of conduction is increased to simulate convection in a molten pool. The enhancement factor for axial, radial and intra-cell conduction is given by

$$FAC = \max\left\{1.0, \left[TKFAC\left(T_{\max} - TKMIN\right)\right]^3\right\} \qquad (2.16)$$

where T_{max} is the larger of the component temperatures and $TKFAC$ and $TKMIN$ are given by sensitivity coefficients C1250 with default values of .01 K^{-1} and 3200. K, respectively. (The default values give an enhancement factor of 10 when T_{max} exceeds the melting point of UO_2 by about 300 K and are primarily intended to eliminate excessive hot spots when rapid convection/radiation, etc. would clearly preclude their existence.) The enhancement factor for conduction in the lower head uses a hard-wired value of $TKFAC$=0.01 and uses the melting temperature of the material between adjacent temperature nodes in the lower head for $TKMAX$.

2.2.1 Axial Conduction

Axial conduction is computed between like components in adjacent axial cells (e.g., cladding-to-cladding). Heat transfer is also calculated between any supporting structure modeling a plate and all components supported by it. In addition, if a given component exists in only one of the two adjacent cells (because of the specification of intact geometry or the failure of the component in one of the cells), conduction will be evaluated between the component and particulate debris in the adjacent cell if it exists and if physical contact between debris and component is predicted. Such contact is assumed if the debris resides in the overlying cell where it is presumed to rest on components in the underlying cell, or if the debris completely fills the available volume in the underlying cell so that it reaches the overlying cell. The heat transfer rate axially from one cell component to another is given by:

$$q_{ij} = K_{eff}\left(T_i - T_j\right) \tag{2.17}$$

where K_{eff} is an effective conductance between the two cells, defined in terms of the individual component conductances by:

$$K_{eff} = \frac{1}{1/K_i + 1/K_j} \tag{2.18}$$

$$K_i = \frac{k_i A_i}{\Delta x_i} \tag{2.19}$$

and where

k_i = thermal conductivity of component in cell i

A_i = axial conduction area of component in cell i

Δx_i = axial conduction distance in cell i

T_i = temperature of component in cell i

For axial conduction, the axial conduction area is taken as the average horizontal cross section of the component, including conglomerate,

$$A_i = \frac{V_{tot,comp,i}}{\Delta z_i} \tag{2.20}$$

and the conduction distance is taken as

$$\Delta x_i = \tfrac{1}{2}\Delta z_i \tag{2.21}$$

where Δz_i is the height of the core cell

Axial conduction is generally insignificant except at the liquid level interface, where it can be very important due to the very steep temperature gradients that can exist there (see Figure 2.2). An approximate analytical model has been implemented in the COR package to more closely approximate this temperature gradient than is possible for the typically coarse grids using Equation (2.17). In this model (as well as in the convection model), the cell components in the level at which the liquid interface resides are represented with two separate regions whose temperatures are tied to the bulk component temperature T_i: a hot, dry uncovered region at temperature T_h, and a cooler wet region covered by pool at temperature T_c. These temperatures are related by energy conservation (assuming constant heat capacities) to the atmosphere and pool fractions of the cell, x_a and x_p respectively:

$$T_i = x_a T_h + x_p T_c \tag{2.22}$$

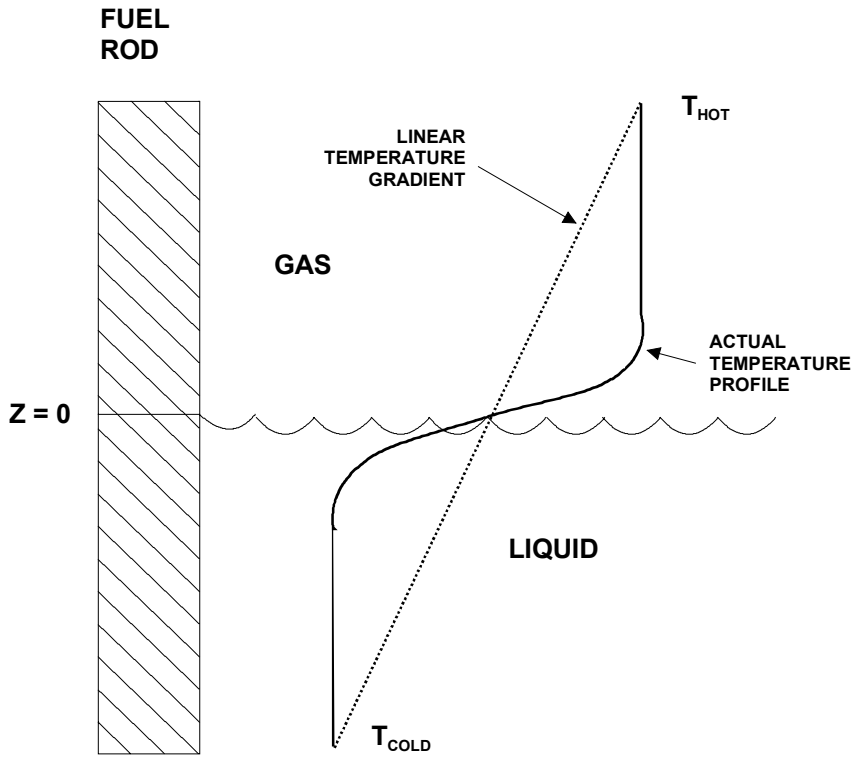

Figure 2.2 Component axial temperature gradient across liquid level.

The temperatures of the two regions are determined by individual energy equations:

$$C_p \, x_p \, (T_c - T_c^o) = C_p \, (T_h^o - T_c^o) \, \max(0, x_p - x_p^o) + [K \, (T_h - T_c) - h_p \, x_p \, A \, (T_c - T_p) + x_p \, Q] \, \Delta t \quad (2.23)$$

$$C_p \, x_a \, (T_h - T_h^o) = C_p \, (T_c^o - T_h^o) \, \max(0, x_a - x_a^o) + [K \, (T_c - T_h) - h_a \, x_a \, A \, (T_h - T_a) + x_a \, Q] \, \Delta t \quad (2.24)$$

where C_p is the total heat capacity of the component ($\sum m_i c_{pi}$), K is an effective axial conductance (discussed below), T_p and T_a are pool and atmosphere fluid temperatures, respectively, and Q is the net component heat input from other sources.

In each of these equations, the first term on the right hand side represents the averaging of a region $|x_p - x_p^o| = |x_a - x_a^o|$ that has just quenched or just uncovered with the old quenched or uncovered regions, respectively. The axial conduction term $K(T_h - T_c)$ is derived from a fin equation, as discussed below. Equations (2.22) through (2.24) can be solved simultaneously to eliminate Q and determine T_c and T_h from known values of x_a, x_p, T_a, and T_p, and new or projected values for the bulk component temperature T_i. The pool and atmosphere heat transfer rates are calculated from these temperatures and the respective fluid temperatures, pool fractions, and heat transfer coefficients.

Because of the large temperature gradient at the liquid level interface, simply using Equation (2.17) with K_{eff} given by Equation (2.18) will significantly underpredict the conduction between the hot and cold regions. Instead, application is made of the one-dimensional conduction equation for fins, given by the ordinary differential equation:

$$k \, \frac{d^2 T}{dz^2} - h \, \frac{A}{V} \, (T - T_f) + q = 0 \quad (2.25)$$

where q is the volumetric heat source, A / V is the surface area to volume ratio and the thermal conductivity k is assumed constant. Assuming the following boundary conditions:

(a) above the interface (z = 0) the fluid temperature is a constant atmosphere temperature T_a; below the interface the fluid temperature is a constant pool temperature T_p;

(b) the heat transfer coefficient is much larger for the pool than for the atmosphere ($h_p \gg h_a$);

(c) T approaches T_h for z above the interface and T_c for z below the interface, the steady state values of which are dependent on the volumetric heat source q;

the approximate solution for the temperature gradient at the liquid interface is:

$$\frac{dT}{dz}(z=0) \approx \sqrt{\frac{h_a\ A}{k\ V}}\ (T_h\ -\ T_c\ ) \tag{2.26}$$

and therefore the value of K used in Equations (2.23) and (2.24) is

$$K = K_i\ \ A_i\ \sqrt{\frac{h_a\ A}{k_i\ V}} \tag{2.27}$$

2.2.2 Radial Conduction

Conduction is calculated between elements of supporting structure (SS) modeling contiguous segments of a plate in radially adjacent core cells. Conduction is also calculated between particulate debris in radially adjacent core cells unless the path is blocked by intact canisters. It is based on equations Equations (2.17) - (2.19), with the conduction area and conduction distance for use in Equation (2.19) taken as

$$A_i = \frac{V_{tot,comp,i}}{V_{tot,cell,i}} A_{rad} \tag{2.28}$$

$$\Delta x_i = \frac{V_{tot,i}}{2\ A_{rad}} \tag{2.29}$$

where $V_{tot,cell,i}$ is the total volume of cell *i* and A_{rad} is the area of the common radial boundary between cell i and cell j. Equation (2.28) accounts for the fraction of the height of the cell that is occupied by the component. It also introduces a factor of (1 - porosity) into the conductance for particulate debris.

2.2.3 Intra-Cell Conduction

As debris accumulates in a core cell and the free volume in the cell vanishes, there will undoubtedly be intimate contact between the debris and any remaining intact core components. Therefore, conduction between the debris and core components in the same cell is calculated from Equations (2.17) - (2.19) with

$$A_i = A_j = \frac{V_{tot,PD}}{V_{tot,PD} + V_{free}} A_{intact} \tag{2.30}$$

$$\Delta x_{intact} = \frac{V_{tot,intact}}{2\,A_{intact}} \tag{2.31}$$

$$\Delta x_{PD} = \frac{V_{bed}}{2\,A_{bed}} \tag{2.32}$$

where

A_{intact} = initial component surface area for the intact component

V_{free} = additional volume available to PD

V_{bed} = total volume of debris bed (including porosity)

A_{bed} = surface area of debris bed (boundary with other components, as opposed to surface area of debris particles)

and a factor of $V_{tot,PD}/V_{bed}$ is included in the conductivity of the particulate debris.

An intact canister (specifically, component CB), will separate particulate debris in the bypass from that in the channel. Under these circumstances, intracell conduction from PD will be calculated only to fuel rods and both canister components (CN and CB). Conduction from PB will be calculated to the outer surface of CB, and to the other structures SS, NS, and OS.

2.2.4 Fuel-Cladding Gap Heat Transfer

Conduction radially across the fuel pellet and the fuel-cladding gap is calculated assuming a parabolic temperature profile across the fuel, negligible cladding thermal resistance, and a constant user-specified gap thickness (input on record COR00001). An effective total gap conductance is calculated by combining in conventional fashion the various serial and parallel resistances:

$$\frac{1}{h_{gap}} = \frac{1}{h_f} + \frac{1}{\dfrac{1}{\dfrac{1}{h_g} + \dfrac{1}{h_{CF}}} + h_{rad}} \tag{2.33}$$

where

$$h_f = 4\ k_f\ /\ r_f \tag{2.34}$$

$$h_g = k_g \ / \ \Delta r_g \tag{2.35}$$

$$h_{rad} = \frac{4 \ \sigma \ T_a^3}{\frac{1}{\varepsilon_f} + \frac{1}{\varepsilon_c} - 1} \tag{2.36}$$

and where

σ = Stefan-Boltzmann constant

r_f = radius of fuel pellet

Δr_g = thickness of fuel-cladding gap

k_f = fuel thermal conductivity

k_g = gap gas thermal conductivity

h_{CF} = conductance calculated by control function

T_f = fuel bulk temperature

T_c = cladding bulk temperature

T_a = average temperature = $(T_f + T_c) / 2$

ε_f = fuel surface emissivity (default value, 0.8)

ε_c = cladding inner surface emissivity (default value, 0.325)

The term representing the thermal resistance of the fuel pellet, $1/h_f$, is combined in series with an effective resistance of the gap. This gap resistance includes radiation across the gap in parallel with the conductive resistance of the gap gas. An additional resistance, $1/h_{CF}$, calculated via a control function and added serially to the conductive resistance of the gap gas, may be specified by the user on record COR00004. The fuel and cladding emissivities used to calculate radiation across the gap are stored in sensitivity coefficient array C1101.

The total effective gap conductance is then used to calculate the heat transfer rate from the fuel to the cladding by the equation:

$$q_{gap} = h_{gap} \ A_f \ (T_f^{\tilde{n}} - T_c^{\tilde{n}}) \tag{2.37}$$

where A_f is the surface area of fuel pellet and the superscript "$\tilde{n}$" denotes projected new-time temperature values. Because of the tight coupling between the fuel and the cladding, an implicit treatment is necessary to prevent numerical oscillations for reasonable time steps. The projected temperatures are found as solutions of the equations

$$C_f\left(T_f^{\tilde{n}} - T_f^o\right) = \left(\Delta E_{cond} + \Delta E_{conv} + \Delta E_{rad} + \Delta E_{oxid}\right)_f - q_{gap}\,\Delta t \tag{2.38}$$

$$C_c\left(T_c^{\tilde{n}} - T_c^o\right) = \left(\Delta E_{cond} + \Delta E_{conv} + \Delta E_{rad} + \Delta E_{oxid}\right)_c + q_{gap}\,\Delta t \tag{2.39}$$

where C_f and C_c are the total heat capacities of the fuel and cladding, respectively, and the ΔE terms on the right hand sides are other terms in their respective energy equations. These terms, which account for conduction, convection, radiation, and oxidation, are calculated as described in the corresponding sections of this report. The projected temperatures are used only in evaluating the gap heat transfer.

2.2.5 Consideration of Heat Capacity of Components

The heat transferred between components by conduction is evaluated from a numerically implicit form of Equation (2.17)

$$\begin{aligned} q_{12}\,\Delta t &= K_{eff}\left[\left(T_1^o - \frac{q_{12}\,\Delta t}{C_1}\right) - \left(T_2^o + \frac{q_{12}\,\Delta t}{C_2}\right)\right]\Delta t \\ &= K_{eff}\,\frac{C_1 C_2}{C_1 C_2 + (C_1 + C_2)K_{eff}\,\Delta t}\left(T_1^o - T_2^o\right)\Delta t \end{aligned} \tag{2.40}$$

Here C_i is again the total heat capacity of component i.

2.2.6 Effective Heat Capacity of Cladding

The formulation of gap heat transfer in Section 2.2.4 implicitly considers the finite heat capacities of the fuel and the cladding. Equations (2.38) (2.39) are solved for T_c in the form

$$T_c = \frac{\left(\Delta E_{cond} + \Delta E_{conv} + \Delta E_{rad} + \Delta E_{oxid}\right)_c}{C_{CL} + \dfrac{C_{FU}\,h_{gap}\,A_f\,\Delta t}{C_{FU} + h_{gap}\,A_f\,\Delta t}} + \text{other terms} \tag{2.41}$$

which may be interpreted as defining an effective heat capacity

$$C_{CL,eff} \equiv C_{CL} + \frac{C_{FU}\, h_{gap}\, A_f\, \Delta t}{C_{FU} + h_{gap}\, A_f\, \Delta t} \tag{2.42}$$

for the cladding. This effective heat capacity implicitly accounts for energy transferred to the fuel pellets through the relatively tight coupling of CL to FU. It is used in estimating the temperature change of cladding in Equation (2.40) and in several other heat transfer models.

2.2.7 Conduction to Boundary Heat Structures

Optionally, conduction from a designated component in the outermost radial ring to the radial boundary heat structures specified on input records CORZjj02 may be calculated. The heat flux is given by

$$q_{C-HS} = \frac{T_C \; - \; T_{HS}}{\mathrm{R}} \tag{2.43}$$

where T_C is the temperature of the core component and T_{HS} is the temperature of the first node of the heat structure (typically an insulator), and R is the total contact resistance, defined as

$$\mathrm{R} = R_{gap} + R_{dif} \tag{2.44}$$

where

$$R_{gap} = \Delta r_{gap} \; / k_{gap} \tag{2.45}$$

$$R_{dif} = \sqrt{\frac{\pi\, \Delta \mathrm{t}}{(\mathrm{k}\, \rho\, c_p)_{\mathrm{HS}}}} \tag{2.46}$$

In the above equations, Δr_{gap} is the thickness of a gap between the core component and the heat structure, k_{gap} is the thermal conductivity of the gap material (calculated from the Material Properties package), Δt is the COR package time step, and k, ρ, and c_p are the thermal conductivity, density, and specific heat, respectively, of the heat structure material. The thermal diffusive resistance R_{dif} is used to mitigate temperature oscillations that may arise from the numerically explicit coupling between the COR and Heat Structure packages. The user may specify on input record COR00011 which core component is used in this model, what the gap material and thickness are, and the value of the thermal diffusion constant $(\pi / \mathrm{k}\, \rho\, \mathrm{c_p})^{1/2}$ for the heat structure (since these properties are not currently accessed from the MP package).

2.3 Convection

Convective heat transfer is treated for a wide range of fluid conditions. Emphasis has been placed on calculating heat transfer to single-phase gases, since this mode is the most important for degraded core accident sequences. A simple set of standard correlations has been used for laminar and turbulent gas flow in both forced and free convection; these correlations give the Nusselt (Nu) number as a function of Reynolds (Re) and Rayleigh (Ra) numbers. Because the numerical method is only partially implicit, the dependence of heat transfer coefficients on surface and fluid temperatures can induce numerical oscillations in calculated temperatures. The calculated heat transfer coefficients for both vapor and liquid heat transfer are therefore "relaxed" by averaging each with its previously calculated value to mitigate the oscillations.

Since the COR cell nodalization is typically much finer than the Control Volume Hydrodynamics (CVH) nodalization, approximate temperature and mass fraction distributions in the control volumes interfacing with the core and lower plenum must be calculated in the COR package to properly determine the convective heat transfer rates for each COR cell. This temperature distribution is calculated in the COR package in what is termed the "dT/dz" model, which is described separately in Section 2.5.

In previous versions of MELCOR, limitations in several models made it difficult—if not impossible—to perform calculations using a fine CVH nodalization with one control volume for each core cell or small number of core cells. MELCOR 1.8.4 included improvements in the dT/dz model and incorporates a core flow blockage model (in the FL package). These make such calculations more practical, although some penalty in terms of increased CPU time requirements should still be expected. It is recommended that the new default dT/dz modeling should be used (*no* CORTIN records), and that the flow blockage model be invoked and momentum flux terms calculated in the core flow paths (see the FL Package Users' Guide). In the discussion that follows, all fluid temperatures refer to local temperatures, whether calculated by the dT/dz model or taken directly from a fine-scale CVH nodalization.

Heat transfer rates are calculated for each component by the equation:

$$q = h_{rlx} \; A_s \; (T_s - T_f) \qquad (2.47)$$

where

h_{rlx} = relaxed heat transfer coefficient

A_s = component surface area for heat transfer, accounting for the effects of conglomerate debris (see Section 3.1.5)

T_s = component surface temperature

T_f = local fluid temperature

MELCOR 1.8.4 and earlier versions used estimated new-time component temperatures in an effort to prevent numerical oscillations in the component heat transfer rates. This approach has been replaced by a semi-implicit calculation of the gap term, described in Section 2.2.4, that has been found to be more effective and reliable.

The unrelaxed heat transfer coefficient, h_{corr}, is calculated from various correlations for the Nusselt number, which will be discussed in the following subsections:

$$\mathrm{Nu} = h_{corr} \; D_h \; / \; \mathrm{k} \tag{2.48}$$

where

D_h = hydraulic diameter for each component surface, defined by the user on input record CORijj04

k = fluid thermal conductivity

Relaxed heat transfer coefficients for COR subcycle n are given by

$$h^n_{rlx,f} = f_{old,f} \; h^{n-1}_{rlx,f} + \left(1 - f_{old,f}\right) h_{corr,f} \tag{2.49}$$

where $f_{old,f}$ is the fraction of the old value to be used for fluid f (vapor or liquid), adjustable through sensitivity coefficient array C1200 with default values of 0.5 and 0.9 for vapor and liquid heat transfer, respectively.

2.3.1 Laminar Forced Convection

For laminar forced flow in intact geometry, the Nusselt number is given by a constant, representing the fully developed Nusselt number for constant heat flux, multiplied by a developing flow factor:

$$Nu = C(n) \; g_{dev} \tag{2.50}$$

where the constant C(n) is currently defined for both rod bundle arrays (n=1) and circular tubes (n=2) to be 4.36 and is implemented as sensitivity coefficient array C1212. The developing flow factor is currently that used in MARCH 2 in connection with gaseous diffusion-limited oxidation [8], with the Prandtl number used instead of the Schmidt number:

$$g_{dev} = 1 + \frac{0.00826}{F(z) + 0.0011} \tag{2.51}$$

In Equation (2.50), the constants have been implemented in sensitivity coefficient array C1213, and *F(z)* is a nondimensional entrance length:

$$F(z) = \frac{(z - z_0)}{D_h \; Re \; Pr} \tag{2.52}$$

where $(z - z_0)$ is the distance from the flow entrance, D_h is the hydraulic diameter, Re is the Reynolds number, and Pr is the Prandtl number. In the present version of the code, $(z - z_0)$ is set to 1000 m, effectively eliminating any developing flow effects.

2.3.2 Turbulent Forced Convection

For turbulent flow in channels, the Dittus-Boelter correlation [9] is used:

$$Nu = 0.023 \; Re^{0.8} \; Pr^{0.4} \tag{2.53}$$

The coefficients and exponents in Equation (2.53) are implemented in sensitivity coefficient array C1214.

Rather than defining a critical Reynolds number controlling whether laminar or turbulent correlations are used, both correlations are evaluated and the maximum of the turbulent and laminar Nusselt numbers is used to calculate the forced convection heat transfer coefficient.

2.3.3 Laminar and Turbulent Free Convection

For laminar free convection in narrow channels, the following correlation for an enclosed air space between vertical walls is used [10]:

$$Nu = 0.18 \; Ra_f^{1/4} \; (L / D_h)^{-1/9} \tag{2.54}$$

where *L* is the channel length. For turbulent free convection a similar correlation is used, differing only in the default values for the multiplicative constant and the exponent for the Rayleigh number [10]:

$$Nu = 0.065 \; Ra_f^{1/3} \; (L / D_h)^{-1/9} \tag{2.55}$$

The coefficients and exponents in Equations (2.54) and (2.55) have been implemented as sensitivity coefficient arrays C1221 and C1222, respectively.

As for forced convection, the maximum of the laminar and turbulent Nusselt numbers is used to evaluate the free convection heat transfer coefficient. The maximum of the forced and free convection heat transfer coefficients is then used in Equation (2.47) to calculate

the heat transfer rate for a given component. This treatment alleviates some numerical difficulties that may occur if ranges are defined for the various flow regimes, with discontinuities in Nusselt number at the transition points between regimes.

2.3.4 Convection from Particulate Debris

For particulate debris, correlations for isolated spherical particles are currently used in the COR package for convection to gases. (Surface areas for particulate debris are normally so high that practically any correlation will almost completely equilibrate the gas temperature with the debris temperature.) For forced convection, the following correlation is used [11]:

$$Nu = 2.0 + 0.6\ Re_f^{1/2}\ Pr_f^{1/3} \tag{2.56}$$

For free convection, the Reynolds number is replaced by the square root of the Grashof number [11]:

$$Nu = 2.0 + 0.6\ Gr_f^{1/4}\ Pr_f^{1/3} \tag{2.57}$$

The coefficients and exponents in Equations (2.56) and (2.57) have been implemented as sensitivity coefficient arrays C1231 and C1232, respectively. In both equations, the properties are evaluated at the film temperature (i.e., the average of the debris and dT/dz model fluid temperatures). The maximum of the free and forced convection Nusselt numbers is once again used to calculate the heat transfer coefficient.

2.3.5 Boiling

By default for liquid-covered components, the COR package uses the correlations from the HS package to treat boiling (see the HS Reference Manual). However, by changing the default value of sensitivity coefficient C1241(5), the simplified boiling curves from the MARCH 2.0 code [3] can be used to calculate the heat transfer coefficient:

$$h = 34.5\ P^{1/4}\ \Delta T^{1.523} \qquad (\Delta T < 23.4\,\mathrm{K}) \tag{2.58}$$

$$h = 1.41(10^7)\ P^{1/4}\ \Delta T^{-2.575} \qquad (\Delta T \geq 23.4\,\mathrm{K}) \tag{2.59}$$

where

P = pressure

ΔT = surface superheat, (T_s - T_{sat})

and the constants have been implemented as sensitivity coefficient arrays C1241 and C1242.

For the film boiling regime ($\Delta T \geq 23.4$ K), a radiation component is added to the convective heat transfer coefficient:

$$h_{rad} = \sigma \ \varepsilon \ \frac{T_s^4 - T_l^4}{T_s - T_l} \tag{2.60}$$

where ε is a hardwired constant emissivity of 0.4.

2.3.6 Heat Transfer from Horizontal Surfaces of Plates

For most core components—fuel rods, BWR canisters, control elements, and BWR Control Rod Guide Tubes—convective heat transfer takes place from a lateral (vertical) surface. If there is a water pool in the associated core cell, the component surface will be progressively and smoothly covered or uncovered as the pool surface rises or falls.

Plates, however, have horizontal bottom and top surfaces that can be covered or uncovered with a relatively small change in the pool level. Moreover, different CVH control volumes are ordinarily used to model the regions above and below the core plate, which can be associated with (at most) one of these volumes. Thus, (at least) its other horizontal surface will see fluid in a different control volume than that from which other boundary conditions for the core cell are derived.

When the SS component is used to represent a plate, an optional model exists to calculate heat transfer from its horizontal surfaces to water pools above and/or below. The model may be controlled independently for the two surfaces, and is off by default. If the model is on, the heat transfer coefficient for the top surface is ordinarily evaluated from the built-in pool boiling correlation (Section 2.3.5) and that for the bottom surface from the built in correlation for downward-facing boiling (Section 5.1). Either or both may be overridden by constant values or by values calculated as control functions. In any case, the temperature difference is based on the average temperature of the plate in the core cell and that of the pool.

For either plate surface, the total area is taken as the total cross-sectional area of the core cell. However, the surface of a water pool is not an idealized plane. One would therefore expect some contact with the bottom of the plate while the average pool surface is some finite distance below it, and less-than-complete coverage of the top until the average surface is some finite distance above it. In order to account for this, the fraction of the lower horizontal surface involved in heat transfer to a pool is linearly ramped on as the surface of the pool in the core cell below rises to the bottom surface of the plate. Similarly, the fraction covered above is ramped off as the surface of the pool in the core cell above falls to the top surface of the plate. User input is required for both the clearance below the

plate required for no contact and the pool depth over the plate required for complete coverage.

This model is activated and the necessary input supplied using COR000PC, CORZjjPC, CORRiiPC, and/or CORijjPC records, as described in the COR Package Users' Guide.

2.3.7 Debris Quenching and Dryout

Heat transfer from debris to liquid water pools may occur in two distinct modes. In the falling-debris quench mode, failure of the core support plate triggers the relocation of a large mass of hot debris from the core region to the lower plenum. In this mode it is assumed that transient heat transfer rates may be sufficient to rapidly quench the hot debris and/or generate large steam pressure excursions. Following the quench mode it is assumed that continued decay heat generation in the stationary debris bed in the lower plenum will either boil off any remaining water in the lower plenum or quickly lead to debris-bed dryout with an overlying water pool. The heat transfer from the debris bed to the overlying pool of water following debris-bed dryout is relatively modest and is calculated with an appropriate dryout heat flux correlation described below.

The falling-debris quench model is active by default. If *de*activated through user input, the debris is assumed to relocate instantaneously from the core region to an unquenched debris bed in the lower plenum. The model may be *de*activated by specifying a value of 0.0 for the quench heat transfer coefficient on input record COR00012. No other parameters on this record are then necessary. The heat transfer calculated by the model may or may not be sufficient to fully quench the debris before it reaches the bottom of the lower plenum, depending on the values chosen for the model parameters described below.

Beginning from the time of core support plate failure in each radial ring, the elevation of the leading edge of the falling debris is determined assuming a constant user-specified descent velocity (default of 5 m/s). The axial elevation of the leading edge of the falling debris is given by

$$z_d = z_{csp} - v_d \ (t - t_{fail}) \qquad (2.61)$$

where z_{csp} is the initial elevation of the core support plate, v_d is the velocity of the falling debris, t is the current time and t_{fail} is the failure time of the support plate in the particular ring. Debris from core cells above elevation z_d will be relocated downwards subject to the availability of free volume and the absence of additional supporting structures.

When the leading edge of the falling debris enters the pool of water in the lower plenum, quench heat transfer begins. The heat transfer surface area is the value calculated assuming the debris particles have an equivalent spherical diameter equal to the user-specified hydraulic diameter for particulate debris (input on record CORijj04). The user-specified quench heat transfer coefficient (input on record COR00012) is assumed to

remain constant until the leading edge of the falling debris reaches the bottom of the lower plenum (the elevation of the lower head). After that time a decay factor initially equal to unity is applied to the user-specified heat transfer coefficient.

The decay factor is intended to simulate the reduction in heat transfer that occurs during the transition from the quench period to the debris bed configuration. During this period of transition, additional hot debris from the core region may relocate to the lower plenum as a result of radial spreading between the rings in the core region. Therefore, the decay factor has a time constant equal to the time constant for radial spreading of solid debris (see Section 3.2.4). The decay factor also includes a term to arrest the decay as long as significant amounts of debris continue to migrate into the failed ring from other core regions. Soon after the bulk of the debris has relocated the decay factor will quickly decrease. When the value of the decay factor falls below 0.01, it is assumed that the transition to a stable debris bed geometry is complete, and all subsequent debris-to-pool heat transfer in that radial ring will be limited by the dryout heat flux correlation discussed below. The time-dependent heat transfer decay factor, f(t), is given by

$$f(t+\Delta t) = \min\ [\,1, f(t)\ \exp(-\Delta t\ /\ \tau_{spr}\ ) + V_{cor}\ /\ V_{LP}\,] \qquad (2.62)$$

where τ_{spr} is the time constant for radial spreading of solid debris described in Section 3.2.4, V_{cor} is the volume of debris which relocates into the ring from radial spreading in the core region during the core time step Δt and V_{LP} is the volume of debris in the ring beneath the level of the core support plate.

During the short period between the failure of the core support plate and the time at which the leading edge of the falling debris reaches the lower head, the models for candling, dissolution and radial spreading of debris in the affected ring are deactivated. This action is taken because those models implicitly assume a stationary debris configuration. In addition to the quench heat transfer coefficient, the user may specify a reactor vessel failure pressure (default value of 2.0e7 Pa). When the differential pressure between the lower plenum CVH volume and the reactor cavity CVH volume reaches the failure pressure, it is assumed that the lower head in all the core rings contained in the lower plenum CVH volume fails totally. When this happens all of the debris in the core cells above the failed lower head is ejected immediately, and further quench heat transfer in those rings is suppressed. Currently, it is suggested that users do not specify a failure pressure in excess of the critical pressure of water (22. MPa) because the CVH package may encounter problems above that pressure.

Because of the relatively low value of the default value for the failure pressure (compared to actual failure pressures that may be much higher) the quench model may have a rather limited range of usefulness for some PWR calculations. If the PWR relief valves cycle around 16-17 MPa, then there is very little margin (3-5 MPa) for steam generation between the relief pressure and the critical pressure; hence, even modest fuel-coolant interactions following support plate failure tend to cause "vessel failure."

For stationary particulate debris beds in liquid water pools, the heat transfer rate will be limited by hydrodynamic phenomena that limit the amount of liquid that can reach the debris particles. The conceptual view taken in the COR package is that liquid water will move downward from above to cool the debris, with vapor produced moving upward to restrict the flow of liquid. At some total bed heat flux, this vapor prevents any more liquid from reaching the debris. This is the point of incipient dryout.

The COR package uses the Lipinski zero-dimensional correlation [12] to calculate the dryout heat flux, q_d, which is then applied as a limiting maximum heat transfer rate from a particulate debris bed (using the cell cross-sectional area rather than the total particulate surface area) which may occupy one or more axial levels:

$$q_d = 0.756\ h_{lv} \left[\frac{\rho_v\ (\rho_l - \rho_v)\ g\ d\varepsilon^3\ (1 + \lambda_c / L)}{(1-\varepsilon)\left[1 + (\rho_v / \rho_l)^{1/4}\right]^4} \right]^{1/2} \tag{2.63}$$

In this equation, h_{lv}, ρ_l, and ρ_v are the latent heat and liquid and vapor densities of water, respectively, g is the gravitational acceleration, d is the debris particle diameter, ε is the bed porosity, L is the total bed depth, and λ_c is the liquid capillary head in the debris bed,

$$\lambda_c = \frac{6\ \sigma\ \cos\theta\ (1-\varepsilon)}{\varepsilon\ d\ (\rho_l - \rho_v)\ g} \tag{2.64}$$

where σ is the water surface tension and θ is wetting angle. The leading constant, the nominal capillary head for 0.5 mm particles in water (approximately 0.089 m), and the minimum bed porosity allowed in the correlation are accessible to the user as sensitivity coefficient array C1244. A default minimum porosity of 0.15 was selected to ensure some heat transfer occurs from molten debris pools. The actual capillary head is adjusted for particle diameter size within the model.

If one or more axial levels give heat transfer rates totaling the dryout maximum, no heat transfer is calculated for particulate debris or other intact structures below this axial level. Furthermore, in cells in which debris is undergoing quenching at the rate given by the dryout heat flux, no convective heat transfer to the pool is calculated for other components in that cell.

2.4 Oxidation

Oxidation of Zircaloy by both steam (H_2O) and oxygen (O_2), and of steel by H_2O is modeled in the COR package. Metal oxidation is calculated using standard parabolic kinetics, with appropriate rate constant expressions for Zircaloy and steel, limited by gaseous diffusion considerations if necessary. There are two options for modeling the reactions of B_4C. The simple default model developed by ORNL for the MARCON 2.1B code [2] treats only

oxidation by H_2O. It gave satisfactory results in oxidizing environments. However, in reducing environments the simple model tends to seriously underpredict the methane generation rate, which can lead to underestimation of the risk from the release of volatile methyl iodide. Hence, use of the optional advanced B_4C reaction model is recommended if reducing atmospheres (high hydrogen concentrations) are expected. It also includes the effects of O_2. The advanced model, also developed at ORNL, is used in the BWRSAR code, which is the successor to MARCON.

Irrespective of the modeling option, the B_4C reaction will not begin until the steel control blade sheaths have failed (B_4C is not exposed to steam until failure occurs). Failure is assumed to occur when the mass of intact steel in the control blade component falls below a user specified fraction (adjustable through sensitivity coefficient C1005, default value of 0.9) of its initial value. The intact steel is consumed by both steel oxidation and dissolution/melting. Following failure of the steel, the reaction is permitted to begin if steam or oxygen is available and the B_4C component temperature is above a user-adjustable threshold (sensitivity coefficient C1005, default value 1500 K). Both the simple and advanced models can be used either with or without the eutectics model described in Section 2.7. If the eutectics model is active, then any B_4C that is dissolved in the eutectic mixture is considered to be unavailable for reaction. The fraction of the initial mass of B_4C that is permitted to react can be arbitrarily limited by the user. The default maximum reaction consumption fraction of 0.02, specified by sensitivity coefficient C1005, was chosen on the basis of experimental observations [13].

Zircaloy oxidation is calculated for cladding, both canister components, and control rod guide tubes; steel oxidation is calculated for the other structure (SS and NS *or* OS) components. Both Zircaloy and steel oxidation are calculated for particulate debris. Oxidation of conglomerate debris (i.e., material that has melted and refrozen onto another existing component) is also modeled but may be selectively deactivated (on MELCOR input record CORTST01) independent of the oxidation of intact components. The oxidation model uses surface areas that account for the effects of conglomerate debris refrozen on the components; calculation of these surface areas is described in detail in Section 3.1.5. For BWR cores, oxidation of both sides of the canister walls (which may be exposed to differing environments) is modeled. A control function may be input on record CORijj07 to shut off oxidation on a cell by cell basis to simulate, for example, the effects of flow blockage. In addition, minimum and maximum oxidation cutoff temperatures have been implemented as sensitivity coefficient array C1004, with default values of 1100 K and 9900 K, respectively.

The effects of steam (or oxygen) starvation and flow blockage are simulated by explicitly considering the direction of flow within the CVH control volumes representing the core fluids (as determined by the dT/dz model setup described in Section 2.5) and by evaluating the unblocked flow area along the portion of the radial rings located within these CVH volumes. The allocation of steam and oxygen to the rings is based on the fraction of the total unblocked flow area of the CVH volume represented by each ring. Furthermore,

oxidizers in each ring are partitioned among the surfaces of each COR cell (see Section 2.4.4) to remove any dependence of oxidation results on the order of surface processing. The partial pressures of steam and oxygen and the amounts available in the control volume interfaced to a COR cell are appropriately decreased and, for the case of steam, the hydrogen partial pressure and mass are increased. (These local gas concentrations are also used in the convection model to obtain local properties for the heat transfer correlations.)

2.4.1 Zircaloy and Steel

The reaction equations for Zircaloy are given by:

$$\mathrm{Zr} + 2\,H_2\mathrm{O} \rightarrow ZrO_2 + 2\,H_2 + Q_{ox} \tag{2.65}$$

$$\mathrm{Zr} + O_2 \rightarrow ZrO_2 + Q_{ox} \tag{2.66}$$

For the purposes of oxidation, steel is divided into the constituent elements iron (Fe), chromium (Cr), nickel (Ni), and carbon (C) according to the mass fractions specified by the user (optionally) in Material Properties package input (converting to moles using the atomic weights for each element). The reaction with steam equations for these species are given by:

$$\mathrm{Fe} + H_2O \rightarrow \mathrm{Fe\,O} + H_2 + Q_{ox} \tag{2.67}$$

$$2\,\mathrm{Cr} + 3\,H_2O \rightarrow Cr_2O_3 + 3\,H_2 + Q_{ox} \tag{2.68}$$

$$\mathrm{Ni} + H_2O \rightarrow \mathrm{Ni\,O} + H_2 + Q_{ox} \tag{2.69}$$

$$\mathrm{C} + H_2O \rightarrow \mathrm{CO} + H_2 + Q_{ox} \tag{2.70}$$

The reaction of steel with O_2 is not calculated currently in the COR package. The reaction energies from Equations (2.65) - (2.70) are calculated from the enthalpies of the reactants and products. Since the equations of state used for the core materials currently do not have reference points consistent with each other or with the CVH and NCG equations of state for fluid materials, the following treatment must be used to obtain the reaction energies for arbitrary temperature T:

$$Q_{ox}(\mathrm{T}) = Q_{ox}(T_0) + H_{rp}(\mathrm{T}) - H_{rp}(T_0) \tag{2.71}$$

$$H_{rp}(\mathrm{T}) = H_r(\mathrm{T}) - H_p(\mathrm{T}) \tag{2.72}$$

where

Q_{ox} = reaction energy generated

H_r = enthalpy of reactants

H_p = enthalpy of products

T_0 = reference temperature

The reference temperature used is 298.15 K and the reaction energies at this temperature are set to *nominal* values of 5.797(10^6) J/kg_{Zr} for the Zircaloy-H_2O reaction, 1.2065(10^7) J/kg_{Zr} for the Zircaloy-O_2 reaction, -2.495(10^5) J/kg_{Fe} for the iron-H_2O reaction and 2.442(10^6) J/kg_{Cr} for the chromium-H_2O reaction. The reaction energy for steel is determined by mass weighting the reaction energies for Fe and Cr by the relative masses of the two components in the steel composition (nickel, carbon and other components in the steel are currently ignored irrespective of their relative mass). All actual reaction energies during a transient are evaluated at the control volume temperature using Equations (2.71) and (2.72) and, for Zircaloy and steel oxidation, deposited in the component being oxidized.

Solid-state diffusion of oxygen through an oxide layer to unoxidized metal is represented by the parabolic rate equation:

$$\frac{d(W^2)}{dt} = K(T) \tag{2.73}$$

where W is the mass of metal oxidized per unit surface area and $K(T)$ is a rate constant expressed as an exponential function of surface temperature T. Equation (2.73) is integrated analytically over a time step Δt assuming a constant temperature [hence constant $K(T)$] for the component:

$$(W^{n+1})^2 = (W^n)^2 + K(T^n)\ \Delta t \tag{2.74}$$

For the Zircaloy-H_2O reaction, the rate constant is evaluated using the Urbanic-Heidrich constants [14], which are implemented (along with the transition temperatures of 1853 K and 1873 K) in sensitivity coefficient array C1001:

$$K(T) = 29.6\ \exp\left(\frac{-16820.0}{T}\right) \quad \text{for } T < 1853.0 \tag{2.75}$$

$$K(T) = 87.9\ \exp\left(\frac{-16610.0}{T}\right) \quad \text{for } T \geq 1873.0 \tag{2.76}$$

Linear interpolation is used between 1853.0K and 1873.0 K.

For the Zircaloy-O_2 reaction, the rate constant is evaluated using constants from Reference [15], which are also implemented in sensitivity coefficient array C1001:

$$K(T) = 50.4 \exp\left(\frac{-14630.0}{T}\right) \tag{2.77}$$

For the steel-H_2O reaction, the rate constant is evaluated using constants from White [16], which are implemented as sensitivity coefficient array C1002:

$$K(T) = 2.42 \cdot 10^{9} \exp\left(\frac{-42400.0}{T}\right) \tag{2.78}$$

For very low oxidant concentrations, gaseous diffusion may limit the reaction rate. A mass transfer coefficient is calculated via a heat-mass transfer analogy from the heat transfer correlations in Section 2.3 by substituting the Schmidt number for the Prandtl number and the Sherwood number for the Nusselt number. The oxidation rate when limited by gaseous diffusion is given by:

$$\frac{dW}{dt} = \frac{MW \; k_c \; P_{ox}}{n \; R \; T_f} \tag{2.79}$$

where

MW = molecular weight of metal being oxidized

k_c = mass transfer coefficient

P_{ox} = partial pressure of oxidant (H_2O or O_2)

n = number of moles of oxidant (H_2O or O_2) consumed per mole of metal

R = universal gas constant

T_f = gas film temperature, $(T + T_{gas}) / 2$

The gaseous diffusion oxidation rate is used if it is less than the rate calculated by Equation (2.74). Although the molecular weight MW and the number of moles n of H_2O consumed are defined by the reaction, the quantity (MW/nR) has been implemented for reactions with H_2O as sensitivity coefficient array C1003 to allow the user a measure of separate control over the gaseous diffusion oxidation rate. That sensitivity coefficient is multiplied by two internally in the code to obtain an equivalent value for gaseous diffusion of oxygen ($n_{H2O} = 2n_{O2}$).

For the oxidation of Zircaloy in environments containing both H_2O and O_2, the maximum oxidation rate calculated for the two gases is used:

$$\frac{dW}{dt} = \max\left[\left(\frac{dW}{dt}\right)_{H_2O}, \left(\frac{dW}{dt}\right)_{O_2}\right] \tag{2.80}$$

There are two options for partitioning the oxidant consumption between the oxygen and steam. The default option is recommended and does not permit the consumption of steam until all of the available oxygen has been consumed. This option is equivalent to assuming that all hydrogen produced by steam oxidation is instantaneously converted back to steam by combustion with the available oxygen. The default option should prevent time step reductions associated with the normal combustion of in-vessel hydrogen by the BUR package. For the second option the reactions given by Equations (2.65) and (2.66) are proportioned by the relative rates:

$$f_{H_2O} = \frac{\left(\frac{dW}{dt}\right)_{H_2O}}{\left(\frac{dW}{dt}\right)_{H_2O} + \left(\frac{dW}{dt}\right)_{O_2}} \tag{2.81}$$

$$f_{O_2} = 1 - f_{H_2O} \tag{2.82}$$

2.4.2 Simple Boron Carbide Reaction Model

In the simple default B_4C reaction model, the B_4C in BWR control blades is reacted with steam using the model from MARCON 2.1B [2]. This model uses three reaction equations:

$$B_4C + 7H_2O \rightarrow 2B_2O_3 + CO + 7H_2 + Q_1 \tag{2.83}$$

$$B_4C + 8H_2O \rightarrow 2B_2O_3 + CO_2 + 8H_2 + Q_2 \tag{2.84}$$

$$B_4C + 6H_2O \rightarrow 2B_2O_3 + CH_4 + 4H_2 + Q_3 \tag{2.85}$$

Chemical equilibrium of reaction products is assumed, and the model uses the steam and hydrogen partial pressures and B_4C temperature to determine the relative extent of each reaction. The equilibrium CO/CO_2 and CO/CH_4 mole ratios $y_{CO/CO2}$ and $y_{CO/CH4}$, respectively, are given by the expressions:

$$y_{CO/CO_2} = \frac{P_{H_2}}{P_{H_2O}} \exp\left[\frac{-3605.0}{T} + 3.427\right] \quad (2.86)$$

$$y_{CO/CH_4} = \frac{P_{H_2O}}{(P_{H_2})^3} \exp\left[\frac{-27350.0}{T} + 30.50\right] \quad (2.87)$$

where the steam and hydrogen partial pressures are in atmospheres. The extents of reactions (2.83) - (2.85), expressed as relative percentages of *CO*, CO_2, and CH_4 produced (x_{CO}, x_{CO2}, and x_{CH4}, respectively), can then be given in terms of the CO/CO_2 and CO/CH_4 mole ratios as:

$$x_{CO} = \frac{1}{1 + 1/y_{CO/CO_2} + 1/y_{CO/CH_4}} \quad (2.88)$$

$$x_{CO_2} = x_{CO} / y_{CO/CO_2} \quad (2.89)$$

$$x_{CH_4} = 1 - x_{CO} - x_{CO_2} \quad (2.90)$$

The reaction energies (in J/kg-mole B_4C reacted) for reaction Equations (2.83) - (2.85) are given by the equations:

$$Q_1 = 8.238(10^8) - 58380.0\ T \quad (2.91)$$

$$Q_2 = 8.674(10^8) - 67060.0\ T \quad (2.92)$$

$$Q_3 = 1.056(10^8) - 61430.0\ T \quad (2.93)$$

The gaseous reaction products are transferred to the CVH package, while the B_2O_3 generated is transferred to the Radionuclide (RN) package as an aerosol. All the energy generated by the B_4C reaction is added to the CVH package. The reaction energies calculated by Equations (2.91) - (2.93) above are inconsistent with reaction energies that would be calculated using the present equations of state for the noncondensible gases and the B_4C and B_2O_3 (i.e., the temperature dependence implied by those equations is not consistent with the actual temperature dependence of the equations of state used). This discrepancy is ignored at present, due to the lack of reliable enthalpy data for B_4C and B_2O_3.

The B_4C oxidation rate is given as a fractional change per second in the initial (intact) B_4C mass by:

$$\frac{d\left(M_{B_4C}/M^{o}_{B_4C}\right)}{dt} = \frac{9.973(10^{6})}{60.}\ \exp\left(\frac{-22647.2}{T}\right) \qquad (2.94)$$

The constants in Eq. (2.94) are programmed as sensitivity coefficients C1006. Given the amount of B_4C reacted, the amounts of the various products are calculated from Equations (2.83) - (2.90) above.

2.4.3 Advanced Boron Carbide Reaction Model

In the optional advanced B_4C reaction model the B_4C in BWR control blades is reacted with vapors in the surrounding atmosphere using the model from BWRSAR and SCDAP [17]. This model determines the equilibrium composition in each control volume that is achieved when the Gibbs free energy of the system is minimized. The difference between the initial composition in the control volume and the equilibrium composition determines the rate of consumption of the reactants. The algorithm that is used to determine the composition that minimizes the free energy is based on the Swedish SOLGASMIX computer code [18]. In this method, the quantity

$$\frac{G}{RT} = \sum_i n_i \left[\left(\frac{g^o}{RT} \right)_i + \ln(a_i) \right] \qquad (2.95)$$

is minimized with respect to the variables n_i for constant temperature and pressure values, where G denotes the total free energy of the system, R the gas constant, T the thermodynamic temperature, n_i the number of moles of the i^{th} species, g^o the standard chemical potential, and a the activity. The values for n_i corresponding to the equilibrium mixture must be non-negative and the mass balance constraints must be satisfied. Lagrange's method of undetermined multipliers is used for determining the constrained minimum, and the logarithmic equations thus obtained are expanded in a Taylor series about initially estimated n_i-values, neglecting terms involving derivatives of second and higher orders. The linear equations represent approximations of the exact expressions, so a series of iterations is performed to obtain the final solution.

The advanced B_4C reaction model assumes that chemical equilibrium is achieved between the reactants during each time step. The mass of reactants considered during each time step is linearly dependent on the size of the time step, so that as the time step size goes to zero, the rate of reaction goes to zero. The mass of B_4C available for reaction during each time step is determined by Eq. (2.94), as in the simple model. The availability of all other reactants is limited by the rate of steam diffusion to the reaction surface during the given time step. For example, if only 5% of the steam in the control volume can diffuse to the surface during the time step, then only 5% of all the other reactants in the control volume (except B_4C) is considered to be available for equilibration with the steam (5% of control volume total) and B_4C (given by Eq. (2.94)). The model considers the following 18

species that contain one or more of the five elements: argon, oxygen, hydrogen, boron and carbon (argon occurs only in elemental form and is included for simulation of fuel damage experiments that employ this inert gas):

H_2 (g)	CO_2 (g)	B (s)	$H_3B_3O_6$ (g)
H_2O (g)	CH_4 (g)	B_4C (s)	HBO_2 (g)
C (s)	O (g)	B_2O_3 (ℓ,s)	BH_3 (g)
CO (g)	O_2 (g)	B_2O_3 (g)	B_2H_6 (g)
	Ar (g)		BOH (g)

The quantity g°/RT is determined from the thermodynamic relationship $g = h - Ts$. The enthalpy h and entropy s are calculated as integrals of the specific heat capacity,

$$h = \int_{298}^{T} c_p \, dT' + h^o_{298}$$

$$s = \int_{298}^{T} \frac{c_p}{T'} \, dT' + s^o_{298} \qquad (2.96)$$

and the specific heat capacity for each species above is expressed as a function of temperature over various temperature ranges,

$$c_p = a + b\,T + c\,T^2 + d/\,T^2 + e/\,T^3 \qquad (2.97)$$

Deviations from ideality are not modeled, so that the activities of all gaseous species are equal to their respective mole fractions in the gas mixture. The condensed species are treated as a mechanical mixture only; their activities are set to unity and they have no effect on the minimization of the Gibbs free energy in Eq. (2.95).

Because a thermochemical reference is used, the heat of reaction is simply the difference between the total enthalpy of the products and that of the reactants.

The reaction products are passed to either the CVH or RN package for tracking and subsequent use as input to the chemical equilibrium routine. Steam, oxygen, hydrogen, carbon monoxide, carbon dioxide, methane and argon are tracked by the CVH package, while elemental boron and carbon and all the boron compounds are tracked by the RN package.

2.4.4 Steam/Oxygen Allocation

As mentioned earlier, steam (and oxygen) from the core region CVH volumes is supplied to the COR Package component surfaces for oxidation purposes in a manner that takes

into account the effects of both steam (and oxygen) starvation and flow blockage. To account for the effect of flow blockage within each core CVH volume, the minimum unblocked flow area for each of the rings interfaced to the volume is evaluated and then summed across all constituent rings. The CVH volume steam allocated to each constituent ring is the fraction of total unblocked flow area of the CVH volume represented by the ring. The calculation of unblocked flow areas may be bypassed if desired by the user (input record CORVOL). The mass of steam within each ring is decremented as oxidation consumes the steam and no sharing of steam among the constituent rings is permitted during a COR subcycle. Thus the situation may arise such that the components of some rings may completely consume the ring inventory of steam while other rings may remain steam rich.

To account for the effect of steam starvation on a ring by ring basis, the processing of oxidation effects is conducted for each radial ring of the CVH volume in the direction of flow. The direction of flow is determined from CVH results or may be set via evaluation of a user prescribed control function (see input record CORRii04). Therefore, if the flow direction is upward, the progression of oxidation processing in the axial direction is from bottom to top. For the up-flow condition, the entire ring inventory of steam is initially allocated to the surfaces of the lowermost axial cell in the ring adjacent to the CVH volume, the inventory adjusted to account for oxidation, and the remaining steam is supplied to the components in the overlying cell in the ring. This axial marching is repeated until the uppermost axial segment of the ring within the CVH volume has been processed. All rings associated with the CVH volume are processed in this manner for each COR subcycle.

A second level of oxidant partitioning is performed at the cell level (axial segment-IA, ring-IR) within the CVH volume during the axial marching process. The object is to make results independent of the order in which the various oxidation reactions are evaluated. A fraction of the total available oxidant (steam or oxygen) available in this level of this ring is allocated to each possible oxidation reaction on each surface in proportion to the area available for that reaction. The reactions may include oxidation of zirconium, steel, and/or B_4C (Sections 2.4.1, 2.4.2, and 2.4.3). The portion of each intact component surface that is not blocked by candled materials (conglomerate debris) and the surface of the conglomerate debris on that component are each considered separately.

Because oxidation is calculated using rate equations subject to availability of steam, it is possible that all of the oxidant allocated to some surfaces may be consumed while only some of the oxidant allocated to other surfaces is consumed. In this situation, the oxidant that was not consumed is reallocated (using the same algorithm) among the starved surfaces, and the oxidation calculations for these surfaces repeated. This process is repeated (a maximum of 10 times) until either

(1) the ring oxidant inventory is exhausted, or

(2) for each surface, either the metal content of each surface is consumed or the limit established by rate considerations is reached.

If the ring oxidant inventory is not exhausted, the calculation proceeds to the next cell in the direction of flow.

Because COR package calculations may result in total blockage (and thus steam/oxygen deprivation) of rings, the effect upon oxidation results and upon accident progression may be significant. Due to this dependence, sensitivity coefficient C1007 has been defined to provide a lower limit on the unblocked area fractions to be used in the partitioning of CVH volume oxidant inventories among the associated rings.

If the calculated unblocked area fraction for a ring falls below the corresponding limit specified for that ring by sensitivity coefficient 1007, then the fraction of CVH volume oxidant inventory allocated to the ring is held at the limit and the remainder of the oxidant is divided among the remaining unblocked rings. If all rings are blocked, then the oxidant is divided among the rings according to the limits prescribed by sensitivity coefficient C1007 and any remaining oxidant is unavailable for oxidation. A check is made during input processing to ensure that the sum of the ring fractions prescribed by sensitivity coefficient C1007 does not exceed unity.

2.5 Control Volume Temperature Distribution (dT/dz) Model

To accurately model the heat transfer to the gas from multiple COR cells interfaced to a single control volume, an estimate of the temperature distribution in the control volume atmosphere must be made in the COR package. Approximate local fluid temperatures are calculated for cells above the uppermost liquid level in the core; the remaining cells use control volume pool and atmosphere temperatures.

The "dT/dz" model used for this approximation assumes steady gas flow through the channel or bypass with known or specified inlet gas temperature and no cross-flow between core rings within any single CVH control volume. The model uses time-smoothed ("relaxed") CVH steam and/or oxygen outflow at the top of the core to determine whether the flow direction is upwards or downwards during each COR package subcycle. The flow relaxation time constant is adjustable through sensitivity coefficient C1030(2), which has a default value of 10. s. (The user can prohibit the consideration of downward flow, in imitation of earlier versions of MELCOR, by changing the default value of sensitivity coefficient C1030(1), but this will degrade the calculation.) Because fluid temperatures are defined in the CVH package only as volume-averaged quantities, and are not defined at particular flow path locations, various methods have been implemented to obtain a suitable inlet temperature for a control volume.

The default treatment is to take the inlet temperature as the temperature of the atmosphere flow actually entering the control volume, as calculated by CVH. If the CVH nodalization permits more than one such flow, a heat-capacity-weighted average temperature of the actual inflows is used. If water is boiling in the CVH control volume, the steam generation is treated as an “inflow” at the saturation temperature.

The default treatment will include the effects of cross flows between control volumes representing different radial portions of the core when a detailed CVH nodalization is used. It also minimizes the discrepancies between the calculated dT/dz temperatures and the CVH temperatures. (Note that donor differencing is used in the hydrodynamic equations, so that fluid is advected out of a control volume with enthalpy corresponding to the CVH temperature. For a core volume, this temperature should therefore correspond to the exit temperature for the portion of the core contained in that volume.) Because CVH and COR equations are not solved simultaneously, imperfections in the coupling may result in apparent discontinuities in the profile of dT/dz temperatures between core cells in different CVH volumes. We have found the consequences to be relatively minor, particularly in comparison to the consequences of major discrepancies between dT/dz and CVH temperatures, which will cause termination of an execution if a temperature becomes nonphysical.

MELCOR 1.8.3 and earlier versions required the user to specify the definition of inlet temperature. This model has been extended slightly to allow consideration of downflow, and is still available (input of IDTDZ=1 on input record COR00006 is required), but its use is now strongly discouraged. (Consideration of downflow may also be disabled, allowing return to the 1.8.3 model, using sensitivity coefficient array C1030(1).) In this older model, the inlet temperature to the control volume atmosphere is taken as the saturation temperature if a pool is present and flow is upwards. Otherwise, there are several options available to the user (via the CORTINxx input record) to control how the inlet temperature to a control volume is determined:

1. As a first option, the user may specify that the inlet temperature for any control volume be taken as the exit temperature from the control volume directly upstream of it, in the direction of assumed axial flow, as calculated with the dT/dz model described below. This option is the default except for the bottommost and topmost control volumes in the reactor vessel that contain core cells, for which it is not applicable.

2. Alternatively, the user may specify that the inlet temperature for a control volume be taken as the CVH atmosphere temperature of some other control volume (or itself), as defined by the user. This option could be used for the lower head volume, for example, where the downcomer atmosphere temperature might be appropriate.

3. As a third alternative, the user may specify that the value of a control function be used as the inlet temperature for a control volume. This option allows the user great flexibility in defining the inlet temperature, and may be appropriate for complex flows or geometries, such as flows from more than one control volume entering the channel or bypass.

4. The model may also be disabled or the current default treatment selected, for specified volumes.

Once the inlet temperature for a control volume is determined, the temperature at each successive COR cell axial location, moving through the core or lower plenum in the direction of flow, is obtained by performing a simple energy and mass balance. The basic energy balance relates the change in energy in a cell, ΔE_{stored}, during a time step to the enthalpy flow through the cell, H_{flow}, and any energy sources, q:

$$\Delta E_{stored} + H_{flow} \ \Delta t = q \ \Delta t \tag{2.98}$$

The terms in Equation (2.98) are expressed in terms of masses, mass flow rates, and temperatures at the entrance and exit to the cell (note the canceling quantities):

$$\Delta E_{stored} = m^n \ h^n - m^o \ h^o = m^o \ c_p \ (T^n - T^o) + (\dot{m}_{in} - \dot{m}_{out}) \ h^n \ \Delta t \tag{2.99}$$

$$H_{flow} = \dot{m}_{out} \ h^n - \dot{m}_{in} \ h^n_{in} = \dot{m}_{in} \ c_p \ (T^n - T^n_{in}) - (\dot{m}_{in} - \dot{m}_{out}) \ h^n \tag{2.100}$$

$$q = (h^* A)_e \ (T_{s,e} - T^n_{out}) + q_{sou} \tag{2.101}$$

where

Δt =time step

m =fluid mass in cell

$\dot{m}$ =mass flow rate

C_p =gas specific heat

h =enthalpy

T =cell temperature

$(h^*A)_e$ =effective average heat transfer coefficient times surface area for the various cell components in contact with the current CVH control volume

$T_{s,e}$ =effective surface temperature for cell components

q_{sou} =source heat rate, from fission product decay heat and B_4C reaction energy deposited in the atmosphere and from heat transfer from heat structures

and superscripts "*n*" and "*o*" represent new and old time values, respectively.

The model solves for the value of T^n, which is then used as T^n_{in} for the next higher cell. Control volume average values for mass and mass flow rates are currently used at the inlet

to the control volume, and are updated for the effects of oxidation for each cell. For multiple core rings within the same control volume, the inlet mass flow rate is multiplied by the fraction of the total flow area for each ring, thus partitioning the flow across all rings.

For the dT/dz model to function correctly and model the phenomena appropriately, it is important that the heat structures representing the radial core boundary (e.g., core shroud) communicate with the fluid temperatures calculated by this model. The outer ring core cells must be specified as the fluid temperature boundary on input records HSCCCCC004 (see the HS Package Users' Guide) unless the IHSDT option switch provided on input record COR00006 has been set to 1.

The heat transfer rates obtained by using the dT/dz temperatures in conjunction with the core component surface areas and temperatures in all the core cells associated with each CVH control volume within the core are summed and compared to the value which would be obtained if the CVH vapor temperature in that volume had been used instead of the dT/dz temperatures. If the heat transfer rates thus obtained are of opposite sign, then it is assumed that the dT/dz model is malfunctioning (probably because prevailing conditions are outside the scope of its intended application) and the dT/dz temperatures are overwritten by relaxing their beginning-of-step values with the value of the CVH vapor temperature in the corresponding CVH volume. Hence, if the model is malfunctioning, then relaxed CVH vapor temperatures are used instead, and the relaxation time constant for the CVH temperatures is adjustable through sensitivity coefficient C1030(3). Also, if the dT/dz model is deactivated by user input, then relaxed CVH temperatures are always used in place of results from the deactivated model.

2.6 Power Generation

2.6.1 Fission Power Generation

For ATWS accident sequences (or for fission-powered experiments), fission power will be generated in addition to the decay heat. The COR package contains a simple model that calculates the fission power as a function of downcomer liquid level using the Chexal-Layman correlation [19]:

$$q_f = 0.037 \left(C_u H_r\right)^{0.7} \left(P / P_r\right)^{0.3} \left(H / H_r\right)^{0.7} \tag{2.102}$$

where H is defined in terms of the downcomer liquid level L relative to the top of active fuel and the distance L_f below the top of active fuel where fission power drops to zero:

$$\mathrm{H} = \max\left[0.0, \left(\mathrm{L} + L_f\right)\right] \tag{2.103}$$

$$L_f = 2.4384 \left(P / P_r\right)^{0.45} \tag{2.104}$$

and

q_f =fraction of full operating power, which is defined by the Decay Heat package on input record DCHFPOW

C_u =dimensional constant = 3.28084 m^{-1}

H_r =arbitrary reference height, selected as 1 m

P =system pressure

P_r =reference pressure, with default value 7.65318 MPa

L =height of downcomer water relative to the top of active fuel

The Chexal-Layman correlation is based largely on work presented in Reference 17, in which steady state power levels were calculated using coupled, 3-D neutronic and thermal-hydraulic models of the reactor power and fluid flow. The correlation assumes that the core inlet enthalpy is always at saturation. The constants in this correlation are implemented in sensitivity coefficient array C1301.

The downcomer liquid level must be calculated by a control function specified on record COR00004. Alternatively, this control function may directly calculate the fission power and the Chexal-Layman correlation is not used, as discussed in the input description for record COR00004.

The energy generated in the fission power model (as well as the decay heat if the RN Package is inactive) is distributed over the core cells using the radial and axial relative power densities input on records CORZjj03 and CORRii03. The user has the option (as described in the input description for record COR00004) for the fission energy to be deposited in the intact fuel components of all core cells (not lower plenum cells), or only in the intact fuel component of cells that are fully or partially liquid covered. For the latter case, the radial and axial relative power densities for these cells are renormalized to achieve this distribution.

Further, because this energy is not all deposited at the point of the fission (some of it is carried by energetic particles and radiation, e.g., gamma rays), the user has the option to specify the distribution of the total fission power in a core cell over the components and materials within that cell using sensitivity coefficients arrays C1311 and C1312. (Direct transport of fission power to adjacent core cells is not modeled.) These coefficients specify relative absorbing efficiencies for the core materials and core components for a fraction, f_{esc}, of the fission power that is specified to "escape" the fuel. A single absorption efficiency is used for steel and steel oxide, and a single coefficient for Zircaloy, ZrO_2, and Inconel in grid spacers. The default values of these coefficients were modified in MELCOR

1.8.4 to model generation of fission power in components other than intact fuel to simulate gamma and neutron heating in non-fuel components. Thus,

$$P_{i,j,k} = P_T F_{cell} \left[(1 - f_{esc}) \frac{M_{i,j,k,UO_2}}{\sum_{k'} M_{i,j,k',UO_2}} + f_{esc} F_{i,j,k} \right] \tag{2.105}$$

is the fission power deposited in component *k* in cell *i,j* (radial ring *i*, axial level *j*), where

$$F_{cell} = \frac{f_i f_j \sum_k M_{i,j,k,UO_2}}{\sum_{i'} \sum_{j'} f_{i'} f_{j'} \sum_k M_{i',j',k,UO_2}} \tag{2.106}$$

is the fraction of the total fission power, P_T , born in cell *i,j*. Note that it is assumed that the fraction of that power born in component k is proportional to the UO_2 mass in component *k*, and the term involving

$$F_{i,j,k} = \frac{\sum_m f_m M_{i,j,k,m}}{\sum_{k'} \sum_m f_m M_{i,j,k',m}} \tag{2.107}$$

represents the absorption by materials in that component of fission power not initially deposited in UO_2. For these equations,

f_i =radial relative power density (input record CORRii03)

f_j =axial relative power density (input record CORZjj03)

$M_{i,j,k,m}$ =mass of material m in component k in cell i,j

f_m =relative material absorbing efficiency for escaping fission energy (sensitivity coefficient array C1311)

f_{esc} =fraction of fission energy escaping UO_2 (1 - C1312(1) from sensitivity coefficient array C1312)

The sum on k´ in Equation (2.107) extends only over active components, as specified by the remainder of sensitivity coefficient array C1312. The sum over cells in Equation (2.106) extends only over the core region, that is, only over axial levels j>NTLP, where NTLP is the value input on record COR00000, and it is to be understood that $P_{i,j,k}$ is non-zero only for active components (as specified by sensitivity coefficient array C1312) in the core region. Therefore, no fission power will be associated with components in the lower plenum. Note that the sum of $F_{i,j,k,m}$ over all materials and components is unity, as is the

sum over components of UO_2 mass fractions, so that the sum of $P_{i,j,k}$ over all components is simply $P_T F_{cell}$, the total fission power generated in that cell.

2.6.2 Decay Power Distribution

A model for distribution of decay power was added to MELCOR 1.8.4 to account for distribution of gamma ray energy from fission product decay to components other than intact fuel. This model resembles the fission power distribution model described in the preceding subsection with two important exceptions: the calculation of average specific power (W/kg-UO_2) in the cell differs, and decay power is distributed among components within cells throughout the entire lower plenum and core region. In addition, separate sensitivity coefficient arrays, analogous to C1311 and C1312, are used in the calculation. Implementation of the model, including determination of default values of the model parameters for BWRs and PWRs, is described in detail in Reference 16.

Decay heat generated in the core is produced by unreleased fission products, which are assumed to remain with the UO_2 material when it is relocated from intact fuel pellets to other components. As with the model for fission power, a fraction of the decay power is assumed to remain with the component containing the fission products, with the remainder absorbed by various materials in that and other components in the same cell. The net decay power deposited in component *k* in cell *i,j* is calculated as

$$DH_{i,j,k,net} = \left(1 - f'_{esc}\right) DH^0_{i,j,k} + f'_{esc} \; DH^0_{i,j} \; F'_{i,j,k} \tag{2.108}$$

where $DH^0_{i,j,k}$ is the decay heat born of fission products associated with component *k* in cell *i,j*

$$DH^0_{i,j} \equiv \sum_{\mathrm{k}} DH^0_{i,j,k} \tag{2.109}$$

and

$$F'_{i,j,k,m} = \frac{\sum_m f'_m M_{i,j,k,m}}{\sum_{k'} \sum_m f'_m M_{i,j,k',m}} \tag{2.110}$$

represents the absorption by materials in component *k* of decay power escaping the UO_2 in which it was born. Here

$M_{i,j,k,m}$ = mass of material m in component *k* in cell *ij*

as in Section 2.6.1,

f'_m = relative material absorbing efficiency for escaping decay gammas (sensitivity coefficient array C1321)

f'_{esc} = fraction of decay energy escaping UO_2 (1 - C1322(1) from sensitivity coefficient array C1322)

and the sum on k' extends only over active components as specified by the remainder of sensitivity coefficient array C1322.

When the RN package is active, the decay power $DH^0_{i,j,k}$ is calculated from the fission product inventories tracked for each component in each cell, using the specific power attributed to each radionuclide class as a function of time by the Decay Heat (DCH) package. As a result, the decay heat per unit mass of UO_2 is not the same for all components. In particular, the decay power in intact fuel pellets in various core cells will reflect differences in initial fission product inventories corresponding to the power densities in those cells, while the decay power in particulate and conglomerate debris will reflect the initial inventories in the fuel pellets that originally contained the UO_2. In addition, all decay power densities will reflect differences in release resulting from the differing temperature histories of the UO_2 carrying the fission products.

If the RN package is not active, information on the distribution of fission products is not available. In this case, the total decay heat can only be approximately distributed over the UO_2 content of the active core components and debris in the cavity. The radial and axial power densities are considered for the UO_2 remaining in intact fuel pellets but—because of the absence of tracking information—the average specific power must be assigned to UO_2 in all other locations. This average specific decay power (W/kg-UO_2) is calculated from the whole core decay power provided by the Decay Heat package as

$$DH(t) = \frac{DH_T(t)}{M_{UO2,cor}(0) + M_{UO2,cav}(0)} \qquad \text{(RN package not active)} \qquad (2.111)$$

where

DH_T = whole core decay power (Watts)

$M_{UO2,cor}$ = total UO_2 mass in the core (kg)

$M_{UO2,cav}$ = total UO_2 mass in the cavity (kg).

The decay heat attributed to UO_2 in the various components in cell *i,j* is then calculated as

$$DH^0_{i,j,FU} = \mathrm{DH(t)}\ \frac{f_i\ f_j\ M_{i,j,FU,UO_2}}{\sum_{i'}\sum_{j'} f'_i\, f'_j\, M_{i',j',FU,UO_2}} \sum_{i'}\sum_{j'} M_{i',j',FU,UO_2} \qquad (2.112)$$

$$DH^0_{i,j,k} = \mathrm{DH(t)}\ M_{i,j,k,UO_2} \qquad (k \neq FU) \qquad (2.113)$$

where

f_i =radial relative power density (input record CORRii03)

f_j =axial relative power density (input record CORZjj03)

as in Section 2.6.1. Note that

$$\sum_i \sum_j \sum_k DH^0_{i,j,k} = DH(t)\ \ M_{UO_2,cor}(t) \qquad (2.114)$$

so that the average decay power density in UO_2 in the core and lower plenum is simply the average power density *DH(t)* from the Decay Heat package.

2.7 Material Interactions (Eutectics)

The material interactions model is invoked by entering integer 1 on input record COR00006. When the model is active the conglomerate debris materials associated with any component are treated as part of a coherent mixture. In the formulation of the model, some of the materials are treated as mutually miscible, while all the others are considered mutually immiscible and treated as they are when the model is inactive (i.e. they melt and relocate independently of one another). As currently implemented, when the model is active all the materials are part of the miscible mixture. The material interactions model can only be activated during MELGEN execution and cannot be deactivated on a restart.

2.7.1 Mixture Formation

Molten material can enter the conglomerate debris mixture in one of three ways: (1) as a normal liquid formed when an intact solid reaches its melting point, (2) as a eutectic reaction product formed when two intact solids in mechanical contact within a core component reach their eutectic temperature, or (3) through the dissolution of an intact solid by an existing liquid mixture in the same core cell (e.g. the dissolution of UO_2 fuel by the liquid mixture associated with the cladding in the same core cell as the fuel). Currently, there are three eutectic reactions considered which lead to early failure of fuel and control rods: (1) the eutectic reaction between Zircaloy cladding and Inconel grid spacers can lead to early failure of fuel rods, (2) the eutectic reaction between Zircaloy guide tubes and steel cladding can lead to early failure of PWR control rods and (3) the eutectic reaction between

B_4C powder and steel cladding can lead to early failure of BWR control rods. The threshold for the first two reactions is taken at 1400 K, and that for the B_4C-steel reaction at 1520 K, based on References [20] and [21], but these temperatures may be modified independently with sensitivity coefficients C1011. The molten material is placed in the conglomerate debris array associated with the component.

2.7.2 Mixture Properties

The properties of the mixture are mass weighted averages of the constituent properties. The solidus and liquidus temperatures of the mixture depend upon the composition of the mixture and are currently calculated as a mole weighted combination of the solidus temperatures determined by considering every binary combination of material pairs in the mixture. That is, the mixture solidus temperature is given by:

$$TS_{mix} = \frac{\sum_{j}\sum_{i\neq j} f_i \quad f_j \quad TS_{ij}}{\sum_{j}\sum_{i\neq j} f_i \quad f_j} \tag{2.115}$$

where the f's are mole fractions and TS_{ij} is the solidus temperature for a mixture of materials *i* and *j* with the same relative proportions as in the total mixture. TS_{ij} can be obtained from pseudo-binary phase diagrams or simple mole weighting of the individual solidus temperatures. Presently, TS_{ij} is given by the mole weighted average of the two solidus temperatures for all material pairs except for those listed in Table 2.2. For the pairs listed in the table, the solidus temperature is given by the mole weighted average of the eutectic temperature and solidus temperature of the component present in excess of the eutectic molar composition. (The molar ratios and eutectic temperatures in Table 2.2 are currently hardwired and not implemented as sensitivity coefficients.) Equation (2.115) correctly reduces to TS_{ij} when only materials *i* and *j* are present in the mixture.

Table 2.2 Core eutectic reactions [20, 21].

Material Pairs		Molar Ratio	Eutectic Temperature
Zr	Inconel	0.76 / 0.24	1210
Zr	steel	0.76 / 0.24	1210
ZrO_2	UO_2	0.50 / 0.50	2800
Zr	B_4C	0.43 / 0.57	1900
steel	B_4C	0.69 / 0.31	1420
Zr	Ag-In-Cd	0.67 / 0.33	1470

The liquidus temperature is set equal to the solidus temperature plus 0.01 K (an artificially small melting range is used to avoid the separation of a two phase mixture into a solid and liquid of vastly different temperatures, which may occur under the assumption of congruent melting that requires the solid and liquid to have the same composition).

The specific enthalpy is calculated in three temperature ranges as follows (refer to Figure 2.3) [22]:

1. For temperatures less than the calculated solidus, the mass weighted individual enthalpies are summed with the exception that extrapolated solid enthalpies are used for any material that would ordinarily be liquid.

2. For temperatures greater than the calculated liquidus, the mass weighted individual enthalpies are summed with the exception that extrapolated liquid enthalpies are used for any material that would ordinarily be solid.

3. Otherwise, linear interpolation in enthalpy is used between the solidus and liquidus. The difference in enthalpy is the latent heat of fusion.

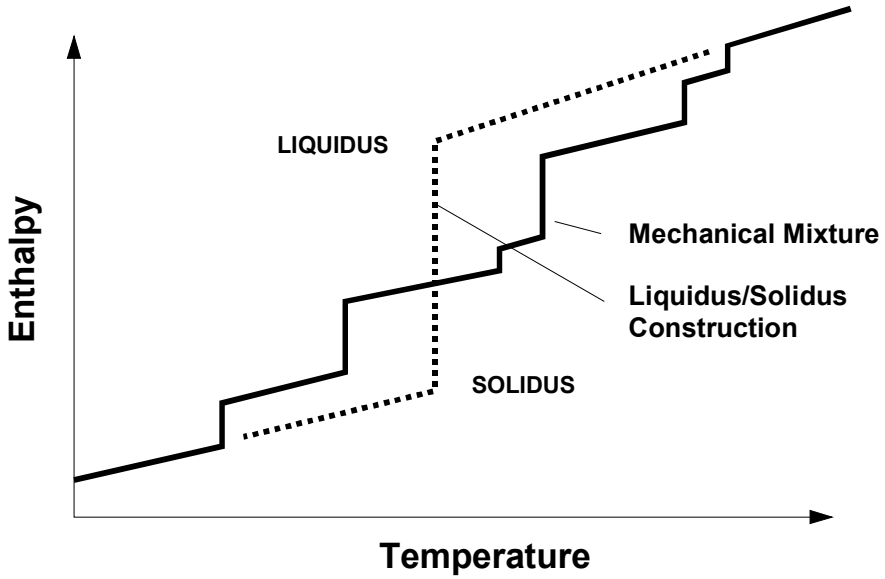

Figure 2.3 Two-phase construction for material mixture [22].

The Zircaloy and steel included in the mixture will oxidize unless disabled by user input on record CORTST01. The oxidation will reduce the metallic content of the mixture and increase the oxidic content.

2.7.3 Chemical Dissolution of Solids

If the enthalpy of the molten mixture exceeds its liquidus enthalpy, then the mixture will begin to dissolve certain solids if they are present in the same core cell. The dissolution of solids proceeds sequentially, and at most two distinct solids may be attacked by the mixture associated with a component on any given time step. Table 2.3 lists the hierarchy used in determining which solids are dissolved by the mixtures associated with each core component (intact fuel does not have a mixture associated with it). Note that certain solids are attacked only if the oxide shell surrounding the component has been breached, while others are attacked only if the shell is intact. Holdup by oxide shells is described in detail in Section 3.1.3. The hierarchy listed is based upon the assumed arrangement of materials in intact core components. For example, it is assumed that a eutectic mixture that escapes from a PWR control rod must dissolve the ZrO_2 oxide shell that surrounds fuel rods before it can dissolve the UO_2 pellets within. Similarly, mixtures originating from BWR control blades encounter canisters. It should be noted that most intact components are eventually converted into particulate debris, so that even though the eutectic associated with BWR control blades is not assumed to reach intact fuel, once the blade becomes particulate debris the eutectic may have access to UO_2.

Table 2.3 Solid dissolution hierarchy.

Component	Solids Dissolved by Mixture
cladding	UO2 from intact fuel
	ZrO2 from intact cladding
canister	ZrO2 from intact canister
	ZrO2 from intact cladding (A)
	UO2 from intact fuel
other structure SS, NS, or OS (steel only)	steel oxide from the same other structure
other structure NS or OS (BWR control rod)	steel oxide from the same other structure
	ZrO2 from intact canister (A)
	Zr from intact canister (A)
other structure NS or OS (PWR control rod)	steel oxide from the same other structure (B)
	Zr from the same other structure
	ZrO2 from intact cladding (A)
	UO2 from intact fuel (A)
particulate debris	UO2 from particulate debris
	ZrO2 from particulate debris
	ZrO2 from intact cladding
	UO2 from intact fuel
(A)	indicates solid is attacked only if there is no holdup of the mixture in the component.
(B)	indicates solid is attacked only if the mixture is being held up by

Component	Solids Dissolved by Mixture
cladding	UO2 from intact fuel
	ZrO2 from intact cladding
	the component

Dissolution will proceed until the addition of solid lowers the updated gross mixture enthalpy to the liquidus enthalpy associated with the updated mixture composition or until the parabolic rate limitation associated with the dissolution reaction has been exceeded for the given time step. The solution is iterative, and the parabolic rate limitations are given by [20]:

$$(x_j^f)^2 = (x_j^i)^2 + K_j \ \Delta t \qquad (2.116)$$

$$K_j = A_j \ \exp\left(B_j / T\right) \qquad (2.117)$$

where

x_j^f = final mass fraction of material j

x_j^i = initial mass fraction of material j

Δt = time step (s)

T = component temperature (K)

and the constants A_j and B_j may be adjusted through sensitivity coefficient array C1010. Default values for ZrO_2 and UO_2 are taken from Reference [18]:

$A_{ZrO2} = 1.47 \times 10^{14}$ $A_{UO2} = 1.02 \times 10^{15}$

$B_{ZrO2} = 8.01 \times 10^{4}$ $B_{UO2} = 8.14 \times 10^{4}$

These constants are based upon experiments using molten Zircaloy to dissolve UO_2 and ZrO_2, but the limits are applied to the dissolution of those solids by any mixture, irrespective of its composition. Consequently, as the fraction of Zircaloy in the mixture becomes small, the results from the model become suspect, and users are urged to conduct sensitivity studies to determine the effect of variations in the values of the constants in Equation (2.117). For the remaining materials, parabolic rate correlations have not been identified and no limitation is applied, although a limitation could be activated by supplying appropriate values for the sensitivity coefficients in Equation (2.117).

3 Core/In-Vessel Mass Relocation Models

This section describes the mass relocation models in the COR package. Candling of molten core materials, the transport of additional unmolten materials with the molten material, the radial relocation of molten pools, and the formation of flow blockages and molten pools are described in Section 3.1. The models for the radial relocation of molten pools and particulate debris are described in Section. Formation of particulate debris by various means from intact component, radial spreading of this debris, and its axial relocation by gravitational settling and collapse of supporting components is described in Section 3.2. The model that limits volumes available to accept the relocation of particulate debris (new in MELCOR 1.8.5) is described in Section 3.2.3.

3.1 Candling

The term *candling* is used here to refer to the downward flow of molten core materials and the subsequent refreezing of these materials as they transfer latent heat to cooler structures below. The COR package candling model is semi-mechanistic, based on fundamental thermal/hydraulic principles, but with incorporation of user-specified refreezing heat transfer coefficients defined for each material on record COR00005. The model is adaptable to steady flow of either films or rivulets (with smaller contact area than a film) by appropriate adjustment of these refreezing coefficients.

The model does not solve a momentum equation for a flow velocity. Instead it assumes steady generation and flow of molten material, with all material generated within a time step reaching its final destination within that step. For a steady melt generation rate, the amount of material entering into the candling model is proportional to the time step, and, for small time steps, the amount of material that refreezes at a particular location is also approximately proportional to the time step. In other words, if for a given time step a certain amount of molten material is calculated with varying amounts refreezing at different axial locations, the assumption is that for a time step twice as large, twice as much molten material would be generated and approximately twice as much would refreeze at each location. Thus, the cumulative behavior of the model should be relatively independent of time step history. For situations involving release of a larger amount of molten material built up over several time steps, alternative assumptions are used regarding the flow of that material and its contact time with structural surfaces to avoid time step dependencies, as described in Section 3.1.2.

3.1.1 Steady Flow

Following the heat transfer and oxidation calculations, molten material may exist on the surfaces of components in various locations in core. This molten mass is assumed to have been generated at a constant rate over the time step, Δt. The candling model follows it

as it flows down (because of gravity) through a column of cells. (A model to hold up molten material by an oxide shell until it is breached is described below.)

The amount of mass that refreezes on each lower cell component is determined by integrating the heat transfer rate between the molten film and the component:

$$q = h_m \; P_w \; \Delta z \; (T_m \; - \; T_s) \tag{3.1}$$

over the time step Δt, where

h_m = user-specified refreezing heat transfer coefficient

Δz = cell height

P_w = film or rivulet width (area of contact divided by Δz)

T_m = temperature of the molten film

T_s = temperature of the component

As energy is transferred between the melt and the component, their temperatures change. To account for this, implicitly projected new temperatures are used in Equation (3.1)

$$T_s = T_s^o + \frac{q \, \Delta t}{C_{ps}} \tag{3.2}$$

$$T_m = \max\left(T_m^o - \frac{q \, \Delta t}{M_m c_{p,m}}, T_{mp} \right) \tag{3.3}$$

where

T_m^o = temperature of the component before candling

C_{ps} = total heat capacity of the component

M_m = molten mass that enters the cell on surface s

$c_{p,m}$ = molten film specific heat capacity

T_m^o = temperature of molten film entering the cell

T_{mp} = melting point of film material

and Equation (3.3) reflects the fact that although the molten film may carry a superheat

$$Q_{sh} = M_m \; c_{p,m} \; (T_m \; - \; T_{mp}) \tag{3.4}$$

it will not be cooled below its melting point.

Equations (3.1) to (3.3) may be solved in the form

$$Q \equiv \mathrm{q}\,\Delta t = h_m \; P_w \; \Delta \mathrm{z} \max\left(\Delta T_1 \, , \Delta T_2\right) \Delta t \tag{3.5}$$

$$\Delta T_1 = \frac{C_{ps} \, M_m c_{p,m}}{C_{ps} \, M_m c_{p,m} + \left(C_{ps} + M_m c_{p,m}\right) h_m \; P_w \; \Delta \mathrm{z} \; \Delta t} \left(T_m^o - T_s^o\right) \tag{3.6}$$

$$\Delta T_2 = \frac{C_{ps}}{C_{ps} + C_{ps} \; h_m \; P_w \; \Delta \mathrm{z} \; \Delta t} \left(T_{mp} - T_s^o\right) \tag{3.7}$$

If Q is less than Q_{sh}, sensible heat is transferred but no mass is refrozen. If Q is greater than Q_{sh}, a mass

$$\Delta M_m = \frac{\mathrm{Q} \; - \; Q_{sh}}{H_f} \tag{3.8}$$

is refrozen as conglomerate debris on the component surface, and then thermally equilibrated with the component.

If the underlying component is cladding, its effective heat capacity from Equation (2.42) is used for C_{ps}. This includes the effects of coupling to underlying fuel pellets. However, the candling calculation is performed after other heat transfer has been evaluated, so that the results are not included in the implicit fuel-cladding gap heat transfer calculation described in Section 2.2.4. Therefore, only the appropriate fraction of the candling heat transfer to cladding from Equation (3.5) is transferred to the cladding, with the remainder going directly to the underlying fuel.

$$Q_{CL} = \frac{C_{CL}}{C_{CL,eff}} Q \tag{3.9}$$

$$Q_{FU} = Q - Q_{CL} \tag{3.10}$$

Molten mass is relocated downward in stepwise fashion according to Equation (3.8) until it has all refrozen on components in one or more lower cells or until it encounters a blockage (see Section 3.1.2). Figure 3.1 illustrates several steps in this process. The material refrozen on a component is termed *conglomerate* debris (as opposed to particulate debris), and becomes an integral part of that component.

If the material interactions (eutectics) model is not active, materials candle independently whenever their melting point is reached; otherwise, the molten portion of the conglomerate debris mixture candles as a congruently freezing mixture (i.e. when it freezes, the solid formed has the same composition as the liquid remaining).

Molten material originating in one type of component refreezes on the same component type in lower cells unless that component does not exist in those cells. If the originating component type does not exist in a cell, the molten material refreezes on an alternate component that depends on the originating component type and whether the cell is in the core or lower plenum. The definition of alternate refreezing components is summarized in Table 3.1. As indicated there, in the core the alternate refreezing component for material originating in all components except particulate debris is particulate debris, in either the channel or the bypass, as appropriate to the originating component. The alternate component for material originating in particulate debris in the channel is cladding, and for particulate debris in the bypass it is NS or OS (presumably representing a control blade). In the lower plenum, a second alternate refreezing component is taken as SS or OS (presumably representing CRGTs), if present. If neither the originating component nor an alternate refreezing component is found in a cell, the molten material falls through to the next lower cell.

Table 3.1 Alternate refreezing components.

Cell Location	Originating Component Type				
	CL	CN/CB	XS (A)	PD	PB
Core	PD fallthru	PD fallthru	PB/PD (B) fallthru	CL fallthru	NS/OS (C) fallthru
Lower Plenum	PD SS/OS (D) fallthru	PD SS/OS (D) fallthru	PB/PD (B) SS/OS (D) fallthru	CL SS/OS (D) fallthru	NS/OS (C) SS/OS (D) fallthru
(A) XS denotes any of SS, NS, or OS					
(B) PB/PD denotes PB if there is a distinct bypass, otherwise PD					
(C) NS/OS denotes whichever is used in the calculation					
(D) SS/OS denotes whichever is used in the calculation					

The volume occupied by molten and refrozen material during candling is tracked, and any related changes in component volumes are communicated to the CVH package as virtual volume changes. (The term "virtual volume" refers to space occupied by relocatable non-CVH materials in a control volume. Changes in virtual volume affect liquid levels, pressure calculations, and so forth. For a detailed discussion of virtual volume concepts, see the CVH Package Reference Manual.)

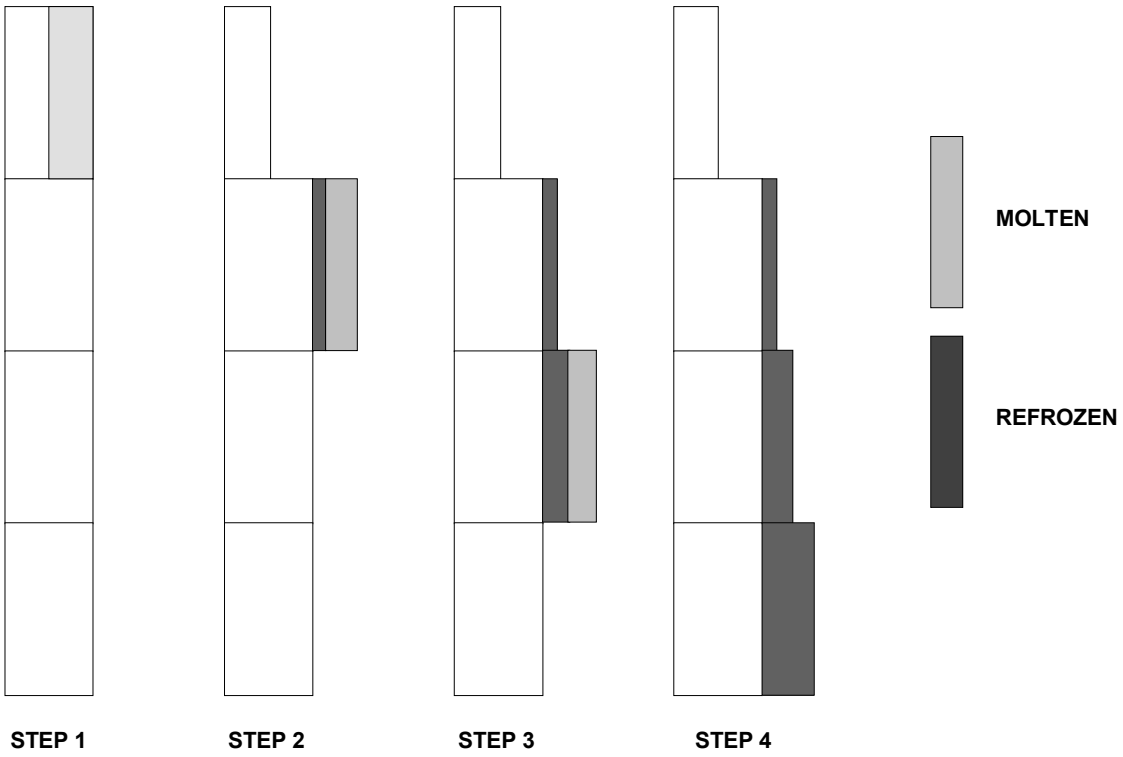

Figure 3.1 Candling process steps.

3.1.2 Flow Blockages

Flow blockages are allowed to form, as illustrated in Figure 3.2, whenever refrozen material completely fills all the available volume in a COR cell. In a core cell that contains an intact canister, the channel and bypass regions may be blocked independently. When candling material reaches a flow blockage (or the lower head), some material may remain molten because the designated refreezing component in the cell above the blockage cannot absorb the latent heat. Any such material becomes conglomerate debris associated with particulate, even if no particulate debris previously existed in that cell, and may form a molten pool. Molten material will be transferred between radial rings to achieve a uniform surface level across the pool as discussed below in Section 3.2.1. Candling of molten pools accumulated above a blockage after failure of that blockage is discussed below in Section 3.1.3.

Relocation of core materials may result in a reduction of area and increase of flow resistance, or even total blocking of flow, within various parts of the core. The effects on hydrodynamic flows may be modeled by using the core flow blockage model in the hydrodynamics package, which requires input of FLnnnBk records for the associated flow paths. In addition to modeling the change in flow area, this model calculates the change in flow resistance. The resistance is based on a model for flow through porous media when particulate debris is present; otherwise, the input flow resistance for intact geometry

is simply modified to account for any change in flow area. This model, described in Section 6.7 of the CVH/FL Reference Manual, uses a porosity based on the ratio of available hydrodynamic volume to total volume (see Section 3.2.3 below); a minimum porosity is imposed by sensitivity coefficient C1503(1), with a default value of 10^{-3}.

MELCOR 1.8.5 also includes a model for the opening of a flow path between the channel and bypass regions of the core upon failure of the canister in a BWR.

Activation of these models is *not* automatic. Input on FLnnnBk records is required to specify which core cells are associated with each flow path involving the core. Furthermore, because only CVH and FL model the flow of water and gases, the effects of blockages on circulation can be modeled only to the extent that the CVH/FL nodalization can resolve that circulation. For more details, see discussion in Section 1.5.5 of the COR Users' Guide and input instructions in the FL Users' Guide.

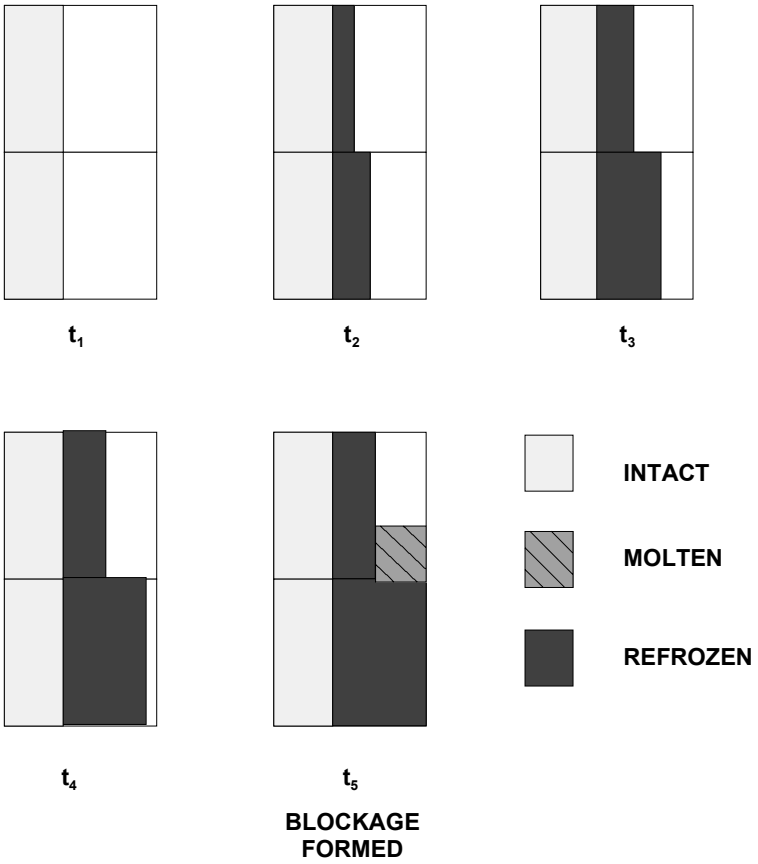

Figure 3.2 Flow blockage formation during candling.

3.1.3 Holdup by Oxide Shells

A model has been implemented in the COR package for an oxide shell to hold up molten material until the shell is breached. Molten material is held up within a component if the oxide thickness is greater than a critical value Δr_{hold}, if the component temperature is less than a critical value T_{breach}, and if no candling from the component in that cell has yet taken place. The parameters Δr_{hold} and T_{breach} may be set independently for steel and Zircaloy via sensitivity coefficient array C1131. The default values for these sensitivity coefficients are currently set so that there is holdup by Zircaloy oxide but not by steel oxide.

When an oxide shell is first breached, or when a flow blockage or crust first fails, the assumption built into the candling model of constant generation of melt over the time step is no longer valid. Behavior of the model, i.e., the amounts of mass refrozen in lower core

cells as described in Section 3.1, would thus be highly dependent on the size of the current time step. Therefore, for those situations involving the sudden release of a large mass of molten material, M_m, built up over perhaps several previous time steps, application of the candling model is modified slightly. For breach of an oxide shell, a constant time step Δt_{break} is used in Equation (3.3) to avoid time step dependencies. For failure of a flow blockage holding up a molten pool, a time step $\Delta t_{contact}$ is used in Equation (3.3). This time step is calculated as a function of a parameter Γ_{max}, which represents a maximum flow rate (per unit surface width) of the molten pool after breakthrough:

$$\Delta t_{contact} = \max \left[\Delta t, \frac{M_m \ \Delta z}{\Gamma_{max} \ A_s} \right] \tag{3.11}$$

In other words, a large molten pool is allowed to discharge at a maximum rate of Γ_{max} and the amount refreezing onto structures below will be a linear function of the total mass of the pool. Both Δt_{break} and Γ_{max} are accessible in sensitivity coefficient array C1141; their default values of 1 s and 1 kg/m-s have been set so that this model is only active for large molten pools breaching a crust.

3.1.4 Solid Material Transport

A simple model has been implemented to allow transport of unmolten secondary materials (currently ZrO_2, UO_2, steel oxide, and control poison) via the candling process. This model could be used to treat the breaking off of pieces of thin oxide shells that are carried with the molten material or to simulate the dissolution of UO_2 by molten Zr. On input record COR00007, the user may specify relocation of a secondary material, ΔM_s, as either an input fraction F_1 of the molten mass ΔM_m deposited on a component:

$$\Delta M_s = F_1 \ \Delta M_m \tag{3.12}$$

or in fractional proportion to its existing fraction within a component:

$$\Delta M_s = F_2 \ \frac{M_{s,total}}{M_{m,total}} \ \Delta M_m \tag{3.13}$$

where F_2 is an input parameter specifying the fraction of direct proportional relocation, $M_{s,total}$ is the total secondary material mass in the component in the cell of origin, $M_{m,total}$ is the total material mass (molten and solid) in the cell of origin, and ΔM_m is the secondary material mass deposited with refrozen material ΔM_m .

This model is inactive if the COR materials interactions (eutectics) model, which is described in Section 2.7 and treats dissolution mechanistically, is active.

3.1.5 Radial Relocation of Molten Materials

There are two radial relocation models—the first relocates molten core material that still exists following the candling/refreezing algorithm just described. The second, which relocates particulate debris, is essentially similar. Both models are intended to simulate the gravitational leveling between adjacent core rings that will tend to equalize the hydrostatic head in a fluid medium. Either of the two radial relocation models can be deactivated by user input on MELCOR input record CORTST01, but they are both active by default.

The molten material radial relocation model considers each axial level of the core independently, and is invoked after the axial relocation (candling) model. A simple algorithm loops over all adjacent pairs of radial rings between which relocation is possible, and compares the calculated liquid levels in the two. If the levels are unequal, then a calculation is performed to determine the volume of molten material, V_{eq}, that must be moved between the rings to balance the levels. Radial relocation is assumed to be blocked by the presence of an intact BWR canister structure in either ring. In addition, radial relocation is not allowed within a core plate. The actual implementation prevents such relocation to or from a core cell containing supporting structure modeled as a plate or, for the older representation using combined other structure, between cells *in level IAXSUP* containing other structure.

The relocation rate has a time constant of τ_{spr}, which may be adjusted by user input, so that the actual volume relocated, V_{rel}, during the core time step, Δt_c, is given by:

$$V_{rel} = V_{eq} \left[1 - \exp\left(-\Delta t_c / \tau_{spr}\right)\right] \qquad (3.14)$$

The default value of 60 s for τ_{spr} was chosen as an order-of-magnitude value based on engineering judgment and recommendations of code users. It is accessible as sensitivity coefficient C1020(2).

If the volume of the material that must be relocated is trivial [specifically, less than 0.01 m^3/kg times the mass below which any component will be eliminated, C1502(1), which has a default value of 1.0×10^{-12} kg], then no relocation is performed during that time step; otherwise, the fraction of the molten material that must be transferred from the "deep" ring to the "shallow" ring is determined by dividing the mass of melt that must be relocated by the total mass of melt in the deep ring. That fraction of molten mass is then transferred from each core component in the deep ring to the conglomerate debris associated with the particulate debris component in the shallow ring, and the component volumes in each ring

are adjusted accordingly. Any fission product transfers or virtual volume adjustments resulting from the relocation are performed by calls to interface routines with the RN Package and CVH Package, respectively.

Radial relocations are directed inward preferentially; that is, at each axial level the algorithm begins at the innermost ring, marches radially outward and transfers molten material from ring i to ring i-1 if the liquid level in ring i exceeds that in ring i-1. Following the march from ring 1 outward, a reverse march is made inward from the outermost ring to perform any outward relocations from ring i to ring i+1 still required to achieve a uniform liquid level across the axial level.

3.1.6 Surface Area Effects of Conglomerate Debris

The addition of conglomerate debris refrozen on component structures affects the surface area exposed to fluid convection, oxidation, and further refreezing during candling. For fuel rods and particulate debris, conglomerate debris can fill interstitial spaces, thus occluding some or all of the surface of the underlying component. The following paragraphs describe in detail a model specifically developed for fuel bundles. The general form of this model is incorporated into the COR package for all core components, but with different coefficients for each. With the default values of these coefficients, it is actually used only for fuel rods and particulate debris.

Consider the candling process idealized for a fuel rod unit cell as shown in Figure 3.3. Molten debris refreezing on the rod is assumed to begin forming a half-cylinder on the rod at the point directly adjacent to the next rod [Figure 3.3(a,b)]. As this half-cylinder of conglomerate continues to grow, its surface area expands, and the intact area shielded also grows, albeit at a lesser rate. Eventually it meets the conglomerate on the adjacent rod, and forms a bridge between the two rods [Figure 3.3(c)]. As additional material is added, more of the intact rod is covered by the conglomerate, until a cylindrical void region centered in the interstitial region among a set of four rods is created [Figure 3.3(d)]. This central void then shrinks to nothing as the interstitial area is completely plugged up [Figure 3.3(e)].

For purposes of calculation, the above-described process is divided into three stages. The first stage lasts until the conglomerate debris half-cylinders bridge the gap between rods, as shown in Figure 3.3(b). The second stage lasts until that bridge has widened to cover the entire surface area of the fuel rods, forming a central cylindrical void, as shown in Figure 3.3(c). The third stage continues until the central void is completely plugged up as shown in Figure 3.3(e). The surface area of the conglomerate debris in the unit cell is calculated in approximate fashion from the fraction of the interstitial volume that it occupies.

It is convenient to define areas and volumes relative to the unit cell rod surface area A_i and initial interstitial volume V_i. The latter is related to the volume of the rods by

$$\frac{V_i}{V_{rod}} = \frac{P^2 \; - \; \pi R^2}{\pi R^2} = \frac{\varepsilon_{bundle}}{1 - \varepsilon_{bundle}} \tag{3.15}$$

where P is the rod pitch and R is the rod radius, as defined by the COR0001 input record, and ε_{bundle} is an effective porosity of the rod bundle.

During the first stage, the surface area of the conglomerate debris A_{cd} grows as the square root of its volume V_{cd} up to some critical volume V_{c1} with surface area A_{c1}.

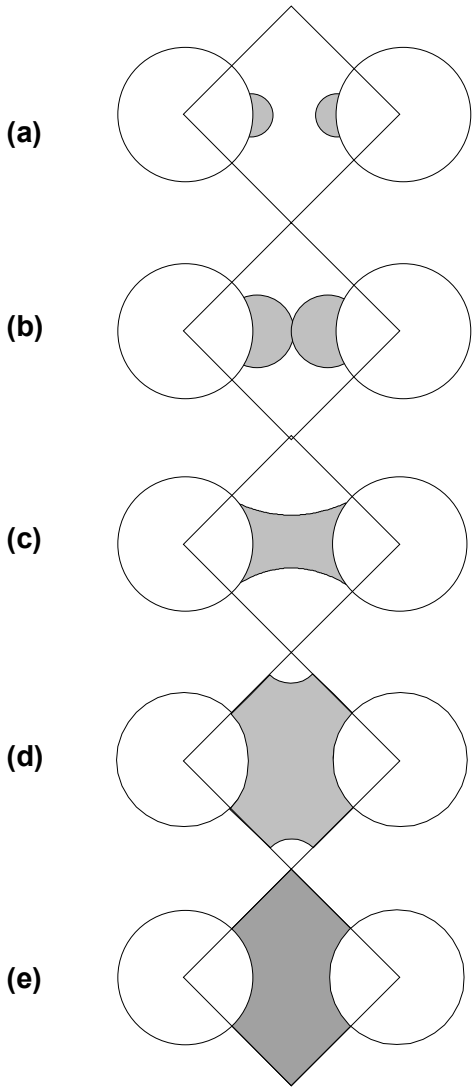

Figure 3.3 Conglomerate debris geometry in fuel rod bundles.

With the definition of Equation (3.15), it may be shown that

$$A_{cd} = A_i \left(\frac{A_{c1}}{A_i}\right)\left(\frac{V_{cd}/V_i}{V_{c1}/V_i}\right)^{1/2} \tag{3.16}$$

$$\frac{A_{c1}}{A_i} = F_{A1,\max} = \frac{P - 2R}{R} \tag{3.17}$$

$$\frac{V_{c1}}{V_i} = F_{V1,\max} = \frac{\pi}{2}\,\frac{(P - 2R)^2}{(P^2 - \pi R^2)} \tag{3.18}$$

During the third stage, beyond some critical volume V_{c2} with surface area A_{c2}, the surface area of the conglomerate debris decreases as the square root of the empty volume (V_i - V_{cd}). In terms of area and volume fractions:

$$A_{cd} = A_i \left(\frac{A_{c2}}{A_i}\right)\left(\frac{1 - V_{cd}/V_i}{1 - V_{c2}/V_i}\right)^{1/2} \tag{3.19}$$

$$\frac{A_{c2}}{A_i} = F_{A2,max} = \frac{P/\sqrt{2} - R}{R} \tag{3.20}$$

$$\frac{V_{c2}}{V_i} = F_{V2,max} = 1 - \pi\,\frac{(P/\sqrt{2} - R)^2}{(P^2 - \pi R^2)} \tag{3.21}$$

A minimum area fraction $F_{A,min}$ may be imposed for the third stage to prevent the surface area of central void from being completely reduced to zero. In any case, the surface area of conglomerate debris will not be reduced below a minimum surface-to-volume ratio as described below.

During the second stage, the surface area of the conglomerate debris is interpolated linearly with volume between A_{c1} and A_{c2}.

The area of the intact rods wetted by the conglomerate, and thus blocked from further oxidation and convection, is treated in two stages. For volumes greater than V_{c2}, the fraction of intact surface area A_i blocked is set to a maximum value:

$$F_b = F_{b,max} \tag{3.22}$$

For volumes less than V_{c2}, the fraction blocked is linearly interpolated:

$$F_b = F_{b,max} \frac{V_{cd}}{V_{c2}} \tag{3.23}$$

The same form is applied for all components. For particulate debris, the user-input porosity of the debris bed is used to replace ε_{bundle} in Equation (3.15); for all other components, the interstitial volume, V_i, is taken as zero. The parameters $F_{A1,max}$, $F_{V1,max}$, $F_{A2,max}$, $F_{V2,max}$, $F_{A,min}$, and $F_{b,max}$ are accessible for each component as sensitivity coefficient array C1151. Currently, all components have default values based on` typical BWR rod geometries with pitch 16 mm and rod radius 6.26 mm. However, they will be used only for fuel rods and particulate debris.

For conglomerate debris that does not occupy interstitial volume (either the component does not have interstitial volume via the porosity input or the debris overflows what is available), a simple surface area to volume ratio is applied to the excess conglomerate debris volume $V_{cd,excess}$:

$$A_{cd,excess} = V_{cd,excess} \; R_{SV} \tag{3.24}$$

The parameter R_{SV} is also accessible in sensitivity coefficient array C1151 with a default value of 100. The surface area of the excess debris is added to the area calculated from Equations (3.16) to (3.23). The total surface area of conglomerate debris (excess plus interstitial) cannot fall below the value obtained by multiplying the debris volume V_{cd} by R_{SV}.

Furthermore, to avoid overheating a vanishing CVH fluid, the sum of the surface areas of the intact component and its associated conglomerate debris, which constitutes the total effective surface area for heat transfer to CVH, cannot exceed

$$A_{tot,\max} = V_{CVH} R_{SVf} \tag{3.25}$$

where R_{SVf} is a limiting surface to volume ratio, accessible in sensitivity coefficient array C1152 with a default value of 1000 m^{-1}.

3.2 Particulate Debris

After core components collapse, the materials that composed them are treated as particulate debris. Once it has been formed, this debris can spread radially and/or settle vertically, subject to the availability of free volume and the presence or absence of support.

3.2.1 Formation of Particulate Debris

The COR package contains several simple models that consider the structural integrity and support of intact components, and convert them to particulate debris when either is lost. Most are logical models rather than structural models; no stress calculations are performed for any component other than supporting structure (SS). Even for SS, such a calculation is optional. Complex debris formation mechanisms, such as quench-induced shattering, have not been implemented into the COR package at this time.

All components other than fuel rods (FU and CL) will be immediately converted to particulate debris whenever the unoxidized metal thickness is reduced below a user-defined minimum value. The thickness criterion is also used for cladding (CL), which is assumed to support fuel pellets (FU), but other criteria are also considered for fuel rods. The user may define one minimum thickness parameter, $\Delta r_{cl,min}$, on record COR00008, with a default of 0.1 mm, that is used for Zircaloy in the cladding and the two canister components (CL, CN, and CB). In calculations using the old combined other structure component (OS), an independent minimum thickness, $\Delta r_{ss,min}$, also input on record COR00008 with a default of 0.1 mm, is applied to the steel in the OS.

For the nonsupporting structure component (NS), the structural metal may be taken either as steel (the default) or as Zircaloy. The default minimum thickness is also 0.1 mm. Both the structural metal to which it will be applied and the minimum thickness may be specified independently for each core cell containing NS.

Setting any Δr_{min} to zero will prevent collapse of the associated components by this mechanism, although MELCOR may still predict their collapse using one of the other criteria described below. If the user has specified electric heating element material in the fuel rods, formation of particulate debris is suppressed, and the minimum thickness parameter $\Delta r_{cl,min}$ must be set to zero.

Unoxidized metal thickness is reduced both by oxidation and by melting and candling of metal. It is considered to be increased, except for the case of cladding, by refreezing of metal candled from above. If candling of molten material is not possible because of a flow blockage or holdup by an oxide shell (Sections 3.1.2 and 3.1.3), the retained metal is considered as part of the unoxidized thickness. In effect, the component is considered to be supported by the oxide shell that contains the held-up melt or by the surrounding pool of molten material. Particulate debris will be formed from CN, CB, or OS whenever the temperature of the component reaches the melting temperature of the associated oxide (ZrO_2 for CN and CB, and steel oxide for OS). The temperature at which NS will be converted to particulate debris, independent of metal thickness, may be independently specified for each core cell containing NS, with a default value of the melting point of the structural metal identified for NS in that cell.

Fuel rods, composed of cladding and fuel pellets (the CL and FU components), are treated somewhat differently. Oxidized rods are assumed to retain their identity until the cladding reaches 2500 K, and to collapse unconditionally if the fuel temperature reaches 3100 K (the approximate melting temperature of UO_2). In MELCOR 1.8.4, the former temperature was taken as 2800 K, the approximate melting temperature of the UO_2/ZrO_2 eutectic, but experience with Phebus has shown that the lower temperature is more appropriate for irradiated fuels. Both temperatures are accessible to the user through sensitivity coefficient array C1132. It is possible for a fuel rod to be hot but unoxidized, either as a result of heating in an inert environment or following total loss of ZrO_2 through candling involving secondary transport (Section 3.1.4) or eutectics (Section 2.7). As currently coded, such a rod will be converted to particulate debris when the remaining metal thickness falls below $\Delta r_{cl,min}$.

Finally, an intact component will be converted to particulate debris whenever support of that component is lost. This support may be provided by either the same component or unfailed supporting structure (SS) component in the cell below; the portion of a fuel rod in level n supports the portion in level n+1, and the core support plate is considered to support all components above it.

If the old representation is being used, support is provided by unfailed “other structure” (OS) component that was initialized with the “tens” digit of the support flag set to 1 on input record CORZjj02. In addition, for this representation only, all components in any level may also be specified as unconditionally supported, i.e. "self supporting," by setting the "ones" digit of the support flag to 1. This is ordinarily done only for the level containing the core support plate, thus modeling it as requiring no external support.

When a component of the core of a BWR collapses to form particulate debris within the core region, this debris can occupy space either inside or outside the channel boxes. In earlier versions of MELCOR, only a single particulate field was available, and all components collapsed to form particulate in the channel. In MELCOR 1.8.5, particulate debris in the bypass (PB) is distinguished from that in the channel (PD). In any core cell with a distinct bypass, the structural components SS, NS, and OS are modeled as collapsing to form PB, while all others collapse to form PD. As this debris is later relocated, it may—depending on geometry—occupy the channel or bypass region of other cells, or be split between them.

Particulate debris is characterized by user-specified particle diameters, D_{pd}, and D_{pb}, entered as hydraulic diameters on input record CORijj04. The two diameters are equal by default, but this is not required. However, there is no provision at this point for considering more than a single representative diameter for either. The surface area of the particulate portion of each type of debris is calculated from D_{px} and the total volume of the particulate, V_{px}, as:

$$A_{s,pd} = \frac{6\ V_{px}}{D_{px}} \tag{3.26}$$

where “x” can be “d” or “b”. The fraction of this area used for oxidizing the Zircaloy portion of the particulate debris is the fraction of the particulate debris volume that is Zircaloy plus ZrO_2. The fraction of this area used for oxidizing the steel portion of the particulate is the fraction of the particulate volume that is steel plus steel oxide. ZrO_2 and steel oxide in particulate debris are modeled to exist as layers covering the Zr and steel, respectively. The particulate areas of the debris are further modified by the addition of conglomerate debris according to the model described in Section 3.1.5 to obtain actual areas for oxidation and heat transfer.

3.2.2 Debris Addition from Heat Structure Melting

During degraded core conditions, many reactor vessel structures that are modeled by the Heat Structures (HS) package in MELCOR are subjected to intense radiative and convective heating, and may be expected to melt. These structures are often designated on input records CORZjj02 and CORRii02 as the radial and axial boundary heat structures for heat transfer from the core. An example of such a structure is the BWR core shroud, a relatively thin (5 cm) structure that surrounds the entire core and extends into the upper plenum.

Although the HS package does not model melting in general, the melting of these structures may be calculated by special application of the HS package degassing model, using material type 'SS' (see the HSDGCCCCCx input records), and the resulting molten steel passed to the COR package. The melting model tracks the mass and volume changes associated with the molten steel added to the core. The model requires that any melting steel HS structure must lie either along the core, corresponding directly with one of the axial segments represented in the COR package, or above the core.

The molten steel produced from the degassing model is passed to the outermost radial ring (NRAD) in the axial segment corresponding to the origin of the melt. It is entered as particulate debris with energy corresponding to fully molten steel with no superheat. The model is flexible to the extent that additional HS package structures above the core can also be identified to melt via the degassing model, with material passed to the uppermost axial segment (NAXL) in the outer ring. Subsequent relocation of the molten steel from its initial core position is performed by the candling model described in Section 3.1 and the particulate debris relocation logic discussed below.

3.2.3 Exclusion of Particulate Debris

Core cells need not be completely filled to block entry of particulate debris; debris can enter a core cell only if there is “free” volume in that cell. The free volume can be less than the

fluid volume, because a component is allowed to exclude particulate (but not fluid or molten materials) from a volume greater than its physical volume. This can represent the natural porosity of a rubble bed, which does not allow other rubble to enter the pores. It can also represent an assumption that other interstitial spaces, such as those within fuel rod bundles, are too small to allow rubble to enter.

All intact components automatically exclude debris from the physical volume that they occupy. In a BWR, all initial components except the control blades are considered to occupy space in the channel region, with the blades occupying space in the bypass. (To be strictly precise, the core support plate is sometimes viewed as occupying space in the bypass, but only in a region where channel and bypass are not distinguished.) Particulate debris can occupy space in the channel (as PD), in the bypass (as PB) or in both.

Particulate debris is treated as forming a porous debris bed, which excludes other particulate debris from an effective bed volume

$$V_{bed} = \max\left(V_{material} , \frac{V_{unmelted}}{1-\varepsilon} \right) \tag{3.27}$$

Here $V_{material}$ is the total volume of material in the particulate, $V_{unmelted}$ is the volume of that portion of the material that has never been melted, and ε is a user-defined porosity. The physical picture is that the unmelted particulate forms a debris bed with porosity ε, but that some or all of the pores may be filled by molten or once-molten materials. For a BWR, this treatment is applied separately to particulate in the bypass and in the channel.

MELCOR 1.8.5 includes a flexible and relatively straightforward capability to model the exclusion of particulate debris from other interstitial spaces. It replaces a limited (and somewhat confusing) model in earlier versions of the code, based on a user-input "porosity" of rod bundles, PORIN. It was applied only to core cells that contained fuel rods. The revised modeling allows all components to exclude particulate debris from some minimum fraction of an associated total volume (channel or bypass) by their simple presence. (In cases where the associated volume is the one actually occupied by the component, particulate debris will continue to be excluded from the total physical volume, if it is greater.)

The "free" volume in a core cell (or in the channel or bypass region of a core cell) represents the volume available for additional particulate debris to relocate into that cell. Such debris may relocate either from the cell above or from an adjacent cell on the same axial level. The free volume is defined as

$$V_{free} = \max\left[V_{total} - \sum_{k} \max\left(V_{material,k} , V_{excluded,k}\right), 0 \right] \tag{3.28}$$

where the sum is over all components. For particulate debris, $V_{excluded,k}$ is the bed volume given by Equation (3.27). For all other components, it is a user defined fraction of the total volume of the cell if the component exists in the cell.

Based on examination of the geometry of typical US reactors, we would expect that no particulate debris could enter fuel bundles so long as there are intact fuel rods present. In BWRs, we would expect that particulate could not enter the unbladed bypass so long as there is intact CN, nor the bladed bypass so long as there is intact NS representing control blades. After the control blades have failed, this debris would be free to enter the bladed bypass, but not the unbladed bypass (assuming that CN was still intact).

The default exclusion fractions, selected in accordance with this picture, are shown in Table 3.2. In the table, “RD” means “fuel rod”; the exclusion is associated with the presence of FU, CL, or both. By default, the presence of intact fuel rods in a core cell excludes particulate debris from the entire channel region, but has no effect on the bypass. The presence of intact CN excludes particulate from 30% of the bypass, representing the unbladed portion, and intact NS representing control blades will exclude it from the remaining 70%. NS representing PWR control rods, SS, and OS have no effect.

Table 3.2 Exclusion of particulate debris by core components

Excluded fraction	Channel	Bypass
RD (FU, CN)	1.0	0.0[a]
CN		0.3[b]
CB		0.0[a]
NS[c]	BWR: 0.7[b] PWR: 0.0[d]	
SS[c]	0.0[e]	
OS[c]	0.0[f]	

[a] The default values for RD and CB will allow failed control blades to slump without melting. A value of 1.0 for CB would exclude particulate from the bypass region so long as CB survives. A value of 1.0 for RD would exclude it from the *original* bypass region—even after the canisters have failed—so long as there are intact fuel rods. Such values could be used to prevent the slumping of unmelted rubble from control blades until the canisters, fuel rods, or both have failed.

[b] By default, CN excludes PB from the unbladed portion of the bypass while NS representing control blades excludes it from the bladed portion. These numbers are intended to represent a typical partition between unbladed and bladed bypass volumes in a BWR, taken here as 30%/70%.

[c] If there is a separate bypass region, SS, NS, and OS occupy that bypass and the exclusion fraction is applied to its volume. If there is none, as for NS or OS representing PWR control rods and most cases of SS or OS representing plates or control rod guide tubes, the fraction is applied to the total (i.e. channel) volume.

[d] In a PWR, NS is used to represent control rods. In Western designs, these rods have little ability to exclude debris in the absence of fuel rods. For a VVER, there are control assemblies that take the place of certain fuel assemblies when the reactor is shut down. If the exclusion fraction for NS is set to 1.0, particulate debris will be prevented from entering these control assemblies until the control elements fail.

[e] SS is used to model core plates and BWR control rod guide tubes. This value will allow particulate to enter core plates and be supported there, and to fill around BWR control rod guide tubes without restriction.

[f] The old combined “other structure” component OS, may represent either supporting structures or control structures. Therefore, values appropriate to each cell must be specified by the user.

Other analysts might want to examine the consequences of other assumptions, or might want to apply MELCOR to different reactor designs. For example, when VVER reactors are shut down, some of the fuel bundles are lowered out of the main core, with their place taken by control elements. Under the assumptions appropriate to US designs, these control elements would have no capability to exclude debris and, when the upper core starts to collapse, the resulting debris would immediately spread into the rings containing these elements and fall to the lower plenum. Therefore, the default exclusion fractions can be modified globally, level by level, ring by ring, or cell by cell through user input. Consequences of default and alternate values are indicated in footnotes to the table.

These constraints on availability of space are considered in the models for radial and axial relocation of debris described in the following subsections. The absence of free volume is not allowed to prevent particulate debris from being *formed* in a core cell. For example, whenever a control rod or blade disintegrates, it is converted to particulate debris in place. The debris must be allowed to occupy the space previously occupied by the blade, even if geometric restrictions might have prevented any rubble from falling into that space. In addition, if a support plate has failed and lost the ability to support particulate debris, the absence of free volume within the plate is not allowed to prevent the passage of particulate debris *through* it. This allows such particulate to continue to relocate downward to space available below the plate. Note that free volume in the sense discussed here is not relevant to the relocation of molten materials, which can fill all volume not physically occupied by materials, i.e., it is the volume available to fluids.

3.2.4 Radial Relocation of Particulate Debris

The particulate debris leveling model is very similar to the molten material leveling model described in Section 3.1.5 except that material is moved only from the particulate debris component in the "deep" ring to the particulate debris component in the "shallow" ring. The time constant for particulate debris relocation has an *ad hoc* default value of 360 s, is accessible as sensitivity coefficient C1020(1). There is no consideration of an angle of repose; debris is completely leveled across the core. Particulate debris relocation is subject to the same constraints concerning BWR canisters and core support plates as molten material relocation. Component volumes and associated fission products are adjusted following relocations.

3.2.5 Gravitational Settling

The downward relocation of particulate debris by gravitational settling is modeled in MELCOR as a constant-velocity process, with the velocity given by VFALL from the COR00012 input record. Each ring in the COR nodalization is treated independently. For a given ring, each core cell containing particulate debris is considered in turn as a potential

source of falling debris, working from the bottom up. The model first determines how far particulate from that cell can fall during the time step, subject to limitations of available volume and support. Falling debris can be stopped by the absence of available space (a "blockage") or by encountering a structure that can support it, typically, a support plate with the capability to support particulate. Note that, because of the debris exclusion model discussed in Section 3.2.3, core cells can be blocked without being completely filled.

Once the lowest core cell that particulate can reach has been determined, the algorithm fills the available space from that level up until the debris in the source cell has been exhausted or all available volume has been filled. It then moves on to consider the next higher cell in the ring as a possible source of slumping debris, subject to the updated availability of space.

The model accounts for the distinction between particulate in the channel (or what was originally the channel), PD, and that in the bypass (or what was originally the bypass), PB. It allows particulate debris to slump from the channel or bypass of one cell into the channel and/or bypass of the cell below, depending on the conditions in those cells. The situation is complicated by the fact that the distinction between channel and bypass does not exist everywhere in the core. For example, cells such as those in the lower plenum that never contained canisters—and therefore can have no "bypass" region—are permitted to contain only PD. Thus, any debris that slumps into such a cell as PB must be considered there as PD. In addition, the distinction is almost entirely lost for cells that originally contained canisters once those canisters fail, and all particulate debris in such a cell is considered as well mixed and equilibrated. (However, separate volumes in the "channel" and the "bypass" must be calculated for such cells in order to define the volumes displaced in the associated CVH control volumes, which do remain distinct.)

The details of the algorithm implemented are as follows, where it is to be understood that "intact canister" means "component CB present in the cell":

1. The split between channel and bypass regions is preserved when particulate debris slumps from a core cell with an intact canister into another core cell with an intact canister. That is, debris in the channel passes into the channel while debris in the bypass passes into the bypass;

2. All particulate debris that originates in, or enters, a core cell where there is no intact canister to separate channel and bypass is treated as mixed, and any distinction between origin as PD or PB is lost;

3. Particulate debris that slumps from a core cell without an intact canister into one with an intact canister is split between channel and bypass in proportion to the available cross-sectional areas of the two regions;

4. If the fall of particulate is blocked in the channel or the bypass in a core cell that contains an intact canister, it will fill that region from the blocked level up. If

both are blocked, it will fill each independently, based on debris entering the corresponding region. If there is sufficient debris to fill all available volume in the channel or bypass to a point above which there is no intact canister, any remaining debris will be used to fill from that cell upwards;

5. If the fall of particulate is blocked in a core cell that does not contain an intact canister, it will fill from that level up. If channel and bypass are distinguished in that cell because it originally contained a canister, the particulate debris will be divided between PD and PB in proportion to the available cross-sectional areas of the two regions. If there is sufficient debris to fill all available volume to a point above which there is an intact canister, the two regions will be filled independently, based on the split of debris between them at the point where falling particulate entered the region containing a canister.

3.3 Displacement of Fluids in CVH

When core materials relocate from one core cell to another by any of the mechanisms discussed in the previous sections, they cease displacing fluid in the old location and commence displacing it in the new one. Candled material (conglomerate debris) is treated as occupying space in the same region, channel or bypass, as the component that supports it. As already implied, each core component (fuel rods, control elements, canisters, and particulate debris) is treated as occupying space in an associated CVH control volume. However, the spatial nodalizations used in COR and CVH are largely independent, and may be quite different. The two representations are maintained independently throughout a MELCOR calculation.

In order to treat the displacement of fluid in CVH, each control volume is considered to have "virtual" volume in addition to the current fluid volume. The virtual volume includes the total volume of all core components within the volume. Part or all of it will become available to CVH fluids when and if these core components relocate. The COR package handles relocation by directing CVH to free virtual volume in the original location, and to occupy it in the new location. The vertical distribution of the virtual volume is defined only within the resolution provided by the Volume/Altitude (V/A) table for the CVH volume. (See the CVH/FL Packages Reference Manual for more details about Volume/Altitude tables and virtual volume.) The most detailed agreement will be obtained if the elevations in the CVH V/A table match those in the core nodalization. Checks included as part of MELGEN input processing will generate warning messages if there are not points in the appropriate CVH Volume/Altitude tables in CVH input to correspond to all axial limits of core cells in COR input.

Further checks are included as part of MELGEN input processing to ensure that the CVH and COR representations of the distribution of fluid volume are compatible. If there is an initial inconsistency, an error message will be generated and processing terminated without generation of a restart file. (An option is available to override these checks if the user is

determined to continue with inconsistent data.) Specifically, the tests require that no fluid volume in COR may exceed those in CVH, thus ensuring that core debris cannot overfill the CVH volume. The requirement actually enforced is on the total fluid volume in all core cells (or fractions of core cells) associated with each range of elevations in the V/A tables for each CVH control volume. Separate checks are performed for channel and bypass regions.

One subtle point must be dealt with to maintain consistency between the representations as a simulation progresses. Although each component is assumed to displace fluid in either the channel or the bypass, but not in both, canisters have two sides that interface with different volumes and may oxidize independently. By convention, canisters are assumed to occupy the channel (there would be no essential difference if they were assumed to occupy the bypass). If the interior of a canister is completely filled, any further oxidation of its inner surface will be precluded, but steam and/or oxygen present outside (in the bypass volume) can continue to oxidize its outer surface. Because the volume of oxide produced is greater than the volume of metal consumed, this produces a volume of oxide that cannot be accommodated in the channel, but must be put somewhere.

The solution devised to this conundrum involves “borrowing” the necessary volume from the bypass. Thus, if there is more material associated with channel components than can be accommodated there, the excess will be treated as reducing the fluid volume in the bypass. In a sense, canisters are allowed to occupy bypass volume “when necessary.” Borrowing of channel volume by bypass components is also allowed, in the interest of symmetry, but should be necessary only in cases involving roundoff. The borrowing is, of course, limited to the actual fluid volume available.

A single call at the completion of the advancement in the COR package communicates the net changes in occupied volumes as calculated within the COR package to the CVH package. There, they are converted to the nodalization used by CVH, for later use in advancing the hydrodynamic equations. For each portion (channel or bypass) of each core cell, the quantity actually communicated is the negative of the change in fluid volume rather than the sum of changes in occupied volumes. This “insulates” CVH from the details of volume “borrowed” within the core representation.

As a simulation advances in time, the COR package repeatedly rechecks the internal consistency of its representation of volumes, and warns of any discrepancies that may develop. The treatment of errors is controlled by elements of sensitivity coefficient array, 1504. If the borrowed volume in any core cell exceeds a limit set by C1504(2), a warning message will be issued. (Issuance of the message is terminated after 100 such messages in any execution.) Checking of total volume occupied in a core cell is really only a test on the logical consistency of the coding. If the total occupied volume exceeds that available by more than a limit set by C1504(1), an error message will be issued (also terminated after 100 such messages). If it exceeds that limit by a factor of 100 times, the calculation will be terminated.

If the representations of volumes within CVH and COR are initially consistent, the one in CVH should remain consistent so long as that in COR does. However, even if they are initially consistent, the CVH and COR representations remain independent. Therefore, it is still possible that they will diverge as a result of accumulated roundoff. If the divergence is great enough, the COR package may attempt to relocate debris to regions where there is no volume in CVH to accommodate it. If this occurs, a warning message is issued, but the calculation is allowed to continue.

4 Structure Support Model

4.1 Model for OS

There are no mechanical models for the combined other structure component, OS. Therefore only simple, parametric models are available for its failure. OS initially has the ability to support other intact components and particulate debris in any cell where the support flag for that axial level was specified as ISUP=1x on input record CORZjj02. That ability is lost when the temperature of the OS reaches the failure temperature defined for that axial level by TSFAIL on input record CORZjj04. Failure also occurs if an optional logical control function defined on input record CORijj07 becomes TRUE. On failure, all components supported by the OS are converted to particulate debris (PD) which, with any PD previously supported by the OS, are allowed to fall through to lower cells. (This is done by resetting the “tens” digit of ISUP to 0.) The OS component itself remains in place until it melts.

4.2 Models for SS

The supporting structure component, SS, in any core cell may be treated as representing an edge-supported plate, a grid-supported plate, a BWR core plate, or BWR control rod guide tubes. The model used is determined by user input on records COR000SS, CORZjjSS, CORRiiSS, and/or CORijjSS, where these four models are associated with the keywords “PLATE,” “PLATEG,” “PLATEB,” and “COLUMN,” respectively.

There are differences in the ability of each form of OS to support other intact components and particulate debris, and in the resulting loads on and stresses in the structure. Failure of the structure may be based on the calculated stresses. Parametric models equivalent to those for OS are also available. The consequences of failure (in terms of which components collapse) also differ for the various models. Subsections 4.2.1-4.2.4 describe the four models, while Subsection 4.2.5 describes further flexibility available to the user. Subsection 4.3 describes the failure models.

4.2.1 The PLATEG Model

The PLATEG model represents a plate that is supported by an underlying array or grid of beams, which may be formed as an integral part of the plate. In general, the beams have sufficient strength that their failure is not an issue, and the interest is in failure of the web between them. PLATEG is not dependent on support from SS in any other core cell. After failure, the plate element will remain in place until it melts.

Until it fails, PLATEG in each cell supports itself and intact components and debris above it, and is loaded by that total weight. When failure occurs in any ring, only the capability to support PD and intact components in cells above is removed. Thus, everything resting on the plate will fall, but the plate will remain in place until it melts. The picture corresponds to failure of the plate portion with survival of the grid, and closely resembles the modeling using OS.

For small deflections of solid plates, the stress is related to the bending moment per unit length, M, by

$$\sigma_e = 6\frac{M}{h^2} \tag{4.1}$$

where h is the thickness of the plate.

Only numerical solutions are available for most cases involving uniform loading of plates with underlying supports. If the support involves a rectangular grid of stiff beams of negligible width, the maximum bending moment for use in Equation (4.1) occurs at the point of support at the midpoint of the longer edge, and is given by [23]

$$M = K\,q\,x^2 \tag{4.2}$$

where q is the load per unit area, x is the short dimension of the supporting grid, and K is a function of the aspect ratio of the supporting grid.

The stress in the plate in any ring is calculated as

$$\sigma_{e,ring,PLATEG} = 6\,\frac{K\,q\,x^2}{h^2} = 6\,K\,\frac{x^2}{A_{ring}}\,\frac{1}{h^2}W_{ring} \tag{4.3}$$

Here W_{ring} is the load carried in that ring and A_{ring} is the ring area. By default, the PLATEG model uses a value of K corresponding to a square supporting grid of beams (or an eggcrate plate) and Poisson's ratio $\nu = 0.3$ appropriate to stainless steel, for which

$$K_{square} = 0.0513 \tag{4.4}$$

The value may be changed through user input.

4.2.2 The PLATE Model

The PLATE model represents a simple edge-supported plate that may span more than one ring of the core. It initially supports itself and intact components above it, and is loaded (as a whole) by its own weight and that of the other supported components including particulate debris. Inner rings of the plate are allowed to fail before the outer ones, leaving the outer portion of the core still supported by the annular remains of the plate. If the failure mechanism is stress based, the local stress is calculated as a function of the total load, the position in the plate, and the fraction of the plate that has not yet failed.

When failure occurs in any ring, support is removed for the SS representing the portion of the PLATE in that ring and any surviving inner rings, as is support for intact components and PD in cells above these. Thus, a failed section of the plate and everything resting on it will be converted to PD and allowed to fall, taking with it any as-yet-unfailed inner rings of the plate together with everything resting on them. The outermost ring of the plate is treated as self-supporting until it fails.

As with the PLATEG model, the stress is related to the bending moment per unit length through Equation (4.1). For uniform loading of a round plate of constant thickness, the bending moments vary radially, and the tangential moment is always greater than the radial moment. The value of the tangential bending moment per unit length, denoted as $M_0(r)$, is [24]

$$M_0(r) = K_{M,0}(r)\, q\, a^2 \tag{4.5}$$

$$K_{M,0}(r) = \frac{3+\nu}{16}\left[1 - \frac{1+3\nu}{3+\nu}\left(\frac{r}{a}\right)^2\right] \equiv K_0\left[1 - K_1\left(\frac{r}{a}\right)^2\right] \tag{4.6}$$

where q is the load per unit area, a is the radius of the plate and ν is Poisson's ratio.

Any variation in loading across the plate is neglected, and q is considered to be the total load on the plate divided by its total area. Equations (4.5) and (4.6) capture the variation of the bending moment, and therefore the stress, from the center to the outside of an intact plate.

If an inner ring of the plate fails before the outer ones, it leaves the outer portion of the core still supported by the annular remains of the plate. Although the resulting configuration will surely be messy, one can expect certain qualitative changes in the stress pattern. The decrease in the total load on the plate will tend to decrease stresses while the loss of the

stiffness of the central portion will tend to increase them. The dominant effect of the formation of a central hole in the plate by failure of inner rings is a stress concentration that will tend to accelerate the failure of the innermost surviving ring. The magnitude of the effect decreases as the hole grows to include a substantial fraction of the original plate.

The model implemented in the MELCOR COR package uses a very simple expression to capture these effects, in the form

$$M_0(r;r_0) = K_M(r;r_0)\, q\, a^2 \tag{4.7}$$

$$K_M(r;r_0) = K_{M,0}(r)\left[1-\left(\frac{r_0}{a}\right)^2\right]\left[1+\left(\frac{r_0}{r}\right)^2\right] \tag{4.8}$$

Here r_0 is the size of the hole, the first factor in Equation (4.8) reflects the reduction in load, while the second factor reflects the stress-concentrating effects of the hole. Note that this equation can be considered to be the general form. It is "exact" in the absence of a hole (r_0=0), where

$$K_M(r;0) = K_{M,0}(r) \tag{4.9}$$

and Equations (4.7) and (4.8) become equivalent to Equation (4.5).

The approximation given by Equation (4.8) has been compared [25] to the exact solution for a uniformly loaded annular plate with a free inner boundary and simple edge support at the outer boundary [26]. The simplified form agrees quite well with the exact solution—rather better, in fact, than the "exact" model corresponds to the expected geometry of a degraded core.

Under the assumption of continued uniform loading of the surviving portion of the plate, the total load on the plate may be written as

$$W_{total} = \pi\left(a^2 - r_0^2\right) q \tag{4.10}$$

W_{total} is evaluated as the total load on the entire plate or annulus, summed over all core rings in which an unfailed portion of the plate is present. For a given ring, the stress will be greatest at its inner edge, or at the center of the plate for the innermost ring. Therefore

$$\sigma_{e,ring\,1} = 6K_0 \frac{1}{\pi}\frac{1}{h^2} \quad W_{total} \tag{4.11}$$

$$\sigma_{e,ring\ i>1} = 6K_0 \frac{1}{\pi} \frac{1}{h^2} \left[1 - K_1 \left(\frac{r_{i-1}}{a} \right)^2 \right] \quad \left[1 + \left(\frac{r_0}{r_{i-1}} \right)^2 \right] W_{total} \qquad (4.12)$$

Here r_i is the outer radius of ring i, and the coefficients K_0 and K_1 are defined by Equation (4.6). The values used by default correspond to a Poisson's ratio $\nu = 0.3$, for which K_0=0.206 and K_1=0.576. These coefficients can be changed through user input.

4.2.3 The PLATEB Model

For a BWR, the primary support of the core is the control rod guide tubes (CRGTs), functioning as columns. The core plate is supported by beams, and is loaded only by its own weight and that of debris on it. Although it does not bear the weight of the fuel and canisters, the presence of the plate is required for the CRGTs to support them.

SS representing PLATEB is not dependent on support from SS in adjacent radial rings, or in any other core cell. When the plate fails in any ring, it loses the ability to support PD, which will then fall, but the plate remains in place until it melts.

Stresses in the plate for the PLATEB model are calculated using Equation (4.3) for the case of beam support without cross beams, neglecting the fact that supporting beams span more than one ring of the core. The value of x in this equation is the spacing between the beams. The differences from the PLATEG model are that the loading is limited to the weight of the plate and any PD resting on it, and that the default value of K is taken as

$$K_{beam} = 0.0833 \qquad (4.13)$$

This corresponds to the limit of the grid result cited above for an infinite aspect ratio of the grid and a Poisson's ratio of $\nu = 0.3$. The default may be changed by user input.

4.2.4 The COLUMN Model

SS representing an unfailed COLUMN in a core cell directly supports SS modeled as COLUMN in the level immediately above. Failure of SS representing COLUMN in one core cell implies failure of contiguous COLUMN elements higher in the same radial ring, resulting in their collapse to PD. The lowest element of a COLUMN is treated as self supporting; it will not collapse until it itself fails.

If there is SS modeled as PLATEB in the level above an unfailed COLUMN, the COLUMN indirectly supports (and is further loaded by) intact fuel assemblies, canisters, and control blades in and above that level, but not the plate or any PD. The internal coding logic treats the PLATEB as if it supported the intact components in the levels above (without being loaded by them) by transferring the load to the COLUMN in the cell below. This support

is dependent on the existence of the COLUMN. If it fails (or is initially absent), the fuel assemblies and control blades "supported" by PLATEB will immediately collapse to PD.

For thick columns in compression, the relationship between stress and load is simply

$$\sigma_e = \frac{W}{A_c} \tag{4.14}$$

where W is the load (including the column itself and the indirectly supported fuel assemblies, canisters, and control blades) and A_c is the cross-sectional area. If there are N identical circular columns in a ring of the core nodalization, each with inner radius r_i and outer radius r_o, the stress is evaluated as

$$\sigma_{e,ring,COLUMN} = \frac{1}{N\pi\left(r_o^2 - r_i^2\right)} \frac{M_{column,0}}{M_{column}} W_{ring} \tag{4.15}$$

The factor of the ratio of the original column mass to its current mass is included to account for any reduction in the load bearing area of the column by oxidation or melting.

4.2.5 User Flexibility in Modeling

As noted in preceding subsections, the coefficients in the equations that relate stress to load for the various models can be modified through user input. This capability can be used to model variations in the form of the structure. For example, if a plate is supported on a square grid of columns of radius c and spacing x, the maximum bending moment per unit length is at the support. The value is given by Equation (4.2) with a modulus [27]

$$K_{support} = \frac{(1+\nu)\left[\ln(x/c) - 0.811\right]}{4\pi} \tag{4.16}$$

A value can be computed from this equation (for example, for $\nu = 0.3$ and (x/c)=5, $K_{support}$=0.0826) and used in the PLATEG model to represent a column-supported plate.

MELPROG [28] used this expression for a column-supported plate, and accounted for the effects of holes in the plate by dividing K by a "ligament efficiency" ε. For the case of 4 holes per cell of radius b and spacing d, this is given by

$$\varepsilon = 1 - b/d \tag{4.17}$$

In fact, the results of a full structural analysis (outside of MELCOR) of a more complicated structure could be used to calculate an effective K for use in one of the plate models.

Thus, the relatively simple models could be used to represent quite complicated support structures, should a user so desire.

4.3 SS Failure Models

Several mechanisms for failure of structures are included in the modeling of supporting structures using the SS core component. These include equivalences to the failure temperature and control function models used for the OS core component. There are also mechanical models that consider the stresses in SS, as calculated from the models in the preceding subsections.

The stress-based failure models include the failure of plates and columns by yielding and the failure of columns by buckling. These are both catastrophic failure models. In addition, structures can fail over time by creep at stresses below the yield stress. This possibility is represented using a Larson-Miller creep-rupture model, which is closely related to the (default) zero-dimensional form of the model for failure of the lower head described in Section 5.2.

4.3.1 Failure by Yielding

Unless a parametric model has been specified, failure will occur if the stress in a structural element exceeds the yield stress. For this analysis, the stress is calculated using equations in Section 4.2 for the loading model specified on the relevant CORxxxSS input record. The temperature-dependent yield stress is represented by the following equation, which has a form similar to that used for the lower head

$$\sigma_Y(T) = 260.\times 10^6 \left\{ \left[1+\left(\frac{T}{800.} \right)^{3.} \right]^{-1} - \left[1+\left(\frac{1700.}{800.} \right)^{3.} \right]^{-1} \right\} \tag{4.18}$$

The constants 260. x 10^6, 1700., 800., and 3. were chosen to approximate the data for 304 stainless steel in the Nuclear Systems Materials Handbook [29], have been implemented as sensitivity coefficient array, C1606.

4.3.2 Failure by Buckling

Columns will buckle if the load exceeds the value given by [30]

$$W_{buckl} = \pi^2 E \frac{I}{\ell^2} \tag{4.19}$$

where $\underline{I}$ is the moment of inertia, E is the elastic modulus, and ℓ is the length of the column. For a circular column with outer and inner radii r_o and r_i, respectively, the moment of inertia is

$$I = \frac{\pi}{4}\left(r_o^4 - r_i^4\right) = \frac{\pi}{4}\left(r_o^2 - r_i^2\right)\left(r_o^2 + r_i^2\right) \tag{4.20}$$

Comparison with Equation (4.15) shows that for N identical columns in a ring, buckling will occur if the stress exceeds

$$\sigma_{buckling} < \pi^2 \frac{\left(r_o^2 + r_i^2\right)}{4N\ell^2} \quad E \tag{4.21}$$

The elastic modulus is represented by the following equation, which has a form similar to that for the lower head

$$E(T) = 370. \times 10^9 \left\{ \left[1 + \left(\frac{T}{1650.} \right)^{3.} \right]^{-1} - \left[1 + \left(\frac{1700.}{1650.} \right)^{3.} \right]^{-1} \right\} \tag{4.22}$$

The constants 370.x10^9, 1700., 1650., and 3. were chosen to approximate the data for 304 stainless steel in the Nuclear Systems Materials Handbook [31]. They are implemented as sensitivity coefficient array, C1605.

4.3.3 Failure by Creep

The Larson-Miller creep-rupture failure model [32] gives the time to rupture, t_R, in seconds as

$$t_R = 10^{\left(\frac{P_{LM}}{T} - 16.44\right)} \tag{4.23}$$

where the temperature, T, is in K. The Larson-Miller parameter, P_{LM}, for stainless steel can be fit as a function of the effective stress, σ_e, in Pa=N/m^2, as

$$P_{LM} = 81000 - 7500\log_{10}(\sigma_e) \tag{4.24}$$

from ASME data [33]. The three constants in Equations (4.23) and (4.24) have been implemented as sensitivity coefficient array, C1604.

Because stress and temperature are not constant, a fractional lifetime rule is applied, and failure is assumed to occur when

$$\int \frac{dt}{t_R(t)} \approx \sum \frac{\Delta t_i}{t_R(t_i)} = 1 \qquad (4.25)$$

For the multi-ring geometry of MELCOR, both the loading and the temperature histories—and therefore the Larson-Miller parameter—vary from cell to cell, and SS in different cells is allowed to fail independently. It is therefore necessary to integrate Equation (4.25) separately for each core cell that contains SS subject to a stress-based failure model.

5 Lower Head Model

The lower head nodalization framework was described in Section 1.1.2; the illustration in Figure 1.5 is repeated here as Figure 5.1 for convenience and with more detail depicting the lower head heat transfer logic. The lower head model physics described in this section is divided into three parts: heat transfer among the model elements, determination of failure at some penetration or gross failure in some ring (when penetrations are absent), and ejection of debris into the reactor cavity. Because much of the phenomena associated with lower head failure is very poorly understood, the lower head model is very simple and parametric, allowing the user significant flexibility in controlling lower head behavior.

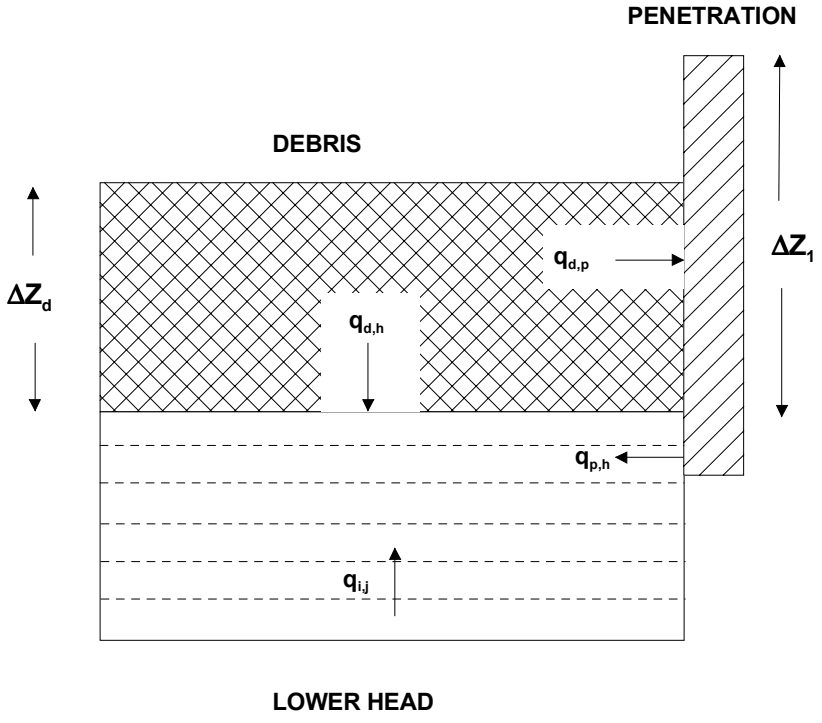

Figure 5.1 Lower head nodalization.

5.1 Heat Transfer

Heat transfer from the debris to the lower head and its penetrations (e.g., instrumentation tubes, control rod guide tubes, or drain plugs) is modeled parametrically using heat transfer coefficients (specified on record COR00009), heat transfer areas (calculated from ring radii specified on record CORLHDii or specified directly on record CORPENnn), and masses (also calculated from composition and nodalization input specified on record CORLHDii or specified directly on record CORPENnn). The heat transfer rate from the debris in the bottommost axial level to the lower head is given by:

$$q_{d,h} = h_{d,h} \; A_h \; \left(T_d \; - \; T_{h,s} \right) \tag{5.1}$$

where

$q_{d,h}$ = heat transfer rate between debris and lower head

$h_{d,h}$ = debris-lower head heat transfer coefficient

A_h = lower head surface area

T_d = debris temperature

$T_{h,s}$ = lower head inner surface temperature

The heat transfer rate from the debris in the bottommost axial level to a penetration is similarly given by:

$$q_{d,p} = h_{d,p} \; \frac{\Delta z_d}{\Delta z_1} \; A_p \; \left(T_d \; - \; T_p \right) \tag{5.2}$$

where

$q_{d,p}$ = heat transfer rate between debris and penetration

$h_{d,p}$ = debris-penetration heat transfer coefficient

A_p = penetration area

Δz_d = debris height in the bottom axial level

Δz_1 = bottom axial level height

T_p = penetration temperature

The penetration area is based on the height of the bottom axial level, Δz_1, and the multiplier $(\Delta z_d - \Delta z_1)$ accounts for the partial covering of the penetration area by the debris of height Δz_d.

The heat transfer rate from the penetration to the top lower head node is based on the conduction area between the penetration and lower head specified by the user:

$$q_{p,h} = k_p \; A_{p,h} \; \frac{T_p - T_{h,s}}{\Delta z_1} \tag{5.3}$$

where

$q_{p,h}$ = heat transfer rate between penetration and lower head

k_p = penetration thermal conductivity

$A_{p,h}$ = conduction area between penetration and head

The conduction area $A_{p,h}$ should be chosen to appropriately model the two-dimensional nature of the heat conduction; note that conduction to only the top lower head node is modeled.

Conduction heat transfer rates within the lower head are given by:

$$q_{i,i+1} = k_i \, \mathrm{FAC} \, A_h \; \frac{T_{h,i} - T_{h,i+1}}{\Delta z_i} \tag{5.4}$$

where

$q_{i,i+1}$ = heat transfer rate from node i to node i+1

k_i = thermal conductivity of mesh layer i

$T_{h,i}$ = temperature of lower head node i

Δz_i = width of mesh layer i

and FAC is a factor to enhance conduction through material that exceeds the melting point, as discussed in Section 2.2. The use of a planar finite-difference equation to model heat

transfer in hemispherical geometry is an adequate approximation because the thickness of the lower head is much smaller than the radius.

Convection heat transfer rates from the penetrations, debris, and inner surface of the lower head to the fluids in the lower plenum control volume ICVHC (specified on record CORijj01), $q_{p,v}$, $q_{d,v}$, and $q_{h,v}$ respectively, are modeled by the methods described in Section 2.3.

Heat transfer from the outer boundary of the lower head to the reactor cavity control volume specified on record CORLHD01 is partitioned between the atmosphere and the pool in the control volume based upon the pool fraction of the surface area of the lower head in each radial ring as follows:

$$q_{h,c} = h_{ATM}(1 - F_{PL})A_h(T_{h,1} - T_{ATM}) + h_{rlx,PL}F_{PL}A_h(T_{h,1} - T_{SAT}) \qquad (5.5)$$

where

h_{ATM} = heat transfer coefficient from lower head to reactor cavity atmosphere

$h_{rlx,PL}$ = relaxed heat transfer coefficient from lower head to reactor cavity pool

F_{PL} = pool fraction of surface area A_h

T_{ATM} = temperature of reactor cavity atmosphere obtained from CVH

T_{SAT} = saturation temperature of reactor cavity pool obtained from CVH

$T_{h,1}$ = lower head outer surface temperature at the beginning of the time step

The first term on the right hand side of Equation (5.5) accounts for heat transfer to the reactor cavity atmosphere, while the second term accounts for heat transfer to the reactor cavity pool. The pool fraction, F_{PL}, is simply the fraction of the area which is immersed in the pool based upon the depth of the pool obtained from the CVH data base at the beginning of each time step. The heat transfer coefficient to the reactor cavity atmosphere, h_{ATM}, is implemented as sensitivity coefficient C1246(1) with a default value of 10 W/m^2-K. The unrelaxed heat transfer coefficient to the reactor cavity pool, h_{PL}, is calculated using a simple downward-facing saturated pool boiling model. Relaxation of h_{PL} is implemented exactly as discussed in Section 2.3. Heat transfer to the pool prior to boiling is currently ignored, as is subcooling of the pool; it is calculated only when the temperature of the outer surface of the lower head exceeds the saturation temperature in the reactor cavity. Hence, the second term on the right-hand side of Equation (5.5) cannot be negative.

The downward-facing saturated pool boiling model treats three heat transfer regimes:

1. fully-developed nucleate boiling with no dependence on the orientation of the boiling surface,

2. transition boiling between the fully developed and film boiling regimes, in which the heat flux is obtained by logarithmic interpolation between the critical heat flux and the minimum heat flux based upon the temperature difference between the surface and saturation, and

3. stable film boiling which depends upon the orientation of the boiling surface.

The boundaries between the heat transfer regimes are determined by a correlation for the critical heat flux, which separates fully developed and transition boiling, and a correlation for the minimum-stable-film-boiling heat flux, which separates transition and stable film boiling. Although heat transfer in the nucleate boiling regime is assumed to be independent of the orientation of the surface, the critical heat flux, which determines its upper limit, is dependent on surface orientation and is given by [34]:

$$q_{CHF}(\theta) = \left(0.034 + 0.0037\theta^{0.656}\right) \rho_v^{1/2} h_{lv} \left[g\,\sigma(\rho_l - \rho_v)\right]^{1/4} \qquad (5.6)$$

where

θ =inclination angle of the surface in degrees ($\theta = 0^\circ$ for a downward-facing surface),

ρ_l, ρ_v =densities of water and steam, respectively,

g =acceleration of gravity,

σ =interfacial surface tension between steam and water,

h_{lv} =latent heat of vaporization of water,

and the constants 0.034, 0.0037 and 0.656 have been implemented in sensitivity coefficient array C1245. Similarly, the minimum-stable-film-boiling heat flux, which separates transition boiling from stable film boiling, is given as a function of θ as [34]:

$$q_{MIN}(\theta) = \left(4.8x10^{-4} + 82.x10^{-4}\theta^{0.407}\right) \rho_v^{1/2} h_{lv} \left[g\sigma\,(\rho_l - \rho_v)\right]^{1/4} \qquad (5.7)$$

where the constants $4.8\text{x}10^{-4}$, $8.2\text{x}10^{-4}$ and 0.407 have also been implemented in sensitivity coefficient array C1245.

In the nucleate boiling regime, the heat flux as a function of the difference between the surface temperature and the saturation temperature, $\Delta T \equiv T_{SRF} - T_{SAT}$, is given by:

$$q_{NB}(\Delta T) = h_{NB}\,\Delta T \tag{5.8}$$

where h_{NB} is given as a function of ΔT (and pressure) by Equation (2.58). In the stable film boiling regime, the heat flux as a function of ΔT is given by:

$$q_{FLM}(\Delta T) = h_{FLM}\,\Delta T \tag{5.9}$$

and the user has two options for determining the h_{FLM} as a function of ΔT. The default option gives the heat transfer coefficient as [35]:

$$h_{FLM}(\Delta T) = 0.142\,k_v\left[\frac{h_{lv}\,\rho_v\,g(\rho_l-\rho_v)}{\mu_v k_v\,\Delta T}\right]^{1/3}(\sin\theta)^{0.3333333} \tag{5.10}$$

where the constants 0.142 and 0.3333333 have been implemented in sensitivity coefficients array C1245. The other option, which is invoked when the user changes the value of sensitivity coefficient C1245(7) to 1.0, gives the heat transfer coefficient as [36]:

$$h_{FLM}(\Delta T) = \left(0.055 + 0.016\,\theta^{0.5}\right)k_v\left[\frac{h_{lv}\,\rho_v\,g(\rho_l-\rho_v)}{\mu_v k_v\,\Delta T}\right]^{1/3} \tag{5.11}$$

where the constants 0.055, 0.016 and 0.5 have been implemented in sensitivity coefficient array C1245.

Equations (5.6) to (5.11) give values of heat fluxes and heat transfer coefficients for particular values of θ (except for Equation (5.8), which is independent of θ). To obtain an average value, f_i, of function $f(\theta)$, which is appropriate for ring i in the lower head model, $f(\theta)$ is averaged over the wetted surface area of ring i as follows:

$$f_i = \frac{\int_{\theta_{i-1}}^{\theta_u} f(\theta)\,\sin\theta\,d\theta}{\cos\theta_{i-1} - \cos\theta_u} \tag{5.12}$$

$$\theta_u = \min[\theta_i, \max(\theta_{i-1}, \theta_{PL})] \tag{5.13}$$

where θ_{PL} is the angle from the bottom of the lower head to the pool surface, $\theta_0 = 0\circ$ and $\theta_{NRAD} = 90\circ$. This averaging results in positive values for all quantities in Equations (5.6) to (5.11), even though the heat transfer coefficient in Equation (5.10) is zero at $\theta = 0^\circ$. Note, however, that specifying very small values of θ_i, (i.e. defining a very small innermost ring) is discouraged because the lower head model does not include azimuthal conduction that tends to limit the formation of local hot spots where boiling heat removal is low (i.e. at the very bottom of the lower head). Hence, the specification of a very small inner ring may

lead to a prediction of vessel failure at a hot spot on the vessel bottom, which would not occur if azimuthal heat conduction in the vessel were modeled.

If the heat flux from Equation (5.8) is set equal to the average heat flux from Equation (5.6) for any ring and solved for ΔT, the result is equal to ΔT_{CHF}, the temperature difference at the critical heat flux for that ring. If the average heat flux from Equation (5.9) is set equal to the average heat flux from Equation (5.7) and solved for ΔT, the result is equal to ΔT_{MIN}, the temperature difference at the minimum-stable-film-boiling heat flux for that ring. Since the actual value of ΔT is known from the data base at the beginning of each COR time step, it can be compared to ΔT_{CHF} and ΔT_{MIN} to determine the appropriate heat transfer regime. If the value is less than ΔT_{CHF}, then fully-developed nucleate boiling occurs and h_{PL} is given by h_{NB} from Equation (2.58). If ΔT is greater than ΔT_{MIN}, then stable film boiling occurs and h_{PL} is given by Equation (5.10) or (5.11), as specified by the user. If the value of ΔT lies between ΔT_{CHF} and ΔT_{MIN}, then h_{PL} is equal to the transition boiling heat transfer coefficient, which is found by logarithmic interpolation as follows:

$$h_{TRN} = \frac{q_{MIN}}{\Delta T}\left(\frac{\Delta T}{\Delta T_{MIN}}\right)^{\left[\frac{\log(q_{CHF}/q_{MIN})}{\log(\Delta T_{CHF}/\Delta T_{MIN})}\right]} \tag{5.14}$$

The net energy transfer for each of the model elements is given by the following equations:

$$C_{p,p}\left(T_p^n - T_p^o\right) = \left(q_{d,p} - q_{p,h} - q_{p,v}\right)\Delta t \tag{5.15}$$

$$C_{p,d}\left(T_d^n - T_d^o\right) = \left(q_s - q_{d,p} - q_{d,h} - q_{d,v} - q_{d,d}\right)\Delta t \tag{5.16}$$

$$C_{p,h,n}\left(T_{h,n}^n - T_{h,n}^o\right) = \left(q_{n-1,n} + q_{d,h} + q_{p,h} - q_{h,v}\right)\Delta t \tag{5.17}$$

$$C_{p,h,i}\left(T_{h,i}^n - T_{h,i}^o\right) = \left(q_{i-1,i} - q_{i,i+1}\right)\Delta t \tag{5.18}$$

$$C_{p,h,1}\left(T_{h,1}^n - T_{h,1}^o\right) = \left(-q_{d,c} - q_{1,2}\right)\Delta t \tag{5.19}$$

where many of these variables were defined in Section 5.1 and

$C_{p,j}$ = total heat capacity of model element j, ($M_j c_{p,j}$)

q_s = debris heat source from oxidation and decay heat

$q_{d,d}$ = debris cell-to-cell heat transfer rate

Δt = COR package time step

and superscripts o and n refer to old-time and new-time temperatures, respectively. All temperatures in Equations (5.1) through (5.4) are considered to be new time temperatures, and Equations (5.5) through (5.8) are solved implicitly for new-time temperatures by matrix inversion.

5.2 Failure

Failure of the lower head will occur if any of four criteria is met:

1. the temperature of a penetration (or the temperature of the innermost node of the lower head) reaches a failure temperature (TPFAIL) specified by the user on record COR00009,

2. a failure logical control function (specified by the user on record CORRii02) is found to be .TRUE. For example, such a control function might refer to a table of differential failure pressures as a function of lower head temperature,

3. overpressure from the falling-debris quench model occurs (see Section 2.3.6). The lower head is allowed to fail from overpressure, with a default failure criterion of 20 MPa that may be changed on input record COR00012 or

4. creep-rupture failure of a lower head ring occurs, in response to mechanical loading under conditions of material weakening at elevated temperatures.

The creep-rupture failure model uses the temperature profile through the lower head to calculate creep based on a Larson-Miller parameter and a life-fraction rule whenever the effective differential pressure across the lower head exceeds a user-specified minimum value (implemented as sensitivity coefficient C1600(3) with a default value of 1000 Pa). The effective differential pressure is the sum of the actual differential pressure between the lower plenum and the reactor cavity and the pressure caused by the weight of any debris resting on the lower head. The lower limit on the effective pressure differential was imposed to bypass the model and save computational resources when the threat of creep-rupture is minuscule.

The model is applied to the load-bearing mesh layers in the lower head, which include all NLH-1 mesh layers by default. However, by entering a positive value for NINSLH on input record COR00000, the user defines the outer NINSLH layers to consist of non-load-bearing insulation. An optional one-dimensional mechanical model that calculates the thermal and plastic strain in each load-bearing mesh layer may be invoked by setting the value of sensitivity coefficient C1600(1) equal to 1.0. By default, however, a zero-dimensional model based on the mass-averaged temperatures in the load-bearing mesh layers is used with the effective membrane stress induced by the effective differential pressure to calculate a single Larson-Miller parameter for each radial ring.

The Larson-Miller creep-rupture failure model [32] gives the time to rupture, t_R in seconds, as:

$$t_R = 10^{\left(\frac{P_{LM}}{T} - 16.44\right)} \tag{5.20}$$

where P_{LM} is the Larson-Miller parameter given by:

$$P_{LM} = 7.722x10^{-4} - 7.294x10^{3} \quad \log_{10} \sigma_e \tag{5.21}$$

where σ_e is the effective stress in Pa and the constants $7.722x10^4$ and $-7.294x10^3$, which are appropriate for reactor vessel carbon steel [37] and 16.44 (Equation (5.21)), have been implemented in sensitivity coefficient array C1601. The life-fraction rule gives the cumulative damage, expressed as plastic strain, $\varepsilon_{pl}(t)$, as:

$$\varepsilon_{pl}(t + \Delta t) = \varepsilon_{pl}(t) + 0.18 \frac{\Delta t}{t_R} \tag{5.22}$$

where the constant 0.18, which has been implemented as sensitivity coefficient C1601(4), implies that failure (defined as when the integrated value of $\Delta t / t_R$ reaches unity) occurs when the strain reaches 18% [36].

For the zero-dimensional default option, the effective stress is given by:

$$\sigma_e = \frac{(\Delta P + \rho_d g \Delta z_d) R_i^2}{R_o^2 - R_i^2} \tag{5.23}$$

where ΔP is the pressure difference across the lower head, ρ_d and Δz_d are the density and depth of the debris resting on the lower head, and R_i and R_o are the inner vessel radius and outer radius of load-bearing vessel steel, respectively. Substitution of σ_e from Equation (5.23) into Equation (5.21) yields a value of P_{LM} for each ring. Substitution of the temperature, mass-averaged over all the load-bearing mesh layers in each lower head ring, and the value of P_{LM} into Equation (5.20) yields t_R (the predicted time lapse until failure for a specimen subjected to the current temperature and stress). And, finally, substitution of t_R into Equation (5.22) yields the accumulated plastic strain at each time step. Failure is declared when ε_{pl} (t) reaches failure strain given by sensitivity coefficient C1601(4), with a default of 0.18, and the mechanical calculation in that ring ceases.

The optional one-dimensional mechanical model predicts the stress-strain distribution through the lower head, and treats stress redistribution from both thermal strain and material property degradation. The elastic modulus as a function of temperature is given by [36]:

$$E(T) = 2.0x10^{11}\left[\frac{1}{1+\left(\frac{T}{900.}\right)^{6.}} - \frac{1}{1+\left(\frac{1800.}{900.}\right)^{6.}}\right] \quad (5.24)$$

where the constants $2.0x10^{11}$, 1800., 900. and 6., which are appropriate for reactor vessel steel, have been implemented as sensitivity coefficient array C1602. The yield stress as a function of temperature is given by [36]:

$$\sigma_Y(T) = 4.0x10^{8}\left[\frac{1}{1+\left(\frac{T}{900.}\right)^{6.}} - \frac{1}{1+\left(\frac{1800.}{900.}\right)^{6.}}\right] \quad (5.25)$$

where the constants $4.0x10^{8}$, 1800., 900. and 6., which are appropriate for reactor vessel steel, have been implemented as sensitivity coefficient array C1603.

The one-dimensional model requires that the stress distribution integrated over the vessel thickness be equal to the imposed load:

$$[\Delta P + \rho_d g \Delta z_d] R_0^2 = \sum_{i}^{N_{NY}} \sigma_i \left(R_i^2 - R_{i-1}^2\right) + \sum_{j}^{N_Y} \sigma_Y(T_j)\left(R_j^2 - R_{j-1}^2\right) \quad (5.26)$$

where the first sum on the right-hand side is over all layers that have not yielded, N_{NY}, and the second sum is over all layers that have yielded, N_Y. The stress, σ_i, in layers that have not yielded is given by:

$$\sigma_i = E(T_i)\left[\varepsilon_{tot} - (\varepsilon_{pl,i} + \varepsilon_{th,i})\right] \quad (5.27)$$

where $E(T_i)$ is the value of the elastic modulus at the average temperature in mesh layer *i*, which is equal to the average of the node temperatures on the two boundaries, ε_{tot} is the total strain across the lower head in the particular ring, which is the same for mesh layers in that ring, and $\varepsilon_{pl,i}$ and $\varepsilon_{th,i}$ are the plastic and thermal strains, respectively, in mesh layer *i*. The thermal strain is given by:

$$\varepsilon_{th,i} = 1.0x10^{-5}(T_i - T_{ref}) \quad (5.28)$$

where the constant $1.0x10^{-5}$ is the linear thermal expansivity, which has been implemented as sensitivity coefficient C1600(2), and T_{ref} is the reference temperature, which is equal to

the initial temperature specified by the user for that ring of the lower head. Equations (5.26) and (5.27) are solved implicitly and iteratively for ε_{tot}, σ_i and $\varepsilon_{pl,i}$ ($\varepsilon_{th,i}$ is known since the temperature profile is known) using Equation (5.20) - (5.22) to update the plastic strain profile with the latest stress profile after each iteration. Failure is declared when ε_{tot} reaches 18% (the use of ε_{tot} rather than ε_{pl} makes little difference because the elastic and thermal strains are insignificant compared to the plastic strain when ε_{tot} becomes large).

Whenever any failure condition is satisfied, an opening with an initial diameter defined by the user on record CORPENnn or with an initial diameter of 0.1 m if there are no penetrations (this gives a relatively rapid ejection of debris without numerical difficulties), is established, and the COR package control function argument COR-ABRCH (see Section 4 of the COR Package Users' Guide) is set to the initial failure flow area calculated from this diameter. COR-ABRCH can then be used to open a valve in the flow path from the lower plenum control volume to the reactor cavity control volume. COR-ABRCH may be increased by additional penetration failures (up to three per radial ring) or by ablation of the failure openings, as described in the next section.

5.3 Debris Ejection

After a failure has occurred, the mass of each material in the bottom axial level that is available for ejection (but not necessarily ejected) is calculated. Two simple options exist. In the default option (IDEJ = 0 on record CORTST01), the masses of each material available for ejection are the total debris material masses, regardless of whether or how much they are molten. Note, however, that this option has been observed to lead to ejection of much more solid debris with the melt than is realistic.

In the second option (IDEJ = 1 on MELCOR record CORTST01), the masses of steel, Zircaloy, and UO_2 available for ejection are simply the masses of these materials that are molten; the masses of steel oxide and control poison materials available for ejection are the masses of each of these materials multiplied by the steel melt fraction, based on an assumption of proportional mixing; and similarly the mass of ZrO_2 available for ejection is the ZrO_2 mass multiplied by the Zircaloy melt fraction. Additionally, the mass of solid UO_2 available for ejection is the Zircaloy melt fraction times the mass of UO_2 that could be relocated with the Zircaloy as calculated in the candling model using the secondary material transport model (see Section 3.1). An option parallel to the methodology used in the materials interactions (eutectics) model has not yet been developed.

Regardless of which of the options described above is chosen, other constraints have been imposed on the mass to be ejected at vessel failure. A total molten mass of 5000 kg or a melt fraction of 0.1 (total molten mass divided by total debris mass) is necessary before debris ejection can begin, to avoid calculational difficulties with the core-concrete interactions modeling. Also, whenever the bottom lower head node exceeds the

penetration failure temperature TPFAIL, gross failure of the lower head in that ring is assumed and all debris in the bottom cell is discharged linearly over a 1 s time step, regardless of the failure opening diameter. However, no mass associated with either the lower head hemisphere or the penetrations is added to the core/lower plenum debris.

Once the total mass of all materials available for ejection has been determined, the fraction of this mass ejected during a single COR package subcycle is determined from hydrodynamic considerations. The velocity of material being ejected is calculated from the pressure difference between the lower plenum control volume and the reactor cavity control volume, the gravitational head from the debris layer itself, and a user-specified flow discharge coefficient input on record COR00009, using the Bernoulli equation:

$$v_{ej} = C_d \left(\frac{2\,\Delta P}{\rho_m} + 2\ g\ \Delta z_d \right)^{1/2} \tag{5.29}$$

where

v_{ej} = velocity of ejected material

C_d = flow discharge coefficient

ΔP = pressure difference between lower plenum control volume and reactor cavity control volume

ρ_m = density of material being ejected

g = gravitational acceleration

Δz_d = debris height

If the expression in parentheses in Equation (5.29) is negative, the ejection velocity is set to zero.

The maximum mass of all materials that can be ejected during a single COR time step is:

$$M_{ej} = \rho_m\ A_f\ v_{ej}\ \Delta t \tag{5.30}$$

where

M_{ej} = maximum mass ejected

A_f = penetration failure area

Δt = time step

The fraction of the total mass available for ejection that actually is ejected during the subcycle is simply M_{ej} divided by the total mass available to be ejected, up to a maximum value of 1.0. This fraction is applied to the mass of each material available for ejection.

Mass and energy that are ejected from the COR package via the foregoing model are transferred to the Transfer Processes (TP) package. That package is a generalized interface utility for mass and energy transfers of core materials between packages and within the radionuclide (RN) package, and performs various bookkeeping functions related to different equation-of-state and mass-species representations between packages. The cavity (CAV), fuel dispersal interactions (FDI), and RN packages may all call the TP package to transfer core materials into their domain. The 'IN' Transfer Process number that specifies the TP package input for transferring masses and energies from the COR package must be specified on record COR00004.

Ablation of the failure opening is modeled by calculating the heat transfer to the lower head by flowing molten debris. A simplified implementation of the ablation model by Pilch and Tarbell [38] is used, which gives the heat transfer coefficient for the flowing molten debris as the maximum of a tube correlation and a flat plate correlation:

$$h_{abl,tube} = 0.023\ K_p\ v_{ej}^{0.8}\ /\ D_f^{0.2} \tag{5.31}$$

$$h_{abl,plate} = 0.0292\ K_p\ v_{ej}^{0.8}\ /\ \Delta z_h^{0.2} \tag{5.32}$$

where

h_{abl} = ablation heat transfer coefficient

K_p = $k\,(\rho / \mu)^{0.8}\ Pr^{1/3}$ (using average property values from [38])

D_f = failure diameter

Δz_h = lower head thickness

The ablation rate is then calculated as:

$$\frac{dD_f}{dt} = \frac{2\ h_{abl}\ \left(T_d\ -\ T_{m,s}\right)}{\rho_s\ \left[c_{p,s}\ \left(T_{m,s}\ -\ T_{h,avg}\right) +\ h_{f,s}\right]} \tag{5.33}$$

where ρ_s, $c_{p,s}$, $h_{f,s}$, and $T_{m,s}$ are the density, heat capacity, latent heat of fusion, and melting temperature of the (lower head) steel, and T_d and $T_{h,avg}$ are the debris and average lower head temperatures. The diameter of the penetration failure is updated explicitly with time using Equation (5.33). The value of the control function argument COR-ABRCH is then redefined to reflect the new failure opening diameter.

6 Discussion and Development Plans

In its inception, MELCOR was envisioned as a PRA tool that was to be fast running, making use of necessarily simplified physics models. In recent years, however, MELCOR has found increasing use as a best estimate tool for severe accident analyses, and many of the physics models, including many in the COR package have been improved considerably. Nevertheless, some of the simplified COR models remain today. In some cases, simplistic parametric models have been implemented until more advances have been made in furthering our understanding of the phenomena. In other cases, more sophisticated models are planned for implementation in the near future.

The following paragraphs are based on assessments of improvement needs for MELCOR in the area of core modeling, including deficiencies identified as part of the MELCOR Peer Review [39], and include work in progress. Suggestions from users regarding additional modification and/or upgrading of the COR package are welcomed and should be directed to the MELCOR Code Development Group using the MELCOR Defect Investigation Report (DIR) forms.

6.1 Radiation

Radiation view factors in the COR package are defined globally, based on simple user input. Since correct characterization of many of these view factors is dependent on local geometry and nodalization, they should be definable on a local cell basis and updated internally with changing geometry. This upgrade would give the user more freedom to satisfactorily model radiative heat transfer within the core, a dominant heat transfer mechanism in reactor accidents.

6.2 Reflood Behavior

To adequately assess the possibly deleterious effects of reflooding and the potential to avoid vessel failure, models to credibly predict the interactions between water and overheated fuel rods or core debris are desirable. This involves the ability to predict quenching rates in the geometries of interest, spallation of oxide from the fuel rod cladding with accelerated oxidation, shattering of the fuel rods during quench, the occurrence and effects of clad ballooning (discussed separately below), and the possibility of forming a molten pool. Models are currently under development for post-1.8.5 MELCOR release.

6.3 Lower Plenum Debris Behavior and Vessel Failure

The COR package in MELCOR does not include consideration of natural circulation of a molten debris pool in the lower head. Such pools can form if the debris temperature and relocation rate are such as to prevent early failure of the bottom head or its penetration (if

there are any), and is of particular importance if the lower head is externally cooled by flooding the reactor cavity with water. It also fails to account for head curvature effects, freezing and remelting of core debris in penetrations, and crust formation, growth, and remelting.

The Bottom Head (BH) package models, developed as part of the BWRSAR program at Oak Ridge National Laboratory (ORNL), address some of these deficiencies. In MELCOR 1.8.4, the BH package was extended to treat PWRs as well as BWRs, and may be invoked by supplying appropriate input as described in the BH package Users' Guide. However, it will not become active in a calculation until complete dryout of the lower head has been achieved; until that time the much simpler models of the COR package will be used.

Either the BH models should be much more completely and tightly coupled into existing COR models, or the domain for each package should be carefully redefined with overlap minimized and interfaces between them and between other MELCOR packages rigorously specified. In either case, the BH lower plenum models should be made more flexible for more complete treatment of different accident scenarios (e.g., debris heat transfer before complete pool boiloff) and to allow greater user control (e.g., with sensitivity coefficients).

6.4 Updating of Core Degradation Models

Understanding of the mechanisms of core degradation has increased significantly since the inception of MELCOR and the original design of the degradation models. There has been an increased appreciation of the importance of melting and materials interactions compared with rubble formation. In addition, application of the code has been expanded from PRA calculations for which simple parametric models would be adequate, to source term calculations requiring more detailed validation against the latest experimental data. Some improvements to core degradation models were made for MELCOR 1.8.4. In the course of this work, it became apparent that the basic modeling approach should be reexamined to determine if changes are be necessary to accommodate models that reflect current understanding of the important phenomena. Some such improvements have been made in MELCOR 1.8.5, and others are being considered for later versions of the code.

APPENDIX A: Sensitivity Coefficients

This appendix gives the sensitivity coefficients associated with various correlations and modeling parameters described in this reference manual.

Equation	Coefficient	Value	Units
(2.75), (2.76)	C1001(1,1)	29.6	$kg^2(Zr)/m^4$-s
	C1001(2,1)	16820.0	K
	C1001(3,1)	87.9	$kg^2(Zr)/m^4$-s
	C1001(4,1)	16610.0	K
	C1001(5,1)	1853.0	K
	C1001(6,1)	1873.0	K
(2.77)	C1001(1,2)	50.4	$kg^2(Zr)/m^4$-s
	C1001(2,2)	14630.0	K
	C1001(3,2)	0.0	$kg^2(Zr)/m^4$-s
	C1001(4,2)	0.0	K
	C1001(5,1)	10000.0	K
	C1001(6,2)	10000.0	K
(2.78)	C1002(1)	2.42E09	$kg^2(steel)/m^4$-s
	C1002(2)	4.24E04	K
(2.79)	C1003(1)	0.00548	$kg(Zr)-K/Pa-m^3$
	C1003(2)	0.00504	$kg(steel)-K/Pa-m^3$
§2.4	C1004(1)	1100.0	K
	C1004(2)	9900.0	K
§2.4	C1005(1)	0.0	-
	C1005(2)	2.E-2	-
	C1005(3)	9.E-1	-
	C1005(4)	1500.	K
§2.4	C1006(1)	1.662E5	s^{-1}
	C1006(2)	2.26472E4	K
§2.4	C1007(1..NRAD,1)	0.0	-
	C1007(1..NRAD,2)	0.0	-
§2.7.3	C1010(1,2)	1.47E14	-
	C1010(2,2)	8.01E4	K
	C1010(1,3)	1.02E15	-
	C1010(2,3)	8.14E4	K
	otherwise		
	C1010(1,J)	-1.	-
	C1010(2,J)	0.0	K
§2.7.1	C1011(1)	1400.	K
	C1011(2)	1400.	K
	C1011(3)	1520.	K

Equation	Coefficient	Value	Units
§3.1.5 §3.2.4	C1020(1)	360.0	s
	C1020(2)	60.0	s
	C1020(3)	0.0	-
	C1020(4)	0.0	-
	C1020(5)	1.0	-
§1.1.1	C1021(1)	1.0	s
§2.5	C1030(1)	0.0	-
	C1030(2)	10.	s
	C1030(3)	1.	s
(2.33)	C1101(1)	0.8	-
	C1101(2)	0.325	-
§3.1.3	C1131(1)	0.00001	m
	C1131(2)	2400.0	K
	C1131(3)	0.001	m
	C1131(4)	1700.0	K
§3.2	C1132(1)	2500.0	K
	C1132(2)	3100.0	K
(3.11)	C1141(1)	1.0	s
	C1141(2)	1.0	kg/m-s

Equation	Coefficient	Value	Units
(3.16) - (3.24)	C1151(l,1)	0.556	-
	C1151(l,2)	0.807	-
	C1151(l,3)	0.143	-
	C1151(l,4)	0.396	-
	C1151(l,5)	0.0	-
	C1151(2,6)	1.0	-
	C1151(6,6)	1.0	-
	C1151(9,6)	1.0	-
	otherwise		
	C1151(l,6)	0.0	-
	C1151(l,7)	100.0	1/m
(3.25)	C1152(1)	1000.	1/m
(2.49)	C1200(1)	0.5	-
	C1200(2)	0.9	-
(2.50)	C1212(1)	4.36	-
	C1212(2)	4.36	-
(2.50)	C1213(1)	0.00826	-
	C1213(2)	0.00110	-
(2.53)	C1214(1)	0.023	-
	C1214(2)	0.8	-
	C1214(3)	0.4	-
(2.54)	C1221(1)	0.18	-
	C1221(2)	0.25	-
	C1221(3)	-1./9.	-
(2.55)	C1222(1)	0.065	-
	C1222(2)	1./3.	-
	C1222(3)	-1./9.	-
(2.56)	C1231(1)	2.0	-
	C1231(2)	0.60	-
	C1231(3)	0.5	-
	C1231(4)	1./3.	-
(2.57)	C1232(1)	2.0	-
	C1232(2)	0.60	-
	C1232(3)	0.25	-
	C1232(4)	1./3.	-
(2.58)	C1241(1)	34.5	$W/m^2\text{-}K\text{-}Pa^{1/4}\text{-}K^{1.523}$
	C1241(2)	0.25	-
	C1241(3)	1.523	-
	C1241(4)	23.4	K

Equation	Coefficient	Value	Units
§2.3.5	C1241(5)	0.0	-
(2.59)	C1242(1)	1.41E07	W/m^2-K-$Pa^{1/4}$-$K^{-2.575}$
	C1242(2)	0.25	-
	C1242(3)	-2.575	-
(2.61)	C1244(1)	0.756	-
	C1244(2)	0.089	m
	C1244(3)	0.15	-
(5.6)	C1245(1)	0.034	-
	C1245(2)	0.0037	-
	C1245(3)	0.656	-
(5.7)	C1245(4)	4.8E-4	-
	C1245(5)	8.2E-4	-
	C1245(6)	0.407	-
§5.1	C1245(7)	0.0	-
§5.1	C1245(8)	0.142	-
	C1245(9)	0.3333333	-
§5.1	C1245(10)	0.055	-
	C1245(11)	0.016	-
	C1245(12)	0.5	-
§2.2	C1250(1)	3200.	K
	C1250(2)	0.01	K^{-1}
(2.102)	C1301(1)	0.037	-
	C1301(2)	0.3	-
	C1301(3)	0.7	-
	C1301(4)	2.4384	m
	C1301(6)	7.65318E06	Pa

Equation	Coefficient	Value		Units
		BWR	PWR	
§2.6.1	C1311(1)	0.735	0.500	-
	C1311(2)	0.400	0.541	-
	C1311(3)	0.292	0.565	-
	C1311(4)	0.263	0.234	-
§2.6.1	C1312(1)	0.9	-	
	C1312(2)	1.0	-	
	C1312(3)	1.0	-	
	C1312(4)	1.0	-	
	C1312(5)	1.0	-	
	C1312(6)	1.0	-	
	C1312(7)	1.0	-	

Equation	Coefficient	Value		Units
		BWR	PWR	
	C1312(8)	1.0	-	
	C1312(9)	1.0	-	
		BWR	PWR	
§2.6.2	C1321(1)	0.735	0.500	-
	C1321(2)	0.400	0.541	-
	C1321(3)	0.292	0.565	-
	C1321(4)	0.263	0.234	-
	C1321(5)	0.400	0.541	-
	C1321(6)	0.292	0.565	-
	C1321(7)	0.400	0.541	-
§2.6.2	C1322(1)	0.9	-	
	C1322(2)	1.0	-	
	C1322(3)	1.0	-	
	C1322(4)	1.0	-	
	C1322(5)	1.0	-	
	C1322(6)	1.0	-	
	C1322(7)	1.0		
	C1322(8)	1.0	-	
	C1322(9)	1.0	-	
§1.2	C1401(1)	1.6	-	
	C1401(2)	0.8	-	
	C1401(3)	-1.0	-	
	C1401(4)	20.0	-	
	C1401(5)	0.5	-	
	C1401(6)	1.0	-	
§1.1.1	C1501(1)	0.5	-	
	C1501(2)	0.5	-	
	C1501(3)	0.5	-	
	C1501(4)	0.5	-	
	C1501(5)	0.5	-	

Equation	Coefficient	Value	Units
§1.2	C1502(1)	1.0E-6	kg
	C1502(2)	10.0	kg
§3.1.2	C1503(1)	1.0E-3	-
§3.3	C1504(1)	10*unit roundoff	-
	C1504(2)	1.E-4	-
§5.2	C1600(1)	0.0	-
(5.28)	C1600(2)	1.E-5	K^{-1}
§5.2	C1600(3)	1.E3	Pa
(5.21)	C1601(1)	-7.294E3	-
	C1601(2)	7.722e4	-
(5.20)	C1601(3)	16.44	-
(5.22)	C1601(4)	0.18	-
(5.24)	C1602(1)	2.E11	Pa
	C1602(2)	1800.	K
	C1602(3)	900.	K
	C1602(4)	6.	-
(5.25)	C1603(1)	4.E8	Pa
	C1603(2)	1800.	K
	C1603(3)	900.	K
	C1603(4)	6.	-
(4.23)	C1604(1)	-7.5E3	-
	C1604(2)	8.1E4.	-
(4.24)	C1604(3)	16.44	-
(4.22	C1605(1)	370.E9	Pa
	C1605(2)	1700.	K
	C1605(3)	1650.	K
	C1605(4)	3.0	-
(4.18)	C1606(1)	260.E6	Pa
	C1606(2)	1700.	K
	C1606(3)	800.	K
	C1606(4)	3.0	-

References

1. F. Kreith, Principles of Heat Transfer, 3rd Edition, Intext Educational Publishers, New York, NY, pp. 251-273 (1973).

2. L. J. Ott, C. F. Weber, and C. R. Hyman, "Station Blackout Calculations for Browns Ferry," Proceedings of the Thirteenth Water Reactor Safety Research Information Meeting, Gaithersburg, MD (October 1985).

3. R. O. Wooton, P. Cybulskis, and S. F. Quayle, "MARCH 2 (Meltdown Accident Response Characteristics) Code Description and User's Manual," NUREG/CR-3988, BMI-2115 (August 1984).

4. D. L. Hagrman, G. A. Reymann, and R. E. Mason, MATPRO-VERSION 11 (Revision 1) A Handbook of Materials Properties for Use in the Analysis of Light Water Reactor Fuel Rod Behavior, NUREG/CR-0497 and TREE-1280 Rev. 1 (February 1980).

5. L. J. Ott, Thermal-Hydraulic Test Facility Bundle 3 In-Core Instrumentation and Operating History, NUREG/CR-2609, Chapter 8 (August 1982).

6. C. B. Ludwig and C. C. Ferriso, "Prediction of Total Emissivity of Nitrogen-Broadened and Self-Broadened Hot Water Vapor," J. Quant. Spectrosc. Radiat. Transfer, 7, pp. 7-26.

7. J. P. Holman, Heat Transfer, McGraw-Hill, Inc., New York, NY, pp. 305-307 (1976).

8. M. P. Manahan, "An Improved Zircaloy-Steam Reaction Model for Use with the MARCH 2 (Meltdown Accident Response Characteristics) Code," Proceedings of the International Meeting on Light-Water Reactor Severe Accident Evaluation, Cambridge, MA (August 1983).

9. F. W. Dittus and L. M. K. Boelter, University of California Pubs. Eng., 2, p. 433 (1930).

10. M. Jacob, Heat Transfer, Vol. I, John Wiley & Sons, Inc., New York, NY (1949).

11. R. B. Bird, W. E. Stewart, and E. N. Lightfoot, Transport Phenomena, John Wiley & Sons, Inc., New York, NY (1960).

12. R. J. Lipinski, A Model for Boiling and Dryout in Particle Beds, NUREG/CR-2646, SAND82-0765 (June 1982).

13. G. W. Parker and A. L. Sutton, Jr., "Boron Control Material Behavior in Large-Scale, Core-Melt Experiments," presented at the Severe Fuel Damage and Source Term Research Program Review Meeting, Oak Ridge Associated Universities Conference Center, Oak Ridge, TN, April 7-10, 1986.

14. V. F. Urbanic and T. R. Heidrich, "High-Temperature Oxidation of Zircaloy-2 and Zircaloy-4 in Steam," J. Nuc. Matls., 75, pp. 251-261 (1978).

15. A. S. Benjamin, D. J. McCloskey, D.A. Powers, and S. A. Dupree, Spent Fuel Heatup Following Loss of Water During Storage, SAND77-1371, NUREG/CR-0649, Sandia National Laboratories, Albuquerque, NM, March 1979.

16. J. F. White et al., "Fifth Annual Report--High Temperature Material Programs, Part A," GEMP-400A (February 1966).

17. Fred Griffin, "BWR Control Blade Channel Box Interaction and Melt Relocation Models for SCDAP," Letter Report ORNL/NRC/LTR-92/12/R2 to Dr. Yi-Shung Chen, Accident Evaluation Branch, Division of Systems Research, RES USNRC, December 30, 1993.

18. G. Eriksson, "Thermodynamic Studies of High Temperature Equilibria: XII. SOLGASMIX, a computer program for calculation of equilibrium compositions in multiphase systems," Chemica Scripta, 8, 1975, pp. 100-103.

19. "Reducing BWR Power by Water Level Control During an ATWS, a Quasi-Static Analysis," NSAC-69, S. Levy, Inc. Final Report (May 1984).

20. P. Hofmann et al., “Reactor Core Materials Interactions at Very High Temperatures,” Nuclear Technology, 87, pp. 146-186, August 1989.

21. W. Hering and K. Muller, “Modelling of Eutectic Interactions in KESS-III (Module EUTECT),” International CORA Workshop 1992, Karlsruhe, FRG, October 5-8, 1992.

22. R. K. Cole, et al., CORCON-Mod2: A Computer Program for Analysis of Molten-Core Concrete Interactions, NUREG/CR-3920, SAND84-1246, August 1984, pp. 64-65.

23. R. J. Roark and W. C. Young, Formulas for Stress and Strain, Fifth Edition, McGraw-Hill Book Company, New York, NY, 1982, Case 8 of Table 26.

24. Ibid. The equation is extracted from Case 10 of Table 24.

25. R. K. Cole, Jr., “Modifications to MELCOR to Improve Modeling of Core Structure Supports, Final Implementation Report,” letter report to Mr. John Ridgely, USNRC, April 15, 1999.

26. R. J. Roark and W. C. Young, op. cit., Case 2a of Table 24.

27. S. Timoshenko and S. Woinowsky-Krieger, Theory of Plates and Shells, Mcgraw-Hill Book Company, New York, NY, Second Edition, 1959. Parameters are taken from Table 58.

28. R. C. Schmidt et al., MELPROG-PWR/MOD1 Models and Correlations, SAND89-3123, June 1992.

29. Nuclear Systems Materials Handbook, Vol. 1 – Design Data, “Yield strength, minimum expected.”

30. T. H. Lin, Theory of Inelastic Structures, John Wiley and Sons, NY, 1983.

31. Nuclear Systems Materials Handbook, Vol. 1 – Design Data, “Young’s modulus, static.”

32. F. R. Larson and J. Miller, “A Time-Temperature Relationship for Rupture and Creep Stress,” Transactions of the ASME, pp. 765-775, July 1952.

33. American Society of Mechanical Engineers, “ASME Boiler and Pressure Vessel Code Case N-47-22,” April 5, 1984.

34. M. S. El-Genk and Z. Guo, “Transient Critical Heat Flux for Inclined and Downward-Facing Flat Surfaces,” ANS Proceedings, HTC-6 Volume 6, 1992, National Heat Transfer Conference, August 9-12, 1992, San Diego.

35. T. Y. Chu, "A Correlational Approach to Turbulent Saturated Film Boiling," Journal of Heat Transfer, Volume 115, November 1993.

36. K. B. Cady, V. K. Dhir and R. J. Witt, "Peer Review of Models for Lower Vessel Head Heat Transfer and Larson-Miller Failure Criterion Proposed for Implementation into MELCOR," ERI/NRC 94-202 March 1994.

37. J. L. Rempe et. al., Light Water Reactor Lower Head Failure Analysis (Draft), INEL, NUREG/CR-5642, EGG-2618, December 1991.

38. M. Pilch and W. W. Tarbell, High Pressure Ejection of Melt from a Reactor Pressure Vessel—the Discharge Phase, NUREG/CR-4383, SAND85-0012 (September 1985).

39. B. E. Boyack, et al., MELCOR Peer Review, LA-12240, Los Alamos National Laboratory (March 1992).